UNIVERSITY OF SOUTHAMPTON

DEPARTMENT OF

AERONAUTICS AND ASTRONAUTICS

STRUCTURAL VIBRATIONS IN ACOUSTIC FIELDS

BY J. H. FOXWELL.

CONTENTS

Part I

Part II

ABSTRACT

FACULTY OF ENGINEERING AND APPLIED SCIENCE.

DEPARTMENT OF AERONAUTICS AND ASTRONAUTICS.

Doctor of Philosophy.

STRUCTURAL VIBRATIONS IN ACOUSTIC FIELDS.

by John Henry Foxwell.

Theoretical studies are described on the response of certain structures to acoustic waves. The most general problem treated is the response of a long cylindrical shell periodically stiffened both longitudinally and circumferentially when excited by obliquely incident plane sound waves. Numerical calculations are given for a structure having similar characteristics to an aircraft fuselage. Calculations of the shell vibration and internal sound field are given.

A simplified mathematical model, related to the phasing of aircraft propellers, is used to show the effect on the internal sound field due to a phase difference between opposite running plane waves incident on the shell.

A procedure is described for calculating the acoustic loading on a rectangular flat plate set in a rigid wall and vibrating in sinusoidal modes. Results are given of the acoustic radiation damping.

Wide frequency band space correlation measurements of the pressure field close to a two-inch diameter cold air jet are described. The results are shown to be consistent with the hypothesis that the pressure field close to the jet is convected at a speed related to the local speed in the jet. Using the convection hypothesis a generalised non-dimensional form of the space correlation is derived and both model and full scale measurements are shown to conform.

The convection model predicts the form of the narrow frequency band space-correlation function. This function is required for the calculation of structural response to jet noise. An approximate form of this function is utilised in a calculation of the response of a flat panel close to an air jet.

Space correlation measurements in the region within five jet diameters of the orifice of a full scale jet engine exhaust show the acoustic nature of the radiated noise showing the pressure field propagating at the speed of sound as opposed to the near pressure field of the jet turbulence propagating downstream at about one half of the local jet speed.

CHAPTER I

INTRODUCTION

Two of the many noise problems arising in the field of aeronautics are the fatigue of structure situated close to intense noise sources and the acoustical comfort of passengers. This thesis presents a theoretical approach to the transmission of acoustic energy through aircraft structures and a further examination of some of the parameters revealed by Powell (Ref.16) as being of major importance in the assessment of the stress levels experienced by structures subjected to acoustic excitation.

Before stating more explicitly the particular problems which are investigated in this work, it is worthwhile to consider briefly the existing theory of acoustic transmission. In architectural acoustics where wall structures are massive, the acoustic transmission loss of a wall can be satisfactorily calculated by the so called "mass law". This "law" is easily derived by considering the wall as a single degree of freedom vibrating structure with one resonant frequency. In normal building construction, this resonant frequency is very low since the mass of the wall is great in relation to its stiffness. At frequencies above resonance the mass of the wall appears as the factor which dictates the amount of acoustic energy which the wall transmits. It has been found by Cremer (Ref.32) that for sound waves at oblique incidence and sufficiently small wave-length the mass law is in error. This is

because flexural waves can be excited in the structure and when the wave-length of these waves matches the trace wave-length of sound-waves across the structure the acoustic transmission loss appears to be much less than the simple mass law would predict. This phenomenon is referred to as the coincidence principle; this and the mass law are well described by Richardson (Ref.32). These theories have been very briefly described in order that they can be discussed in relation to aircraft structure.

The type of structure considered in this work is typical of that used in present day aircraft fuselage construction. This structure consists basically of a cylindrical shell which is supported by circumferential frames and lengthwise stringers. This structure is designed to be as light as possible whilst carrying the loads placed upon it. In consequence of its light weight its acoustic transmission properties are poor compared with traditional building structure. Coupled with the fact that intense noise fields originating from the boundary layer over the fuselage of the aircraft, the noise from the propeller or the jet exhaust, a severe problem is posed; that of achieving an acceptable noise level in the aircraft cabin. This has been approached, principally in the United States, by conducting experiments on many types of sound-proofing in order to arrive at the most effective. To the author's knowledge no satisfactory theory exists for predicting the acoustic transmission properties of aircraft structure. Miller has shown (Ref.4) that the resonant frequencies of the many mode shapes in which a typical aircraft structure can vibrate are distributed over a wide frequency range.

This means that the simple mass law cannot be applied since the fundamental assumption of the mass law is a one-degree of freedom mass-stiffness system with a resonant frequency below the frequency range of interest. With the type of structure under consideration, it is doubtful whether the coincidence principle is valid since this depends on the transmission of flexural waves along the wall or fuselage skin. In fact, these flexural waves will be reflected back at the frame-skin junctions to form standing waves in the structure rather than free flexural waves. In view of the inadequacy of these theories in the special case of aircraft structure a theoretical approach is proposed.

The problem may be stated in the following way; given an aircraft structure and a steady state external acoustic excitation, what is the steady state response of the structure in each of its mode configurations and what is the ratio of the acoustic pressure level at a given point inside the fuselage to a given point outside ? As a first step, the choice of the type of structure and the form of the external acoustic field was made as straightforward as possible, whilst still retaining the essential features of a practical case. Therefore, the most general case treated in this work is the response of a cylindrical structure periodically stiffened with frames and stringers and excited by plane sound waves at oblique incidence to the cylinder axis. Expressions are derived for the modal response and these have been programmed for electronic digital computation. However, before this general case was considered a series of progressively more complicated

problems were solved each of which gave useful ideas as to the course which the investigation should follow. The work of Junger (Ref.3.), Warburton and Arnold (Ref.5.) and Miller (Ref.4) have proved very helpful in developing the type of problem described above.

Plane wave periodic acoustic fields are considered and unfortunately these are seldom met in practice. Even calculations with plane waves prove to be complicated, but this is eased to some extent by automatic computation; however, with representative acoustic fields such as those produced by a propeller or by jet mixing, the calculation becomes very formidable. The principle difficulty lies in the mathematical representation of the incident field. For the discrete frequency components of propeller noise it would be possible by numerical methods to obtain the mode response and hence the internal acoustic field, but for random noise fields such as are produced by jet mixing and boundary layer turbulence only very crude calculations are possible at present.

Acoustic pressure fluctuations generated by the jet mixing process and the turbulent boundary layer are random in nature. This means that although the fluctuations are time dependent it is not possible to write down an explicit function for this time dependency. This is an intrinsic property of the random process. Therefore, in the calculation of structural response due to random loading it is only possible to obtain statistical properties of the response which are related to the corresponding statistical properties of the random incident field through the dynamic properties of the structure. These remarks lead to the work carried out in the second part of this thesis, which describes measurements made in

the noise field close to an air jet exhausting into still air and then considers a response calculation.

The course of the investigation was mainly motivated by the work of Powell (Ref.16), who showed which were the most important parameters in predicting mean square stress levels in structure subjected to random loading. One aim in calculating the structural response to random loading is the assessment of the fatigue life of such structure; the fatigue aspect is not considered in this work but, a knowledge of the mean square stress level, together with controlled laboratory fatigue tests can give a designer a good idea of the likely fatigue life of a given structure. For calculations of the mean square stress level at a given point in a structure in a given mode, Powell, (Ref.16) shows that two functions describing the incident random field are required; these are the power spectral density function which in effect gives the mean square value of the pressure fluctuations as a function of frequency and the space-correlation function of pressure fluctuations on the structure. Many measurements have been made of power spectral densities at points in noise fields produced by jet mixing, but very few space-correlation measurements have been made. The space-correlation measurements reported in this work were made in the noise fields of a small scale cold air jet in the laboratory and on a full scale hot jet in the field; these are considered in turn.

CHAPTER 2.

The one-degree of structural freedom system.

2.1

This chapter is concerned with two problems which, whilst having been simplified to a degree which gives them little practical application, do reveal the important characteristics of the general and more complex problem of a multi-degree of freedom system such as an aircraft fuselage.

2.2

Consider first an infinite, rigid, flat plate situated in an acoustic medium density ρ speed of sound c (see Fig.1). The plate has mass m per unit area and stiffness S per unit area and divides the medium into two regions. The plate is subjected to a simple harmonic forcing function $F(t)$ per unit area (which can be considered as an incident plane-wave sound field).

As the plate vibrates plane waves are generated which may be represented by

$$p_{r_1} = A_1 \exp\left[i\omega t + i\frac{\omega}{c}y\right] \qquad (2.1)$$

$$p_{r_2} = A_2 \exp\left[i\omega t - i\frac{\omega}{c}y\right] \qquad (2.2)$$

and ω is the angular frequency of the incident pressure field $F(t)$.

If continuity is to be satisfied at the plate then the resultant particle velocity in the sound waves at the plate (i.e. at $y=0$) must equal the plate velocity. Now the particle velocity in the sound wave is obtained from the equation of motion of the medium.

$$-\frac{\partial p}{\partial y} = \rho \ddot{\xi} \qquad (2.3)$$

where ξ is the particle displacement. For simple harmonic motion particle velocity V is given by

$$\frac{\partial \xi}{\partial t} = V = -\frac{1}{i\omega\rho}\frac{\partial p}{\partial y} \qquad (2.4)$$

If x is the plate displacement then the boundary condition is

$$-\frac{1}{i\omega\rho}\left(\frac{i\omega}{c}\right)p_{r_1} = -\frac{1}{i\omega\rho}\left(-\frac{i\omega}{c}\right)p_{r_2} = \dot{x} \qquad (2.5)$$

$$\therefore \; -p_{r_1} = p_{r_2} = \rho c\dot{x} \qquad (2.6)$$

The equation of motion of the plate can now be written

$$m\ddot{x} + Sx = F(t) + p_{r_1} - p_{r_2}$$
$$= F(t) - 2p_{r_2}$$

Hence $$m\ddot{x} + 2\rho c\dot{x} + Sx = F(t) \qquad (2.7)$$

This is the equation of motion of the plate taking into account the presence of the surrounding fluid. It is seen at once that there is a "viscous" damping term in the equation. Physically this damping arises from a loss of energy from the vibrating plate due to the radiation of the plane sound waves p_{r_1} and p_{r_2}. Fig. (2) shows the effect of this acoustic damping on the response of a plate with natural frequency $\sqrt{\frac{S}{m}} = 560$ c/s.

2.3

In the problem of the response of an aircraft fuselage to sound waves interest is centred on two aspects; the response of the structure and the transmission of the sound waves to the interior. An extension of the problem in the above section to include the effect of an "interior" should therefore provide an introduction to the more complicated problem.

This problem is the same as in (2.2) but with a rigid wall infinite in extent placed at $y=d$ (see Fig.3). There is now a reflected wave from the wall P_{r_3} and an additional boundary condition at the wall $(y=d)$ where the resultant particle velocity of the incident and reflected waves P_{r_2} and P_{r_3} must be zero. All the sound waves are plane and P_{r_1}, P_{r_2} are as before and P_{r_3} may be written.

$$P_{r_3} = A_3 \exp\left[i\omega t + \frac{i\omega y}{c}\right] \tag{2.8}$$

The boundary conditions are

$$\frac{\partial}{\partial y}\left(P_{r_3} + P_{r_2}\right)_{y=d} = 0 \tag{2.9}$$

$$-\frac{1}{i\omega\rho}\left(\frac{\partial P_{r_1}}{\partial y}\right)_{y=0} = -\frac{1}{i\omega\rho}\frac{\partial}{\partial y}\left(P_{r_3} + P_{r_2}\right)_{y=0} = \dot{x} \tag{2.10}$$

The first of these gives

$$A_3 = A_2 \exp\left[-\frac{2i\omega d}{c}\right] \tag{2.11}$$

and the second

$$A_1 = A_3 - A_2 = \frac{\rho c \dot{x}}{\exp i\omega t} \tag{2.12}$$

The equation of motion of the plate is

$$\begin{aligned} m\ddot{x} + Sx &= F(t) + P_{r_2} + P_{r_3} - P_{r_1} \\ &= F(t) + \exp[i\omega t]\{A_2 + A_3 - A_1\} \\ &= F(t) + \rho c \dot{x}\left(i \cot\frac{\omega d}{c} - 1\right) \end{aligned}$$

$$\therefore\ m\ddot{x} + \rho c\left(1 - i\cot\frac{\omega d}{c}\right)\dot{x} + Sx = F(t) \tag{2.13}$$

Comparing this equation with equation 2.7 it is seen that the damping term is halved, this is because the plate now radiates sound energy from one side only. An additional complex term has also appeared

in the coefficient of $\dot{x}$ this arises from the combination of the sound waves p_{r_2} and p_{r_3} in the cavity.

The solution of 2.13 for the amplitude of the plate motion is

$$|x| = \frac{|F(t)|}{\sqrt{\left\{(S - m\omega^2)^2 + \rho c \cot\frac{\omega d}{c}\right\}^2 + \rho^2 c^2 \omega^2}} \qquad (2.14)$$

Resonances occur when

$$-(S - m\omega^2) = \rho c \omega \cot\frac{\omega d}{c} \qquad (2.15)$$

and the amplitude at such a resonance is limited by the acoustic damping ρc.

Examination of (2.15) shows that since $\cot\frac{\omega d}{c}$ is a cyclic function there are an infinite number of resonant frequencies of the system. This is due to the coupling of the fluid in the cavity to the plate. Fig.4 illustrates the effect where $-(S-m\omega^2)$ and $\rho c \omega \cot\frac{\omega d}{c}$ are plotted against frequency. Also there are frequencies of anti-resonance, that is no motion of the plate; these occur when

$$\cot\frac{\omega d}{c} \to \infty$$

$$\text{ie. } \frac{\omega d}{c} = \pi, 2\pi, \ldots\ldots$$

These correspond to the points A, B, C etc. in Fig.4.

Fig. 5 shows response curves for a plate with a natural fequency at 560 c/s with and without a cavity behind the plate; ω has been chosen such that an antiresonance occurs at 560 c/s.

The physical explanation of this problem lies in the fact that at the frequency corresponding to

$$\cot\frac{\omega d}{c} = \infty$$

the incident, transmitted and reflected sound waves combine to form a

standing wave system with the plate situated at a point of zero pressure gradient, hence the plate has no net exciting force.

A physical explanation using an electrical analogue is given in Ref. 1.

2.4

The results in the previous two sections give the response of a very simple structure to sound waves and show the reaction effects of the acoustic medium on the structure. They are such as to provide a damping to the structure and also a reactance effect (following electrical terminology) which alters the resonant properties of the system as a whole. Further it is possible to compute the value of the sound field within the cavity and thus assess the transmitting properties of this simple structure. From the first problem (without the cavity) the 'mass law' for sound transmission can be derived. The usual situation in 'building acoustics' is that the mass of the structure is large and the stiffness low so that the resonant frequency is low. Therefore, above resonance the wall displacement, and hence the sound transmission, is governed by the $m\ddot{x}$ term in (2.7) and m is the controlling factor. In an aircraft structure resonances occur throughout the audible range and the mass law is no longer valid.

Whilst the above treatments have been idealistic they do reveal the salient points of the problem of a stiffened cylinder which is excited by a sound field; it is this problem which forms the subject of the following chapter.

CHAPTER 3

The Vibrations of a stiffened thin-walled cylinder in an Acoustic Field - No axial modes.

3.1

When a cylindrical structure is in vibration under the action of some forcing function the actual displacement of the structure at a given point is the sum of many separate displacement modes (Ref. 2) of differing amplitude and phase. Hence in order to find the dynamic displacement of a given cylindrical structure it is necessary to find the displacements in all the modes, and sum their effect. For a finite length cylinder each mode takes the form of a certain number of sinusoidal waves round the circumference combined with a number of waves along the length; hence many mode combinations must be investigated. If the problem is restricted to waves in the circumferential direction only with no modes in the axial direction, the problem is considerably simplified and may be considered a special case of the complete problem.

The restricted two-dimensional problem to be dealt with is the response of an infinitely long thin-walled cylinder with periodic frame stiffening to a plane-wave acoustic field; the wave fronts are in a plane which is parallel to the plane formed by the cylinder axis and a cylinder generator.

The method is the same as that used by Junger, that is, the displacements in the radial and circumferential directions are represented by Fourier series each term corresponding to a mode of deformation and

the coefficients to the generalised Lagrangian co-ordinates. The total strain (potential) energies S_t and kinetic energies T_t for the shell and stiffening members may be written in terms of the generalised co-ordinates; these have been developed for stiffened cylinders by Miller (Ref. 4) who has extended the work on uniform shells (Ref. 5, 6).

The Lagrangian equation is used, viz:-

$$\frac{d}{dt}\left(\frac{\partial T_t}{\partial \dot{q}_n}\right) + \frac{\partial S_t}{\partial q_n} = Q_n$$ the generalised force.

The following work extends that of Junger by including the internal field effects and directing the calculation to the solution for the internal sound field besides the modal responses. The generalised force is developed for a general type of simply harmonic pressure field and is then specialised to a plane sound wave.

3.2 The Acoustic Fields.

Consider a cylinder radius a, centre O the origin of co-ordinates r, ϕ, (Fig. 6). The radial and tangential linear displacements are denoted by w, v, respectively with

$$w = \sum_0^n a_r \cos r\phi + b_r \sin r\phi$$

$$v = \sum_0^n c_r \sin r\phi + d_r \cos r\phi \qquad (3.1)$$

The r^{th} term of these Fourier series represents the dynamic deflection in the r^{th} mode. The coefficients, which are functions of time only, and in general are complex, are the generalised co-ordinates whose values are required.

The cylinder is excited by an incident acoustic field $p_0(r, \phi, t)$. On incidence there is a scattering of sound about the cylinder and a

transmission to the interior; these two fields are denoted by $p_s(r,\phi,t)$, $p_i(r,\phi,t)$. The scattered and incident pressure fields combine linearly (since the linear wave equation will be assumed) to the pressure at a point r,ϕ as :-

$$p(r,\phi,t) = p_0 + p_s \qquad r > a \qquad (3.2)$$

$$p(r,\phi,t) = p_i \qquad r < a \qquad (3.3)$$

These are acoustic fluctuations and for not too intense sound fields the linear wave equation may be assumed viz :-

$$\nabla^2 p = \frac{1}{c^2}\frac{\partial^2 p}{\partial t^2} \qquad (3.4)$$

The general solution of this equation is, in polar co-ordinates

$$p = \begin{Bmatrix} \cos n\phi \\ \sin n\phi \end{Bmatrix} \begin{Bmatrix} J_n(kr) \\ Y_n(kr) \end{Bmatrix} \exp[i\omega t] \qquad (3.5)$$

where $k = \frac{\omega}{c}$; J_n, Y_n, are the solutions of Bessel's equation and p is exactly determined by the boundary conditions.

Consider, in turn, the acoustic fields.

3.2.1 The Incident Field.

In practical aircraft situations the incident acoustic field will be either a noise field arising from boundary layer turbulence or the jet efflux, or a complicated non-random field from aircraft propellers. The mathematical representation of these fields is outside the scope of this work although it is possible to proceed for the non-random fields.

For the present purpose a plane sound wave field is chosen which is defined (using the co-ordinate system of Fig. 6) by

$$p_0 = P_0 \exp[ik(x+ct)] = P_0 \exp[ik(r\cos\phi + ct)]$$

$$= P_0 \sum_{1}^{\infty} (J_0(kr) + 2(i)^n J_n(kr)\cos n\phi) \exp[i\omega t] \qquad (3.6)$$

3.2.2 The Scattered Field

The scattered field is defined, through the boundary conditions, by the geometry of the shell and its dynamic deflection.

The boundary conditions to be satisfied are :-

(1) The particle velocity of the scattered plus incident fields at the surface of the cylinder ($r=a$) must equal the velocity of the surface $\dot{w}$.

(2) At infinity the scattered wave must have the form of a diverging wave. (The Sommerfeld radiation condition).

Condition (2) is satisfied by the solution of the wave equation (3.5).

$$p_s = \sum_0^\infty (A_n \cos n\phi + B_n \sin n\phi) H_n^{(2)}(kr) \exp[i\omega t] \qquad (3.7)$$

where $H_n^{(2)}(kr)$ is the Hankel function $= J_n - iY_n$ and

$\lim_{r\to\infty} H_n^{(2)}(kr) \exp[i\omega t] = \sqrt{\frac{2}{\pi kr}} \exp\left[-ik\left(r - \frac{g}{k} - ct\right)\right]$ which has the form of a diverging wave.

Condition (1) determines the constants A_n, B_n in equation (3.7).

3.2.3 The Internal Field

Again the internal field is defined by the shell geometry and its dynamic deflection.

The boundary conditions in this case are :-

(1) The particle velocity in the internal field at the cylinder surface ($r=a$) must equal the velocity of the surface.

(2) At the origin ($r=0$) the pressure must be finite.

Condition (2) leads to the rejection from the solution (3.5) of the function $Y_n(kr)$ which is infinite at $r=0$. This means that the

wave system within the cylinder is stationary.

The solution is therefore :-

$$p_i = \sum_0^\infty (C_n \cos n\phi + D_n \sin n\phi) J_n(kr) \exp[i\omega t] \quad (3.8)$$

where C_n and D_n are determined by condition (1).

3.3 The generalised forces

The generalised force Q_n is defined in the Lagrangian equations as

$$Q_n = \frac{\partial W}{\partial q_n} \quad (3.9)$$

Where W is the work done through the displacement of the loading. The loading/unit/area arises from the acoustic pressures and is, in the radially outward direction

$$[p_i - (p_o + p_s)]_{r=a} \quad (3.10)$$

The forces acting in the tagential (v) direction are viscous forces which are very small compared with the acoustic normal forces, therefore the generalised forces in the C_n and d_n direction are neglected.

Now

$$\delta W = \int_0^{2\pi} (\delta a_r \cos r\phi + \delta b_r \sin r\phi)[p_i - (p_o+p_s)]_{r=a} a\, d\phi \quad (3.11)$$

Two points were raised by Kafka (Ref. 33) in connection with this equation who suggests that in the particular case of a radially uniform pressure field the work δW vanishes. This is true for all the non-zero modes but not true for the radial mode $n=0$. Since, from equation 3.1 there is always an even number of half-waves round the circumference for $n \neq 0$, the work done must always be zero except in the radial displacement mode. The second point deals with the volume displacement under the loading. The work done is quoted as $\int_0^{2\pi} p\,dV$ where in equation 3.11 $dV = \delta a_n a\, d\phi$

A more accurate expression for dV is given involving second order terms in products of the small displacements. It should therefore be noted that equation 3.11 represents the normal linear approximation usually found to be adequate in problems of small vibrations.

The generalised forces per unit length are

$$Q_{ar} = \frac{\delta W}{\delta a_r} = a\int_0^{2\pi}\left[p_i - (p_0+p_s)\right]_{r=a}\cos r\phi\, d\phi \qquad (3.12)$$

$$Q_{br} = \frac{\delta W}{\delta b_r} = a\int_0^{2\pi}\left[p_i - (p_0+p_s)\right]_{r=a}\sin r\phi\, d\phi \qquad (3.13)$$

on substituting for p_i and p_s from equations (3.7) these become

$$Q_{an} = \frac{2a}{\epsilon_n}\left[\pi C_n J_n(ka) - \int_0^{2\pi} p_0\Big|_{r=a}\cos n\phi\, d\phi - \pi A_n H_n^{(2)}(ka)\right]\exp[i\omega t] \qquad (3.14)$$

$$Q_{bn} = \frac{2a}{\epsilon_n}\left[\pi D_n J_n(ka) - \int_0^{2\pi} p_0\Big|_{r=a}\sin n\phi\, d\phi - \pi B_n H_n^{(2)}(ka)\right]\exp[i\omega t] \qquad (3.15)$$

and A_n, B_n, C_n, D_n are found from the boundary condition that the particle velocity and cylinder surface velocity be equal at $r=a$. The particle velocity($\dot{w}$) in a sound wave is given by the equation of motion :-

$$-\frac{\partial p}{\partial r} = \rho\frac{\partial \dot{w}}{\partial t} \qquad (3.16)$$

which for $w = f(r,\phi)\exp[i\omega t]$ gives

$$\dot{w} = -\frac{1}{i\omega\rho}\frac{\partial p}{\partial r} \qquad (3.17)$$

Application of the boundary condition gives

$$\dot{w} = \sum_0^\infty \dot{a}_r\cos r\phi + \dot{b}_r\sin r\phi = -\frac{1}{i\omega\rho}\frac{\partial}{\partial r}\left[p_i\right]_{r=a}$$

$$= -\frac{1}{i\omega\rho}\frac{\partial}{\partial r}\left[p_0+p_s\right]_{r=a}$$

whence

$$A_n = \frac{-1}{\exp[i\omega t]\, H_n'^{(2)}(ka)}\left[\dot{a}_n\, i\rho c + \frac{c}{\pi\omega}\int_0^{2\pi}\left[\frac{\partial p_0}{\partial r}\right]_{r=a}\cos n\phi\, d\phi\right] \qquad (3.18)$$

$$B_n = \frac{-1}{\exp[i\omega t]} \frac{1}{H_n^{(2)\prime}(ka)} \left[b_n i\varrho c + \frac{c}{\pi\omega} \int_0^{2\pi} \frac{\partial p_0}{\partial r}\Big|_{r=a} \sin n\phi \, d\phi \right] \tag{3.19}$$

$$C_n = -\frac{i\varrho c}{\exp[i\omega t]} \frac{\dot{a}_n}{J_n'(ka)} \tag{3.20}$$

$$D_n = \frac{-i\varrho c}{\exp[i\omega t]} \frac{\dot{b}_n}{J_n'(ka)} \tag{3.21}$$

Finally, on substituting these coefficients in equation (3.14) and (3.15), the generalised forces are found to be

$$Q_{an} = -i\pi a \varrho c \frac{2}{\epsilon_n} \left[\frac{J_n}{J_n'} - \frac{H_n^{(2)}(ka)}{H_n^{(2)\prime}(ka)} \right] \dot{a}_n + F_n(t) \tag{3.22}$$

$$Q_{bn} = -i\pi a \varrho c \frac{2}{\epsilon_n} \left[\frac{J_n}{J_n'} - \frac{H_n^{(2)}(ka)}{H_n^{(2)\prime}(ka)} \right] \dot{b}_n + G_n(t) \tag{3.23}$$

where

$$F_n(t) = -\frac{a}{\epsilon_n} 2 \int_0^{2\pi} p_0|_{r=a} \cos n\phi \, d\phi + \frac{H_n^{(2)}(ka)}{H_n^{(2)\prime}(ka)} \frac{ac}{\omega} \int_0^{2\pi} \frac{\partial p_0}{\partial r}\Big|_{r=a} \cos n\phi \, d\phi$$

$$G_n(t) = -\frac{a}{\epsilon_n} 2 \int_0^{2\pi} p_0|_{r=a} \sin n\phi \, d\phi + \frac{H_n^{(2)}(ka)}{H_n^{(2)\prime}(ka)} \frac{ac}{\omega} \int_0^{2\pi} \frac{\partial p_0}{\partial r}\Big|_{r=a} \sin n\phi \, d\phi$$

The first terms in (3.22) and (3.23) can be written in a more convenient form by making use of the following properties of the Bessel functions

$$H_n^{(2)}(x) = J_n(x) - i Y_n(x)$$

$$J_n Y_n' - J_n' Y_n = \frac{2}{\pi x}$$

whence

$$Q_{an} = -[R_A + i X_A] \dot{a}_n + F_n(t) \tag{3.24}$$

$$Q_{bn} = -[R_A + i X_A] \dot{b}_n + G_n(t) \tag{3.25}$$

where

$$R_A = \frac{2\varrho c}{k} \cdot \frac{2}{\epsilon_n} \cdot \frac{1}{J_n'^2 + Y_n'^2}$$

$$X_A = \frac{1}{J_n'} \frac{Y_n'}{J_n'^2 + Y_n'^2} \cdot \frac{2\varrho c}{k} \cdot \frac{2}{\epsilon_n}$$

R_A and X_A are the acoustic radiation and reaction terms and are analogous to the coefficients of $\ddot{x}$ in equation (2.13).
R_A represents the acoustic damping of the structure due to radiation of sound energy away from the system. X_A is the reactance, $R_A + iX_A$ together represent the acoustic impedance of the system at $r=a$.

3.4.1 The Lagrange equations

If the potential (strain) and kinetic energies of the cylinder are known in mode r , together with the generalised forces in that mode then by means of the Lagrange equation the differential equations for the generalised co-ordinates a_r , b_r , c_r , d_r , can be written; the equations can then be solved giving the displacements in mode r . These displacements can then be summed over the n modes to give the total displacements w and v .

Expressions for the ptential and kinetic energies of a uniform cylinder (no stiffening) are given by Warburton and Arnold (Ref. 5) who used expressions derived by Love (Ref. 6) for the stresses in a shell element. A full discussion of the derivation of these formulae and the validity of the assumptions involved is given by Miller (Ref. 4). Miller also derives more exact expressions and extends the analysis to include the effect of stiffening by frames and longerons. In the present calculation the more approximate expressions of Ref. 6 are used and extended to include frame stiffening.

3.4.2 The Structural Energies

Using the co-ordinate system defined by Fig. 6 the strain energy in two dimensions (that is no axial modes) is for the uniform shell.

S_s strain energy/unit length

$$= \frac{E}{2(1-\nu^2)} \int_0^{2\pi} \int_{-h/2}^{h/2} \left[\frac{1}{a}(V_\phi + W) - \frac{z}{a^2}(V_\phi - W_{\phi\phi}) \right]^2 d\phi\, dz \qquad (3.26)$$

where E = Young's Modulus

ν = Poisson's ratio

h = cylinder wall thickness (note:- origin of co-ordinates (V,W) is shell middle surface)

The kinetic energy is approximately

T_s = kinetic energy/unit length

$$= \frac{\rho_s}{2} \int_0^{2\pi} \int_{-h/2}^{h/2} (\dot{V}^2 + \dot{W}^2)\, a\, d\phi\, dz \qquad (3.27)$$

where ρ_s = shell density and a dot denotes differentiation w.r.t time.

Substituting for W and V (3.1) in (3.26) and (3.2), and integrating:-

$$S_s = \frac{1}{\epsilon_n}\left(\frac{h}{a}\right)\frac{E\pi}{(1-\nu^2)} \left[(a_n + nc_n)^2 + (b_n - nd_n)^2 + n^2\beta\{(c_n + na_n)^2 + (nb_n - d_n)^2\} \right] \qquad (3.28)$$

with $\beta = \frac{1}{12}\left(\frac{h}{a}\right)^2$

and $$T_s = \frac{1}{\epsilon_n} \pi \rho_s a h \left[\dot{a}_n^2 + \dot{b}_n^2 + \dot{c}_n^2 + \dot{d}_n^2 \right] \qquad (3.29)$$

In this two dimensional problem the shell is stiffened by frames only. This was done to ease desk computation of results; the added complication of longeron stiffening not being thought worthwhile. To calculate the additional terms in S and T arising from frame stiffening the integrals (3.26) and (3.27) are used but the Z-integration now extends over the depth of the frame. Provided that the ratio frame depth/cylinder radius is small, it was felt that the approximations would be satisfactory. Since there are no modes in the axial direction in this calculation, it is assumed that the 'frame energies' are distributed uniformly along the length of the cylinder.

If d is the frame spacing then from (3.26)

$$S_F = \frac{Ea}{2(1-\nu^2)} \frac{1}{d} \int_0^{2\pi} \int_{depth} b_F \left[\frac{V\phi}{a} + \frac{W}{a} + \frac{2W\phi\phi}{a^2} \right]^2 d\phi\, dz \qquad (3.30)$$

where b_F is the width of the frame (a function of z) and the term $\frac{V\phi}{a^2}$ is neglected in comparison with $\frac{V\phi}{a}$.

Substituting for (W,V) and integrating

$$S_F = \frac{2}{\epsilon_n} \frac{E\pi}{(1-\nu^2)} \left[\frac{A_F}{2ad} n^2 (c_n^2 + d_n^2) + (a_n^2 + b_n^2) \left(\frac{A_F}{2ad} + \frac{n^4 I_F}{2a^3 d} - \frac{n^2 A_F z_F}{a^2 d} \right) + n(a_n c_n - b_n d_n) \frac{A_F}{ad} \left(1 - \frac{z_F n^2}{a} \right) \right] \qquad (3.31)$$

where $A_F = \int_{depth} b_F\, dz$ — frame area

$A_F z_F = \int z b_F\, dz$ — z_F = distance of centre of frame area from skin.

$I_F = \int z^2 b_F\, dz$ — second moment of frame area about skin

The kinetic energy is given by (3.27) with the z-limits changed :-

$$T_F = \frac{2}{\epsilon_n} \frac{\pi \rho_F A_F a}{2d} \left[\dot{a}_n^2 + \dot{b}_n^2 + \dot{c}_n^2 + \dot{d}_n^2 \right] \qquad (3.32)$$

3.4.3 The equations of motion

Having found the generalised forces and the potential and kinetic energies of the shell the Lagrange equations

$$\frac{d}{dt} \left[\frac{\partial}{\partial \dot{q}_n} (T_S + T_F) \right] + \frac{\partial}{\partial q_n} (S_S + S_F) = Q_n \qquad (3.33)$$

may be solved giving

$$\begin{aligned} A\ddot{a}_n + Ba_n + (R_A + iX_A)\dot{a}_n + Cc_n &= F_n(t) \\ A\ddot{b}_n + Bb_n + (R_A + iX_A)\dot{b}_n - Cd_n &= G_n(t) \\ A\ddot{c}_n + Dc_n + Ca_n &= 0 \\ A\ddot{d}_n + Dd_n + Cb_n &= 0 \end{aligned} \qquad (3.34)$$

where

$$A = \frac{2}{\epsilon_n}\rho_s a h\left[1 + \frac{A_F}{hd}\right]$$

$$B = \left(\frac{h}{a}\right)\frac{2}{\epsilon_n}\frac{E\pi}{(1-\sigma^2)}\left[1 + \beta n^4 + \frac{1}{hd}\left\{A_F + n^4\frac{I_F}{a^2} - 2n^2\frac{A_F Z_F}{a}\right\}\right]$$

$$C = n\left(\frac{h}{a}\right)\frac{2}{\epsilon_n}\frac{E\pi}{(1-\sigma^2)}\left[1 + \beta n^2 + \frac{A_F}{hd}\left(1 - n^2\frac{Z_F}{a}\right)\right]$$

$$D = n^2\left(\frac{h}{a}\right)\frac{2}{\epsilon_n}\frac{E\pi}{(1-\sigma^2)}\left[1 + \beta + \frac{A_F}{hd}\right]$$

The equations 3.34 can be solved when $F_n(t)$, $G_n(t)$ are known; for a simple harmonic exciting field

$$F_n(t) = F_n \exp[i\omega t]$$

$$G_n(t) = G_n \exp[i\omega t]$$

putting

$$a_n(t) = a_n \exp[i\omega t]$$

then

$$a_n = \frac{F_n}{(X_M - \omega X_A) + i\omega R_A}$$

$$b_n = \frac{G_n}{(X_M - \omega X_A) + i\omega R_A} \qquad (3.35)$$

$$c_n = \frac{C}{A\omega^2 - D}\, a_n$$

$$d_n = \frac{-C}{A\omega^2 - D}\, b_n$$

where

$$X_M = -A\omega^2 + B + \frac{C^2}{D - A\omega^2}$$

X_M is henceforth termed the mechanical reactance of the vibrating cylinder. In the absence of the acoustic reactance X_A resonance occurs when $X_M = 0$. It will be noticed that the coefficients B, C, D are functions of n, the mode number. Thus there is one X_M for each mode and the zeros give the resonant frequencies (in vacuo) of the cylinder in each mode. However, for vibration in an acoustic medium, it can be seen that the total reactance is $(X_M - \omega X_A)$ and that resonance occurs when this is zero.

Examination of X_A reveals that at the roots of $J_n'(\frac{\omega a}{c})$, X_A becomes infinite, thus there is an anti-resonance effect. If X_A becomes large close to a natural (in vacuo) frequency of the shell then the response curve in the given mode will be quite different to the in vacuo case.

The term $i\omega\rho_A$ represents the "acoustic Damping" of the cylinder i.e., the energy loss due to the radiation of sound by the surface; structural damping of course would have an additional effect on the motion.

3.5 The response of the cylinder to a simple harmonic Plane Wave.

In the preceding sections equations have been derived for the response of a cylinder to a general type of periodic incident field. To carry the work a stage further the computation was done for a particular plane wave incident sound field.

The pressure in a plane wave travelling in the negative x direction (Fig. 6) is expressed by

$$P_0 = P_0 \exp[ik(x+ct)]$$
$$= P_0 \exp[ik(r\cos\phi + ct)]$$

This can be written

$$P_0 = \left[P_0 J_0(kr) + 2\sum_1^\infty P_0 (i)^n J_n(kr)\cos n\phi\right]\exp[i\omega t] \quad (3.36)$$

in which the plane wave is now expressed as a sum of cylindrical waves.

Putting P_0 into (3.22) and (3.23)

$$F_n(t) = F_n \exp[i\omega t] = (i)^n \frac{4P_0\pi a}{\epsilon_n}\left[\frac{H_n^{(2)}(ka)}{H_n^{(2)}(ka)} J_n'(ka) - J_n(ka)\right]$$
$$G_n(t) = \alpha \quad (3.37)$$

Using this and from equation (3.34) the total radial displacement is given by

$$w = \sum_0^n |a_r| \exp[i(\omega t + \delta_r)]\cos r\phi \quad (3.38)$$

where

$$|a_r| = \frac{8 P_0 c}{\epsilon_r \omega} \frac{\left[J_r'^2 + Y_r'^2\right]^{-1/2}}{\left[(X_M - \omega X_A)^2 + \omega^2 R_A^2\right]^{1/2}}$$

$$|b_r| = 0 \qquad (3.39)$$

and

$$\delta_r = \left[\tan^{-1} \left\{ \frac{Y_r'}{J_r'} \frac{(X_M - \omega X_A) - R_A}{(X_M - \omega X_A) + \omega R_A \frac{Y_r'}{J_r'}} \right\} + 90(r+1) \right]^\circ$$

$$|b_r| = 0 \qquad (3.40)$$

The computation of $|a_r|$ has been carried out for the mode $n = 10$ for a frame stiffened cylinder details of which are given in appendix B.

The response curves are shown in Figs. 7 and 8.

3.5.1 Results

Fig. 7 shows the mechanical reactance X_M and the acoustical reactance X_A plotted to the same scale for the mode $n = 10$. From (3.39) it will be seen that resonance occurs when the frequency of the incident wave is such that

$$(X_M - \omega X_A) = 0$$

Therefore the intersections A, B, C... of X_M and ωX_A in Fig. 7 denote resonant points of the system. There are in fact an infinite number of resonant points since ωX_A has a quasi-periodic form and there are thus an infinity of intersections.

Fig. 8 shows the response curve for the mode $n=10$; the resonances A, B, C correspond to the intersections in Fig. 7. The dashed curve shows the response in the absence of acoustic effects (in vacuo).

Consider, now, these effects. Acoustic damping arises from the radiation of sound energy from the vibrating system which represents to the structure a damping of its motion; this damping is given by (3.24).

$$R_A = \frac{2\rho c}{k} \frac{2}{\epsilon_n} \left[J_n'^2 + Y_n'^2 \right]^{-1}$$

Thus from this expression the magnitude of the acoustic damping can be determined for any frequency and mode. Junger (Ref. 8) gives curves of R_A for $n=0\,(1)\,10$ plotted aginst $\frac{\omega a}{c}$.*

The acoustic reactance X_A is mainly responsible for the changes in the response curve from the 'in vacuo' condition (dashed curve). There are three consequences of the effect. Firstly, that whereas in the 'in vacuo' case there is <u>one</u> resonant frequency, in the present system there are many resonant frequencies; this is due to the coupling between the structural vibration and the wave motion within the cylinder. Secondly, there are points in the curve where the response is zero. These arise from standing wave modes which occur in the internal field. The frequency for a given mode n at which this <u>anti-resonance</u> occurs is determined by

---

* Whilst Junger's paper does not consider the transmitted interior field his function for R_A is identical with the result here since there is no energy loss in the internal field.

the roots of

$$J_n'\left(\frac{\omega a}{c}\right) = 0 \qquad \text{(see 3.25)}$$

Under certain conditions this gives rise to the third consequence when the 'in vacuo' resonant frequency of a particular mode lies close to the frequency of anti-resonance due to the internal field. In this case the response curve becomes very different from its shape when acoustic effects are ignored. This last point is well illustrated in Fig. 8.

A calculation was carried out to find the response in each of the first twenty modes to an incident plane wave of 160 db(rel. to 0.0002 dynes/cm^2) intensity and frequency of 577 c/s. These results are shown in Table 1. The total amplitude at $\phi = 0$ (summation (2.38)) is 20×10^{-3} inches. The predominant mode at this frequency is $n = 10$ with an amplitude of 26×10^{-3} inches.

3.6 The transmitted field within the cylinder.

From the expressions already derived it is possible to calculate the distribution of sound within the cylinder. Equation (3.8) gives the value of the interior sound field P_i where the coefficients C_n and D_n are given by (3.20) and (3.21). For the case of plane wave excitation

$$P_i = \sum_0^\infty -i\epsilon_n \frac{J_n(kr)}{J_n'(ka)} \cos n\phi \, a_n \qquad r \leq a \qquad (3.41)$$

Fig. 9 shows the sound pressure level along the $\phi = 0$ axis for an incident plane wave of 160db at 577 c/s; also plotted is the level due to the principal ($n = 10$) mode alone.

From (3.7) and (3.18) the external field pressure $p_0 + p_s$ may be computed. The expression for p_s contains two terms the second of which represents the scattering when the cylinder is rigid and the first the effect of the motion of the cylinder surface. Wiener (Ref. 9) shows the scattering from a rigid cylinder; for $ka > 10$ and $\phi = 0$ there is pressure doubling at the cylinder surface. Motion of the surface causes alleviation of 'pressure doubling' and in the example calculated there is a pressure increase of 5.8 db as opposed to 6 db in the rigid case.

3.7 Conclusion

The main points of the above analysis may be summarised :-

1) Assuming the linearity of the wave equation to hold, which is the case for not too-intense sound fields, then the reflected and transmitted fields can be considered independently of the incident field. This means that the acoustic damping and reactance are independent of the incident field and are inherent properties of the system. In the non-linear case the amplitude of the mode response is not directly proportional to the incident pressure; the independence noted above would not exist.

2) The method enables the response in any mode to be calculated for a given simple harmonic incident field.

3) The interior sound field at any point may be calculated.

4) The acoustic reactance term due to the interior field may modify considerably the 'in vacuo' response of the structure and therefore should be included in any calculations. In particular at frequencies

corresponding to the roots of

$$J_n'\left(\frac{\omega a}{c}\right) = 0$$

the response is zero for the mode considered; this is termed anti-resonance.

5) Close to and outside the cylinder the scattered field P_s causes an increase of sound pressure to a maximum of 6db.

The work in the following chapter extends the above analysis to include axial modes.

CHAPTER 4

The response of a cylinder stiffened with frames and longerons to an oblique plane sound wave.

4.1

The problem on cylinder vibration in the previous chapter was limited to modes round the cylinder; in practice the vibration will involve modes in the axial direction also. The approach to the problem is the same as before but gives much more complicated expressions and requires much computation. With the aid of the Pegasus digital computer, it has been possible to develope a programme to do the computations.

4.2

The problem analysed here is that of a cylinder - length $2L$, with 'heavy' frame stiffening in the middle and at each end which resists radial and circumferential motion but which is free in the axial direction - which is subjected to an oblique plane wave whose axis is at an angle θ to the cylinder axis. 'Light' frame and longeron stiffening is allowed between the 'heavy' frames. The system and co-ordinates are shown in Fig. 10. Again the Lagrange equation is used; the potential and strain energies are given by Miller (Ref. 4) and are included in Appendix A; the deflections of the cylinder surface are defined by

$$\text{axial deflection} = u = \sum_{0}^{\infty}\sum_{0}^{\infty} a_{mn} \cos n\phi \cos \frac{m\pi z}{L}$$

$$\text{circumferential deflection} = v = \sum_{0}^{\infty}\sum_{0}^{\infty} b_{mn} \sin n\phi \sin \frac{m\pi z}{L} \qquad (4.1)$$

radial deflection $= W = \sum_{0}^{\infty}\sum_{0}^{\infty} C_{mn} \sin n\phi \sin \frac{m\pi z}{L}$

It is assumed that the incident exciting field is symmetric on $\phi = 0$; this is not a limitation but merely makes for simplicity in this particular case.

To solve the Lagrange equation the generalised force is required in the u, v, w directions; in the u, v directions the only force acting are viscous ones which can be assumed small (for air) in comparison with the force in the radial (w) direction.

One important approximation is made in the analysis, this concerns the scattered field at the ends of the cylinder. The scattering of the incident field at the ends depends mainly on the shape of the ends, for example, the ends can be flat discs; cones, hemispheres, etc., or combinations of these. In all cases the analytical difficulties of coping with these would be great. The approximation made is therefore that the effect of the end scattering is small and may be ignored. It is felt that this will mean that results will not be reliable near the ends but that away from the ends errors will be small.

4.3.1 The Acoustic Field

There are three sound fields to be considered; the incident field denoted p_0 , the scattered field p_s and the transmitted interior field p_i. p_s and p_i must satisfy the wave equation

$$\nabla^2 p = \frac{1}{c^2} \frac{\partial^2 p}{\partial t^2}$$

the general solution of which is in cylindrical co-ordinates.

$$p = \sum_{s}\sum_{q} \begin{matrix} J_s(k_r) \\ Y_s(k_r) \end{matrix} \begin{matrix} \cos \\ \sin \end{matrix} (s\phi) \begin{matrix} \cos \\ \sin \end{matrix} (qz) \exp[i\omega t] \qquad (4.2)$$

with

$$k_m^2 = \left(\frac{\omega}{c}\right)^2 - q^2$$

P_i and P_s will be determined by the boundary conditions.

4.3.2 The Incident Field

The same remarks apply here as in section 3.2.1; the expression 3.6 however is modified - this will be treated later.

4.3.3 The Scattered Field

There are two boundary conditions to apply on (4.2)

1) at $r=a$ the particle velocity in the resultant sound field ($P_o + P_s$) must equal the surface velocity of the cylinder ($\dot{w}$).

2) the scattered wave must be outgoing.

Condition 2) is satisfied by the function

$$H_s^{(2)}(k_m r) = J_s - iY_s \qquad (4.3)$$

The first condition is written

$$\dot{w} = -\frac{1}{i\omega\rho}\left[\frac{\partial}{\partial r}(P_o + P_s)\right]_{r=a} \qquad (4.4)$$

therefore

$$\sum_0^\infty \sum_0^\infty \dot{c}_{mn} \cos n\phi \sin \frac{m\pi z}{L} = \frac{-k_m}{i\omega\rho} \sum_s \sum_q B_{sq} H_s'^{(2)}(k_m a) \begin{matrix}\cos\\ \sin\end{matrix}(s\phi) \begin{matrix}\cos\\ \sin\end{matrix}(qz) - \frac{1}{i\omega\rho}\left[\frac{\partial P_o}{\partial r}\right]_{r=a} \qquad (4.5)$$

from which it can be seen that

$$s \equiv n$$

$$q \equiv \frac{m\pi}{L}$$

Hence

$$L\pi \dot{c}_{mn} = -\frac{k_m L\pi}{i\omega\rho} B_{mn} H_n'^{(2)}(k_m a) \exp[i\omega t] - \frac{1}{i\omega\rho} \int_0^{2L} \int_0^{2\pi} \left[\frac{\partial P_o}{\partial r}\right]_{r=a} \cos n\phi \sin \frac{m\pi z}{L} \, d\phi \, dz \qquad (4.6)$$

then

$$B_{mn} = -\frac{i\omega\rho}{k_m}\frac{1}{H_n'^{(2)}(k_m a)}\frac{\dot{c}_{mn}}{\exp[i\omega t]} - \frac{1}{H_n'^{(2)}(k_m a)}\frac{1}{\exp[i\omega t]}\frac{1}{\pi k_m L} \times \int_0^{2L}\int_0^{2\pi}\left[\frac{\partial p_0}{\partial r}\right]_{r=a}\cos n\phi \sin\frac{m\pi z}{L}\, d\phi\, dz \qquad (4.7)$$

4.3.4 The Internal Field p_i

Two boundary conditions apply in (4.2) for the internal field.

1) at $r=a$ the particle velocity in p_i must equal the surface velocity of the cylinder ($\dot{w}$)

2) The pressure field must be finite.

Condition 2) leads to the rejection of the function $Y_s(k_m r)$ which $\to \infty$ as $r \to 0$.

Applying condition 1)

$$\sum\sum \dot{c}_{mn}\cos n\phi \sin\frac{m\pi z}{L} = \frac{-k_m}{i\omega\rho}\sum\sum A_{mn} J_n'(k_m a)\begin{matrix}\cos\\ \sin\end{matrix}(s\phi)\begin{matrix}\cos\\ \sin\end{matrix}(qz) \qquad (4.8)$$

from which

$$s \equiv n$$

$$q \equiv \frac{m\pi}{L}$$

Hence

$$A_{mn} = -\frac{i\omega\rho}{k_m}\frac{1}{J_n'(k_m a)}\frac{\dot{c}_{mn}}{\exp[i\omega t]} \qquad (4.9)$$

4.4 The generalised force.

The generalised force in the Lagrangian equations is defined as

$$Q_{mn} = \frac{\partial W}{\partial q_{mn}}$$

where W is the work done through the displacement of the loading. For

this problem the generalised force is required for the modes described by (4.1), therefore

$$\delta W = \int_0^{2\pi} a \int_0^{2L} \left[p_i - (p_0 + p_s) \right]_{r=a} \delta c_{mn} \cos n\phi \sin \frac{m\pi z}{L} \, d\phi \, dz \qquad (4.10)$$

then

$$Q_{mn} = \frac{\delta W}{\delta c_{mn}} = \int_0^{2\pi} a \int_0^{2L} \left[p_i - (p_0 + p_s) \right]_{r=a} \cos n\phi \sin \frac{m\pi z}{L} \, d\phi \, dz \qquad (4.11)$$

Using coefficients determined by the boundary conditions in the previous sections

$$Q_{mn} = \int_0^{2\pi} \int_0^{2L} \left[-\frac{i\omega\rho}{k_m J_n'(k_m a)} \dot{c}_{mn} J_n(k_m r) \cos n\phi \sin \frac{m\pi z}{L} \right.$$

$$- \left\{ p_0 + \left(-\frac{i\omega\rho}{k_m} \frac{1}{H_n'^{(2)}(k_m a)} \dot{c}_{mn} - \frac{1}{H_n'^{(2)}(k_m a)} \frac{1}{k_m \pi L} \int_0^{2\pi} \int_0^{2L} \left[\frac{\partial p_0}{\partial r} \right]_{r=a} \cos n\phi \sin \frac{m\pi z}{L} \, d\phi \, dz \right) \right.$$

$$\left. \left. \times \left(H_n^{(2)}(k_m r) \cos n\phi \sin \frac{m\pi z}{L} \right) \right\} \right]_{r=a} a \cos n\phi \sin \frac{m\pi z}{L} \, d\phi \, dz$$

$$= \frac{i\omega\rho a \dot{c}_{mn}}{k_m} \left[\frac{J_n(k_m a)}{J_n'(k_m a)} - \frac{H_n^{(2)}(k_m a)}{H_n'^{(2)}(k_m a)} \right] \pi L \qquad (4.12)$$

$$- \int_0^{2\pi} \int_0^{2L} p_0 a \cos n\phi \sin \frac{m\pi z}{L} \, d\phi \, dz + \frac{H_n^{(2)}(k_m a)}{H_n'^{(2)}(k_m a)} \frac{a^2}{k_m a} \int_0^{2\pi} \int_0^{2L} \left[\frac{\partial p_0}{\partial r} \right]_{r=a} \cos n\phi \sin \frac{m\pi z}{L} \, d\phi \, dz \qquad (4.13)$$

The first term of this expression for Q_{mn} contains $\dot{c}_{mn}$, the coefficient of $\dot{c}_{mn}$ represents the acoustic impedance of the system. The last two terms of (4.13) give that part of the generalised force due to the incident field p_0.

4.5 The Acoustic Impedance

The acoustic impedance is given by the coefficient of $\dot{c}_{mn}$ in 4.13 namely.

$$Z_A = \frac{-i\omega\rho a\pi L}{k_m}\left[\frac{J_n(k_m a)}{J_n'(k_m a)} - \frac{H_n^{(2)}(k_m a)}{H_n'^{(2)}(k_m a)}\right] \qquad (4.14)$$

There are two cases to consider according as k_m is real or imaginary -

$$k_m = \sqrt{\left(\frac{\omega}{c}\right)^2 - \left(\frac{m\pi}{L}\right)^2}$$

1) k_m real, $\frac{\omega}{c} > \frac{m\pi}{L}$

knowing that (Ref. 12)

$$J_n Y_n' - J_n' Y_n = \frac{2}{\pi x}$$

then

$$Z_A = -(R_A + iX_A)$$

where

$$R_A = \frac{2\omega\rho L}{k_m^2}\left[J_n'^2(k_m a) + Y_n'^2(k_m a)\right]^{-1} \qquad (4.15)$$

$$X_A = \frac{2\omega\rho L}{k_m^2}\frac{Y_n'(k_m a)}{J_n'(k_m a)}\left[J_n'^2(k_m a) + Y_n'^2(k_m a)\right]^{-1} \qquad (4.16)$$

R_A and X_A are the acoustic damping and acoustic reactance terms discussed in 3.5 and the same remarks apply.

2) k_m imaginary $\frac{\omega}{c} < \frac{m\pi}{L}$

The arguments of the Bessel functions are now imaginary; knowing that (Ref. 13)

$$I_n(x) = i^{-n} J_n(ix)$$

$$K_n(x) = \frac{\pi}{2}\exp\left[\frac{i\pi}{2}(n+1)\right] H_n^{(1)}(ix)$$

then

$$Z_A = -iX_A'$$

where

$$X_A' = \frac{\omega\rho a}{|k_m|}\left[\frac{I_n(|k_m|a)}{I_n'(|k_m|a)} + \frac{K_n(|k_m|a)}{K_n'(|k_m|a)}\right] \qquad (4.17)$$

I_n and K_n are the modified Bessel functions which are always real for real positive arguments; hence Z_A is purely reactive at frequencies below $\omega = \frac{m\pi c}{L}$. There is no radiation of sound away from the system and thus no accoustic damping; the physical interpretation of this cut-off effect is discussed by Junger (Ref. 8).

4.6 The generalised force for an oblique plane wave.

A problem of some interest is the excitation of the stiffened cylinder by an oblique plane wave, symmetrical on $\phi=0$ whose axis is inclined at angle θ to the cylinder axis (Fig. 10). The wave, with wave fronts perpendicular to the η axis is

$$p_0 = P_0 \exp\left[i(\omega t - k\eta)\right] \qquad (4.18)$$

now $x = r\cos\phi$

(Fig. 11) $\eta = z\cos\theta + x\sin\theta$

Hence

$$p_0 = P_0 \exp[i\omega t]\exp\left[-ik(z\cos\theta + r\cos\phi\sin\theta\right] \qquad (4.19)$$

$$= P_0 \exp[i\omega t]\exp[-ikz\cos\theta]\left[J_0(kr\sin\theta) + 2\sum_{1}^{\infty}(-i)^n J_n(kr\sin\theta)\cos n\phi\right] \qquad (4.20)$$

The generalised force is given by 4.13; the integral

$$\int_0^{2L} e^{-ikz\cos\theta} \sin\frac{m\pi z}{L}\, dz \qquad (4.21)$$

$$= \frac{\frac{m\pi}{L}}{\left(\frac{m\pi}{L}\right)^2 - k^2\cos^2\theta}\left[1 - e^{-i2kL\cos\theta}\right] \quad k\cos\theta \neq \frac{m\pi}{L} \qquad (4.22)$$

And the generalised force for this case of an oblique plane wave is

$$Q_{mn} = Z_A \dot{C}_{mn} - \frac{\frac{m\pi}{L}}{\left(\frac{m\pi}{L}\right)^2 - k^2\cos^2\theta}\left[1 - e^{-i2kL\cos\theta}\right] 2\pi a P_0 \exp[i\omega t] \times$$

$$(-i)^n\left[J_n(ka\sin\theta) - \frac{H_n^{(2)}(ka)}{H_n'^{(2)}(ka)}\frac{k\sin\theta}{k}J_n'(ka\sin\theta)\right] \qquad (4.23)$$

4.7 The Lagrangian equations and the solution.

The Lagrangian equation for the generalised co-ordinate q_r is

$$\frac{\partial}{\partial t}\left(\frac{\partial T_r}{\partial \dot{q}_r}\right) + \frac{\partial S_r}{\partial q_r} = Q_r \qquad (4.24)$$

where S_r and T_r are the total potential and kinetic energies of the vibrating system in terms of the generalised co-ordinates which in this case are a_{mn}, b_{mn}, C_{mn}. Expressions for these are given in Appendix A whence using these and equation 4.24 the following set of differential equations are obtained (using the notation of Appendix A).

$$\begin{aligned} H\ddot{a}_{mn} + A a_{mn} - B b_{mn} - J\ddot{c}_{mn} - C c_{mn} &= 0 \\ -B a_{mn} + M\ddot{b}_{mn} + D b_{mn} + N\ddot{c}_{mn} + E c_{mn} &= 0 \\ -J\ddot{a}_{mn} + N\ddot{b}_{mn} - G a_{mn} + E b_{mn} + Q\ddot{c}_{mn} + F c_{mn} &= Q_{mn} \end{aligned} \qquad (4.25)$$

Since the solution will be periodic in time t, then

$$a_{mn} = \bar{a}_{mn}\exp[i\omega t] \quad \text{etc.}$$

and putting this into 4.25

$$(A-\omega^2H)\bar{a}_{mn} + (-B)\bar{b}_{mn} + (\omega^2J-C)\bar{c}_{mn} = 0$$

$$(-B)\bar{a}_{mn} + (D-\omega^2M)\bar{b}_{mn} + (E-\omega^2N)\bar{c}_{mn} = 0$$

$$(\omega^2J-G)\bar{a}_{mn} + (E-\omega^2N)\bar{b}_{mn} + (F-\omega^2Q-i\omega Z_A)\bar{c}_{mn} = \{Q_{mn}\}_{P_0} \qquad (4.26)$$

where $\{Q_{mn}\}_{P_0}$ is that part of the generalised force due to the incident field. From the first two of the above $\bar{a}_{mn}$ and $\bar{b}_{mn}$ can be expressed in terms of $\bar{c}_{mn}$ and using these in the third equation the solution for $\bar{c}_{mn}$ is obtained -

$$\bar{c}_{mn} = \frac{\{Q_{mn}\}_{P_0}}{(X_n-\omega X_A)+i\omega R_A} \qquad (4.27)$$

where

$$X_n = \frac{\left\{\begin{array}{l}(\omega^2J-G)\left[(\omega^2J-C)(D-\omega^2M)+B(E-\omega^2N)\right] \\ +(E-\omega^2N)\left[(D-\omega^2M)(E-\omega^2N)+B(\omega^2J-C)\right]\end{array}\right\}+(F-\omega^2Q)}{B^2-(A-\omega^2H)(D-\omega^2M)} \qquad (4.28)$$

X_n is dependent on the structural properties, the frequency and the particular mode mn; it can be considered as the mechanical impedance.

From (4.23) and (4.27)

$$\bar{c}_{mn} = \left[(X_n-\omega X_A)-i\omega R_A\right]\frac{m\pi}{L}\left[1-e^{-i2Lk\cos\theta}\right]\exp[i\omega t]\times$$

$$\frac{\left[2\pi a P_0(-i)^n\left\{J_n(ka\sin\theta)-\frac{H_n^{(2)}(k_m a)}{H_n'^{(2)}(k_m a)}\frac{k\sin\theta}{k_m}J_n'(ka\sin\theta)\right\}\right]}{\left(\frac{m\pi}{L}\right)^2-k^2\cos^2\theta} \qquad (4.29)$$

$$(X_n-\omega X_A)^2+\omega^2R_A^2$$

4.8 Computation and results.

The numerical computation of the above expression for the displacement in the mn^{th} mode is clearly unmanageable other than by automatic computation.

A programme for computing $\bar{c}_{mn}$, has been developed for the Ferranti

"Pegasus" computer and details are contained in Appendix C.

A stiffened cylinder was chosen having the following dimensions:-

radius = 5 ft. skin thickness = 0.048"

length (2L) = 40 ft. frame spacing = 20"

longeron spacing = $\frac{\pi'}{4}$ (40 longerons)

The frame and stiffener geometry is shown in Fig. 11., the frames and stiffeners being rigidly attached to the skin.

The response to a plane wave at several angles of incidence was computed for a frequency of 240 c/s. The programme is arranged so that the acoustic impedances R_A and X_A, the magnitude of the response in the mn^{th} mode $\bar{C}_{mn}$, and the phase angle ϵ_{mn}, are calculated. Table 2 shows the amplitudes in the first one hundred modes for angles of plane wave incidence θ. Fig. 15 shows the amplitudes against θ for the more important modes. It will be noticed that the curves peak quite sharply indicating an angle of maximum acceptance (or generalised force). At this frequency (240 c/s) it is the modes $n=3-6$ coupled with $m=3-6$ that are predominant. At the higher values of n and m the amplitudes become extremely small, indicating that 'panel' modes are not important at this frequency.

It was unfortunately not possible to investigate the modal characteristics at other frequencies but it is felt that such work would yield interesting information. At higher frequencies it is possible that the higher mode numbers will be excited. For propeller noise calculations interest is centred in the low frequency region where the incident pressures are largest but other types of excitation, for example boundary layer fluctua-

tions, the high frequency region is probably equally or more important.

The above calculation can be used to investigate the effect of varying the structural parameters since these can be readily altered in the programme.

A discussion of the limitations of the above theory and possible extensions is deferred until Chapter 7.

CHAPTER 5

The phasing of aircraft propellers - a simple mathematical model.

5.1

The phasing of aircraft propellers is best described by the following diagram -

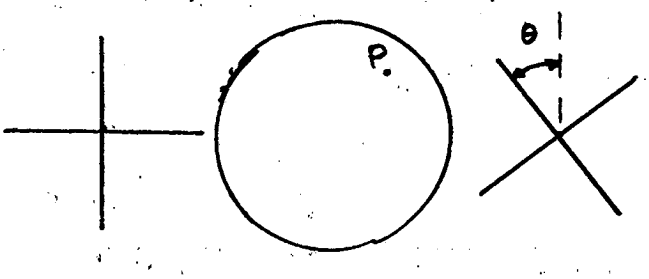

The propellers A and B rotate at the same speed but have a phase angle difference θ as shown. It is clear that the relative phase between similar components of the field from each propeller at a typical point P in the fuselage will depend, among other things, on θ. It is not the purpose here to determine this dependence on θ since this is a problem in propeller noise theory. But, by taking two oppositely running plane waves with phase angle ϵ between them; to find the sound pressure level at a general point P.

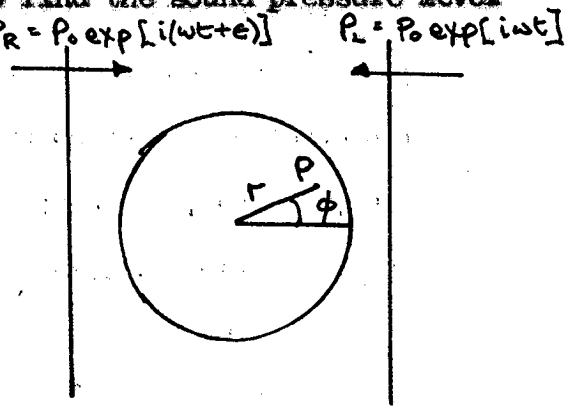

5.2

Consider the plane waves, P_L, P_R of equal amplitude P_0 and frequency ω but with a phase difference ϵ, impinging from opposite sides onto the fuselage structure. An expression is formulated for the sound pressure at a point P inside the fuselage and then minimised with respect to ϵ to find the condition on ϵ. The two-dimensional theory of Chapter 3 is used

here although the problem could be solved for the three dimensional case but with more complicated expressions.

The general expression for the internal sound field at point P (r, ϕ) is given by (Eq. 3.8) -

$$p_i = \sum_0^\infty (C_n \cos n\phi + D_n \sin n\phi) J_n(kr) \exp[i\omega t] \tag{5.1}$$

The incident plane waves p_R and p_L are symmetrical on the $\phi = 0$ axis therefore the whole system has symmetry and 5.1 becomes

$$p_i = \sum_0^\infty C_n \cos n\phi \, J_n(kr) \exp[i\omega t] \tag{5.2}$$

The coefficient C_n is (Eq. 3.20)

$$C_n = \frac{-i\rho c \dot{a}_n}{\exp[i\omega t] J_n'(ka)} \tag{5.3}$$

where $\dot{a}_n$ is the velocity amplitude in the n^{th} radial mode of vibration. Hence from 5.1 and 5.3

$$p_i = -i\rho c \sum_0^\infty \dot{a}_n \frac{J_n(kr)}{J_n'(ka)} \cos n\phi \tag{5.4}$$

The radial velocities of the surface in each mode due to the incident fields p_L and p_R are therefore required, a_n is given by (Eq. 3.35)

$$a_n = \frac{F_n}{(X_M - \omega X_A) + i\omega R_A} \tag{5.5}$$

where F_n is the generalised force in the n^{th} mode; this generalised force will consist of two parts arising from the two opposite running plane waves.

From 3.6 a left running plane wave can be written

$$p_L = p_0 \left[J_0(kr) + 2 \sum_1^\infty (i)^n J_n(kr) \cos n\phi \right] \exp[i\omega t] \tag{5.6}$$

and a right running wave with phase angle ϵ w.r.t p_L is

$$p_R = p_0 \left[J_0(kr) + 2 \sum_1^{\infty} (-i)^n J_n(kr) \cos n\phi \right] \exp[i\omega t] \exp[i\epsilon] \quad (5.7)$$

The generalised force for the n^{th} mode is given by Eq. 3.37 which for p_L is

$$F_{nL} = \frac{4}{\epsilon_n} \left[\frac{H_n^{(2)}(ka)}{H_n'^{(2)}(ka)} J_n'(ka) - J_n(ka) \right] (i)^n p_0 \pi a \exp[i\omega t] \quad (5.8)$$

and for p_R

$$F_{nR} = \frac{4}{\epsilon_n} \left[\frac{H_n^{(2)}}{H_n'^{(2)}} J_n' - J_n \right] \left[(-i)^n p_0 \pi a \exp[i(\omega t + \epsilon)] \right] \quad (5.9)$$

therefore

$$\dot{a}_n = \frac{i\omega 4 p_0 \pi a}{\epsilon_n} \frac{\left[\frac{H_n^{(2)}}{H_n'^{(2)}} J_n' - J_n \right] \left[(i)^n + (-i)^n e^{i\epsilon} \right]}{(X_n - \omega X_A) + i\omega R_A} \exp[i\omega t] \quad (5.10)$$

and

$$p_i(r,\phi) = \exp[i\omega t] 2\omega \rho c p_0 \pi a \sum_0^{\infty} \frac{2}{\epsilon_n} \frac{J_n(kr)}{J_n'(ka)} \frac{\cos n\phi \left[\frac{H_n^{(2)}}{H_n'^{(2)}} J_n' - J_n \right] \left[(i)^n + (-i)^n e^{i\epsilon} \right]}{(X_n - \omega X_A) + i\omega R_A} \quad (5.11)$$

It is this which must be minimised w.r.t ϵ

Eq. 5.11 can be rewritten in the following form

$$p_i = -8 p_0 \rho c^2 \sum_0^{\infty} \frac{2}{\epsilon_n} \frac{J_n(kr)}{J_n'(ka)} \frac{\cos n\phi}{\sqrt{J_n'^2 + Y_n'^2}} \frac{\cos\left(\frac{n\pi}{2} - \frac{\epsilon}{2}\right)}{\left\{ (X_n - \omega X_A)^2 + \omega^2 R_A^2 \right\}^{1/2}} \times \exp\left[i\left(\omega t - \alpha_n - \beta_n + \frac{\epsilon}{2}\right) \right] \quad (5.12)$$

$$= -8 p_0 \rho c^2 \sum_0^{\infty} \Theta_n(r,\phi) \cos\left(\frac{n\pi}{2} - \frac{\epsilon}{2}\right) \exp\left[i\left(\omega t - \alpha_n - \beta_n + \frac{\epsilon}{2}\right) \right] \quad (5.13)$$

with

$$\Theta_n(r,\phi) = \frac{2}{\epsilon_n} \frac{J_n(kr)}{J_n'(ka)} \frac{\cos n\phi}{\sqrt{J_n'^2 + Y_n'^2}} \left\{ (X_n - \omega X_A)^2 + \omega^2 R_A^2 \right\}^{-1/2} \quad (5.14)$$

and

$$\alpha_n = \tan^{-1} \frac{J_n'(ka)}{Y_n'(ka)}$$

$$\beta_n = \tan^{-1} \frac{\omega R_A}{(X_n - \omega X_A)}$$

It can be seen from 5.13 that the effect of the even modes (n even) on the internal field can be removed by putting $\epsilon = \pi$ and the odd modes by putting $\epsilon = 0$.

This arises because the generalised force in these modes is zero under these values of ϵ . In general both the even and odd modes will make significant contributions and hence ϵ will have some value between 0 and π . Returning to 5.13

$$p_i = C_1 \sum_0^\infty \theta_n(r,\phi) \cos\left(\frac{n\pi}{2} - \frac{\epsilon}{2}\right) \cos\left(\frac{\epsilon}{2} - \gamma_n\right) \cos\omega t$$
$$- C_1 \sum_0^\infty \theta_n(r,\phi) \cos\left(\frac{n\pi}{2} - \frac{\epsilon}{2}\right) \sin\left(\frac{\epsilon}{2} - \gamma_n\right) \sin\omega t \qquad (5.15)$$

where

$$C_1 = -\,8\rho c^2 P_0 \qquad \gamma_n = \alpha_n + \beta_n$$

Hence

$$|p_i|^2 = C_1^2 \left[\sum_0^\infty \theta_n(r,\phi) \cos\left(\frac{n\pi}{2} - \frac{\epsilon}{2}\right) \cos\left(\frac{\epsilon}{2} - \gamma_n\right)\right]^2$$
$$+ C_1^2 \left[\sum_0^\infty \theta_n(r,\phi) \cos\left(\frac{n\pi}{2} - \frac{\epsilon}{2}\right) \sin\left(\frac{\epsilon}{2} - \gamma_n\right)\right]^2$$

$$= C_1^2 \sum_0^\infty \sum_0^\infty \theta_r \theta_s \cos\left(\frac{r\pi}{2} - \frac{\epsilon}{2}\right) \cos\left(\frac{s\pi}{2} - \frac{\epsilon}{2}\right) \cos(\gamma_r - \gamma_s) \qquad (5.16)$$

Now $|p_i|$ the amplitude of the sound pressure at $P(r,\phi)$ must be minimised w.r.t ϵ .

$$|p_i| \frac{\partial |p_i|}{\partial \epsilon} = \sum_0^\infty \sum_0^\infty C_1^2 \theta_r \theta_s \cos(\gamma_r - \gamma_s) \left[\frac{1}{2} \sin\left\{\frac{(r+s)\pi}{2} - \epsilon\right\}\right] \qquad (5.17)$$

$$= C_1^2 \sum_0^\infty \sum_0^\infty \frac{\theta_r \theta_s}{2} \cos(\gamma_r - \gamma_s) \left[\sin\frac{(r+s)\pi}{2} \cos\epsilon - \cos\frac{(r+s)\pi}{2} \sin\epsilon\right] \qquad (5.18)$$

$$\frac{\partial |P_i|}{\partial \epsilon} = 0 \qquad \text{for a minimum}$$

$$\therefore \tan\epsilon = \frac{\sum\sum \theta_r \theta_s \cos(\gamma_r - \gamma_s) \sin\frac{(r+s)\pi}{2}}{\sum\sum \theta_r \theta_s \cos(\gamma_r - \gamma_s) \cos\frac{(r+s)\pi}{2}} \qquad (5.19)$$

This expression gives two values of ϵ corresponding to the maximum and minimum values of $|P_i|$. In a numerical example, it will be possible to determine by inspection which is the correct value for a minimum.

5.3 Conclusion

A calculation was done using the results of the work in Chapter 3. The value obtained for ϵ depends on the point P within the fuselage. A calculation was made of the value of ϵ along the $\phi = 0$ axis and the following obtained.

$\frac{r}{a}$	ϵ
1·0	6° 57'
0·8	1° 16'
0·6	12° 33'
0·4	21° 42'

A value $\epsilon = 5°$ was arbitrarily chosen and the sound pressure plotted along the $\phi = 0$ axis for plane waves incident from the right and left.

Fig. 12 shows the results obtained.

5.4 Discussion of Results.

It can be seen from Fig. 12 that considerable attenuation is obtained with alteration of the phase angle between the incident fields. These

calculations have been confined to finding a phase difference between the two incident waves which gives a reduction in sound pressure level along the $\phi = 0$ axis. No calculations have been done at other points within the cylinder space.

The results emphasise the importance of the phase transmitting characteristics of structures.

It should be emphasised that this is a very simplified mathematical model of the state of affairs occuring in a practical case, but nevertheless it indicates the benefit that can be obtained from correct phasing.

CHAPTER 6

Acoustic Radiation Damping from a Flat Finite Rectangular Plate

6.1 Introduction

It was seen in Chapter 4 that a vibrating structure in an acoustic medium experiences a damping due to the radiation of energy away from the system in the form of diverging sound waves. The damping was evaluated for the special case of a circular cylindrical structure vibrating in longitudinal and circumferential modes. A case of some importance is the vibration of a plane elastic plate of rectangular shape and finite size.

Problems concerning the sound transmission properties of such a plate and also the stresses experienced by the plate have so far been extremely hampered by the lack of numerical values for the damping in any particular mode. Indeed, at resonance the damping is the predominant term and thus the accuracy of any numerical result relating to the plate response depends critically on accurate evaluation of the damping.

The method used here to evaluate the radiation damping is the well known Rayleigh formula. The difficulty of this method lies in the evaluation of the resulting integral which has only been solved analytically in restricted cases; in particular to the radiation from a rigid circular piston which is treated in Rayleigh's book. When the radiation of a surface which is free to vibrate in modes in examined it is found that the resulting integrals are very awkward; an analytic solution was sought but

an extensive search in several books of standard integrals was unsuccessful. The integrals are evaluated numerically and this has been done using the 'Pegasus' electronic digital computer.

A similar difficulty in this problem to that in Chapter 4 is encountered; namely, acoustic scattering round the boundaries of the panel. To obviate these, the panel is set in a rigid flat baffle. Since the edge effects are probably not significant away from the edges then for normal size panels, this mathematical restriction is not severe.

In the problem treated the panel radiates on one side only; if the panel radiated to both sides then the numerical answers for the damping would be twice the figures to be quoted.

6.2

The plate length a breadth b is set in an infinite, rigid wall, the co-ordinates are shown in Fig. 13. Consider a fluid in the region to the right of the plate with density ρ velocity of sound c and the plate motion perpendicular to and measured from its median plane to be

$$w = \sum_m \sum_n a_{mn} \alpha_n(x) \beta_m(y) \exp[i\omega t] \qquad (6.1)$$

where α_n, β_m are the mode shapes which depend on the boundary conditions of the plate in the wall, that is the edge fixation. For the purposes of developing the theory the edges have been taken as pin-jointed which is equivalent to zero curvature and therefore zero bending moment round the edges; this leads to

$$w = \sum_1 \sum_1 a_{mn} \sin \frac{n\pi x}{a} \sin \frac{m\pi y}{b} \qquad (6.2)$$

a_{mn} periodic in time, frequency ω rad/s .

The Rayleigh expression for the sound pressure above an infinite flat plate at a general field point r is

$$p = -\rho \frac{\partial \phi}{\partial t}$$

with $$\phi = -\frac{1}{2\pi} \iint \frac{\partial \phi}{\partial n} \cdot \frac{1}{r} \exp[-ikr]\, ds \qquad (6.3)$$

where the double integral extends over the plate area and $\frac{\partial \phi}{\partial n}$ is the normal plate velocity = $\dot{w}$.

From (6.2) and (6.3) there appears to be two methods of evaluating the radiation component of the acoustic loading on the plate. Either the sound pressure can be evaluated a long way away from the plate and then the acoustic intensity integrated over a hemispherical surface the real part of the resulting expression giving the damping; or the pressure at one point on the plate can be found due to the effect of all other elemental areas and then the pressure can be integrated through the modal displacements to find the generalised force which will give a real part, the damping. It was thought that the former method would lead to valid approximations and hence an anlytical result; this was the case with the rigid circular piston which gave a result identical with the second method (treated by Rayleigh) but no success was had with the problem in hand.

Turning to the second method; the generalised force Q_{mn} is

$Q_{mn} = \frac{\partial W}{\partial a_{mn}}$ where δW is the work done by the acoustic field at the plate surface.

$$\delta W = \iint_A \delta a_{mn}\, p(x,y) \sin\frac{n\pi x}{a} \sin\frac{m\pi y}{b}\, dx\, dy \qquad (6.4)$$

$$\therefore Q_{mn} = \iint p(x,y) \sin\frac{n\pi x}{a} \sin\frac{m\pi y}{b}\, dx\, dy \qquad (6.5)$$

Using equations (6.2) and (6.3) and the fact that

$$\frac{\partial}{\partial t} = i\omega$$

the following equation is obtained for $p(x,y)$

$$p(x,y) = \frac{i\omega\rho}{2\pi} \iint_A \sum_1^n \sum_1^m \dot{a}_{mn} \sin\frac{n\pi x'}{a} \sin\frac{m\pi y'}{b} \left(\frac{1}{r}\right) \exp[-ikr]\, dx'dy' \qquad (6.6)$$

where

$$r = \sqrt{(x-x')^2 + (y-y')^2}$$

Hence

$$Q_{mn} = \frac{i\omega\rho}{2\pi} \iint_{AA'} \sum\sum \dot{a}_{mn} \sin\frac{n\pi x'}{a} \sin\frac{m\pi y'}{b} \frac{\exp[-ikr]}{r} \sin\frac{n\pi x}{a} \sin\frac{m\pi y}{b}\, dx\, dx'\, dy\, dy'$$

The real part of the coefficient of $\dot{a}_{mn}$ in this expression is the radiation damping.

$$R.P.\, Q_{mn} = \frac{\omega\rho}{2\pi} \iint_{AA'} \sum\sum \dot{a}_{mn} \sin\frac{n\pi x'}{a} \sin\frac{m\pi y'}{b} \frac{\sin kr}{r} \sin\frac{n\pi x}{a} \sin\frac{m\pi y}{b}\, dx\, dy\, dx'\, dy' \qquad (6.7)$$

The imaginary part of Q_{mn} represents the reactive loading of the fluid on the plate for air. This is small but for water, say, its effect should be included and will alter the resonant frequencies of the modes.

An interesting difference is noted here between the cylinder damping and the plate damping. In the equation of motion for the displacement in the mn^{th} cylinder mode the only damping occuring was one term proportional

to the velocity in that particular mode; in the plate problem the equation of motion for the displacement in the mn^{th} mode contains a set of damping terms proportional to the velocities in all the other modes. All the equations are coupled together through the damping terms. Physically this means that, whereas in the cylinder problem radiated pressure by one mode combination does no work in any other mode, in the plate problem the pressures set up by one mode do work in other modes.

For the present purpose only the damping contributed by the mn^{th} mode is considered.

Denoting the coefficient of $\dot{a}_{mn}$ by $R_{A_{mn}}$ the damping coefficient in the mn^{th} mode becomes from (6.7).

$$R_{A_{mn}} = \frac{\omega\rho}{2\pi}\iint_{A}\iint_{A'} \frac{\sin k\sqrt{(x-x')^2+(y-y')^2}}{\sqrt{(x-x')^2+(y-y')^2}} \sin\frac{n\pi x'}{a}\sin\frac{m\pi y'}{b}\sin\frac{n\pi x}{a}\sin\frac{m\pi y}{b}\,dx\,dy\,dx'\,dy' \tag{6.8}$$

putting $x = a\eta$, $y = b\xi$ (6.8) becomes

$$\frac{R_A}{\rho c A} = \left[\frac{a}{\lambda}\right]\left[\frac{b}{a}\right]\int_0^1\int_0^1\int_0^1\int_0^1 \frac{\sin 2\pi\left[\frac{a}{\lambda}\right]\sqrt{(\eta-\eta')^2+\left(\frac{b}{a}\right)^2(\xi-\xi')^2}}{\sqrt{(\eta-\eta')^2+\left(\frac{b}{a}\right)^2(\xi-\xi')^2}} \sin n\pi\eta'\sin m\pi\xi'\sin n\pi\eta\sin m\pi\xi \; d\eta\,d\eta'\,d\xi\,d\xi' \tag{6.9}$$

Where A = area of the plate = a b

λ = wavelength of the radiated sound field corresponding to the (ω) frequency.

The fraction on the left hand side is the ratio of the plate radiation damping in mode mn to the rigid damping of the plate at high frequencies.

This ratio is a function of the plate aspect ratio $\frac{b}{a}$, the mode mn, and the ratio of a typical plate dimension to the wavelength of the radiated waves. For a given mode mn a family of curves can be plotted of the damping against the non-dimensional frequency parameter for various values of $\frac{b}{a}$.

A solution of the integral was sought without success; therefore recourse was made to the digital computation. The quadruple integral (6.9) can be reduced to a double integral by a Jacobian transformation* (see Appendix D) to the form.

$$\frac{R_A}{\rho c A} = \alpha\beta \int_0^1 \int_0^1 F(u,v)\left[(1-v)\cos n\pi v + \frac{1}{n\pi}\sin n\pi v\right]\left[(1-u)\cos m\pi u + \frac{1}{m\pi}\sin m\pi u\right] du\,dv \qquad (6.10)$$

with $\alpha = \frac{a}{\lambda}$, $\beta = \frac{b}{a}$, $F(u,v) = \dfrac{\sin 2\pi\alpha\sqrt{v^2+\beta^2u^2}}{\sqrt{v^2+\beta^2u^2}}$

6.3 Results

The computation was carried out for the fundamental mode $n=1$, $m=1$, for different aspect ratios over a range of the non-dimensional frequency parameter $\frac{\omega a}{c}$. The acoustic damping is plotted in Fig. 14. These results are utilised later (Chapter 11) in the calculation of panel stresses. This programme should be extended to consider higher mode combinations. Appendix E gives details of the programme and method of operation.

Concluding comments are given in the following Chapter in which also is discussed the work of earlier chapters.

---

* The author is indebted to Dr. J. Cleave for pointing this out.

CHAPTER 7.

Conclusions to Part I.

7.1

Part I of this work has been concerned with theoretical methods for calculating the structural response of progressively more complicated structures when excited by simple harmonic plane sound waves.

The starting point was the simple model of a plane infinite single degree of freedom plate spaced parallel to an infinite sound-hard wall. The model demonstrates the effect which the sound field in the space between the plate and the wall has on the plate response (Fig. 5) and the transmission of sound. This model shows in a simple way the less obvious internal sound field effects which have been found in the next structural model, more complicated, but more representative of an aircraft fuselage.

This model is the periodically stiffened thin-walled infinite circular cylinder excited by plane waves. The calculations show that many modes of vibration are excited but in the particular example taken only a few modes make a significant contribution to the internal sound field (Table 1). The results also show the internal sound field to be far from uniform (Fig. 9).

This model has also been used to show the effect on the internal sound when plane sound waves are incident from opposite directions. The calculations show that a phase difference between these waves can be found which reduces the level of the sound field at points within the fuselage space (Fig. 12).

Finally in this class of problem expressions have been formulated to

deal with the case of obliquely incident phase sound waves allowing longitudinal as well as circumferential modes of vibration of the stiffened cylinder. Calculations have been done for a particular cylinder at one frequency for a range of angles of incidence. Many modes (Table 2) are excited but usually a few predominate and these modes will be responsible for the bulk of the sound transmission to the interior.

Results have also been obtained of the acoustic radiation damping of a rectangular vibrating panel set in a rigid wall using Rayleigh's theory. These results (Fig. 14) will be found useful in a later section of the work dealing with panel response to acoustic noise.

7.2 Future Work.

The present work has been concerned with periodic vibrations of various types of structure. The work is restricted by the requirement of linear vibrations which restricts the magnitude of the amplitudes. A further restriction in the case of stiffened structures arises in that the stiffeners must be close spaced; this is not severe at low frequencies where the lower order modes are predominant. At high frequencies where higher order modes become important, the structural theory will break down. The question of large amplitudes with consequent non-linear stiffness is a difficult one and does not appear to have been solved even for a simple beam. The main difficulty lies in the solution of the differential equation. However, with high acoustic loading the plate is certainly vibrating in a non-linear manner and work in this field is needed. Another assumption is that of mode shape, necessary for the Lagrange approach. Again the question of deriving the mode shape from the differential equation

is the problem; probably here it is specifying the boundary conditions that is difficult. Further no account has been taken of structural damping. The acoustic restrictions are those of linearity and scattering effects. The assumption of linearity precludes very intense sound fields whilst the latter is thought to be significant only near the ends of the structure and does not effect the generalised forces too greatly.

In the three-dimensional stiffened cylinder problem, several interesting points could be pursued namely :-

1) the investigation of the modal response to the oblique plane wave over a frequency range up to the limit of the validity of the structural theory (see Miller Ref. 4).

2) the investigation, using the "Pegasus" programme, of structural changes such as frame and stiffener sizes and spacing (bearing in mind the basic load carrying requirements of these structures).

3) the question of non-linear stiffness at large amplitudes.

4) the extension of the cylinder problem to that of forward flight. This could be done by using the solution to the wave equation in a moving set of co-ordinates for the 'outside' field. This work should lead to the supersonic flutter problem investigated by Prof. J.W. Miles and others.

5) from a practical aspect; the question of the effect of aircraft cabin acoustic absorption on internal sound fields. This work probably lies a long way off.

6) the application of more complicated sound fields such as those from propellers and also the question of propeller phasing discussed in Chapter 5.

7) the investigation of mode shapes in stiffened structures.

Much of the above requires considerable analytical and computational work and careful practical justification would be needed before a project such as item 5 was attempted. In particular, items 3 and 4 seem to be of fundamental interest.

The acoustic damping radiation of flat flexible plates needs further examination and the programme (Appendix E) should be of value here. The question of damping coupling between the modes should also be considered.

In conclusion little or no experimental work has been done in the work discussed in Part 1; such work is desirable to substantiate the theory although the difficulties appear to be formidable.

CHAPTER 8

Noise pressure fluctuations

8.1

So far, consideration has been given only to problems where the incident sound fields are periodic in time where it is possible to specify the incident field completely as a function of time. Such problems have an important practical application; for instance in the solution of structural response to propeller sound fields. The sound field produced by a propeller is essentially complex consisting of Fourier series of harmonic frequencies with each of which there is associated an amplitude and phase which is dependent on the field point considered. Nevertheless each of these harmonics can be treated separately as a function which is completely known (that is at all instants of time) and the summed total effect of these harmonic components can be found on the structure. Two important sources of time dependent pressure fluctuations are excluded from the treatment so far considered; these are the fluctuations caused by the jet efflux of the turbo-jet engine and the fluctuations caused by the turbulent boundary layer. These phenomena are not characterised by the discrete frequency terms as in the propeller case. Indeed, it is not possible to write down an expression for the pressure fluctuations at a given point as a function of time. Such fluctuations go under the heading of noise or random processes.

In acoustics literature the word 'noise' appears to have two distinct and separate meanings under the broad headings of subjective and objective.

Subjectively 'noise' is defined as 'unwanted sound'. In this, as for example disturbance to a conversation, whether of discrete frequency or otherwise, would be defined as noise. It is not this definition of noise which is meant in this work, but rather the objective definition that is the mathematical one that - a noise fluctuation is one that cannot be expressed explicitly as a function of time. The words 'noise' and 'random process' can be taken as synonimous.

8.2 Measurable quantities

In fact the difference between the periodic process and the random process is that, whereas in the former it is possible to predict with certainty what the state of the system will be at time t, in the latter such prediction is not possible but only a probability can be stated that the value of some characteristic fluctuating quantity will be within some prescribed limits. As is stated by Wang and Uhlenbeck (Ref. 14), the random process is defined by a set of probability distributions. A knowledge of the (infinite in the general case) set of probability distributions would define the process completely. From these all the average properties of the process could be obtained. The measurement of these probabilities does not seem to be a practical proposition and the computation from say, an oscilloscope trace would be prohibitive in time. It is clear that whilst no mathematical theory exists which enables the pressure fluctuations to be predicted, some practical form of measurement may be made in order to determine the statistical properties of the process (e.g. the length scale of turbulence and spectra in various directions). It is precisely through

such measurements that insight is gained into the physical processes which should then provide the basic framework for a mathematical analysis. The work on turbulence theory and structure vibration due to noise has shown that there are three measureable quantities of particular importance in the calculation of structural response; these are the space-correlation, auto-correlation and power spectral density functions.

Taking the last one first, it is clear that if one has, say, a random fluctuating pressure, a knowledge of the energy distribution through the spectrum is of first importance. The power spectrum density function $F(f)$ of the random pressure is defined in the following way :-

$$\overline{p^2} = \int_0^\infty F(f)\,df \qquad (8.1)$$

where $\overline{p^2}$ is the time average value of the pressure^2. $F(f)$ has dimensions of $(\text{pressure})^2$/cycle/sec. In the case of a set of discrete frequencies, $F(f)$ would be a spectrum of lines. For a random process the power spectral density function is a continuous function of f .

The auto-correlation function of the pressure $p(t)$ is defined as :-

$$R(\tau) = \overline{p(t)\,p(t+\tau)} = \lim_{T\to\infty} \int_{-\frac{T}{2}}^{+\frac{T}{2}} p(t)\,p(t+\tau)\,dt \qquad (8.2)$$

where τ is the separation in time between two parts of the same signal $p(t)$. The product $p(t)\,p(t+\tau)$ is averaged over an integration time T; for $R(\tau)$ to be accurate this integration time must be much larger than $\frac{1}{f_L}$ where f_L is the limit below which the power spectral density function

is considered to be insignificant. So that for low frequency noise processes, the integration time T must be long in order that the auto-correlation function $R(\tau)$ shall be accurate. There is a well known relationship between the power density spectrum function $F(f)$ and the auto-correlation function $R(\tau)$ first noted by Weiner (Ref. 15). It is that $F(f)$ and $R(\tau)$ are Fourier transforms of each other viz :-

$$R(\tau) = \int_0^\infty F(f) \cos 2\pi f \tau \, df$$

$$F(f) = 4 \int_0^\infty R(\tau) \cos 2\pi f \tau \, d\tau \qquad (8.3)$$

Thus a knowledge of the function $R(\tau)$ can be used to evaluate the power spectral density $F(f)$. A further use for $R(\tau)$ is for the detection of a periodic signal buried in noise, this however is beyond the scope of the present discussion.

The above two functions give information about one signal $p(t)$; they are one-dimensional quantities related to the time domain. In electric circuit theory this is usually adequate but in the phenomena of turbulence and random pressure fluctuation, spatial variations also play a major role. The measureable function which brings in the spatial dimensions is the space-correlation function, or more generally, the space-time correlation function. Consider the pressures at points in space $\vec{r}_1$ and $\vec{r}_2$, $p_1(\vec{r}_1, t), p_2(\vec{r}_2, t)$ then the space time correlation function is

$$R(\vec{r}_1, \vec{r}_2, \tau) = \lim_{T \to \infty} \int_{-\frac{T}{2}}^{+\frac{T}{2}} p_1(\vec{r}_1, t) \, p_2(\vec{r}_2, t+\tau) \, dt \qquad (8.4)$$

and the space-correlation function is

$$R(\vec{r}_1, \vec{r}_2) = \lim_{T \to \infty} \int_{-\frac{T}{2}}^{+\frac{T}{2}} p_1(\vec{r}_1, t)\, p_2(\vec{r}_2, t)\, dt \qquad (8.5)$$

If statistical homogeneity in the region $\vec{r}$ is assumed, $\vec{r}_1$ can be taken as the origin of co-ordinates and R is a function of the separation between the signals, (8.5) becomes

$$R(\vec{r}_1 - \vec{r}_2) = \lim_{T \to \infty} \int_{-\frac{T}{2}}^{+\frac{T}{2}} p_1(\vec{r}_1, t)\, p_2(\vec{r}_2, t)\, dt \qquad (8.6)$$

It is important to note here that not only the distance between the points at which the signals are averaged but the direction also (through the vector difference $\vec{r} = \vec{r}_1 - \vec{r}_2$) is important.

The space-correlation function as shown by Powell (Ref. 16), and as will be shown in a later section, plays a major role in the computation of the generalised force due to random loading on a structure. In turbulence theories where a knowledge of the size and structure of turbulent eddies is required, the space-correlation function is a necessary measurement. The space-time correlation function provides a powerful method for determining the direction of propagation of random wave trains.

The technique of correlation measurement in acoustic noise fields has only recently been developed; the experimenter is presented with a wide field of investigation.

Allied to this, the time needed to accumulate a sensible amount of information is long, even when one has available a continuous primary source. Nevertheless there is no doubt that if a better understanding of random fluctuating processes is to be obtained, such measurements must be made. The succeeding sections of this work describe some experiments on model and full scale jets in which correlation measurements were made. An interpretation is based on the results from a turbulence view-point and also some of the measurements are utilised in a calculation of the stresses induced in a flat panel.

CHAPTER 9

Space-correlation measurements close to a model 2" dia. jet.

9.1

Some time before the author commenced his period of research at the University of Southampton, it was appreciated that a general purpose space-time correlator would be an essential piece of equipment for a more detailed study of random phenomena; in particular those created by jet mixing but also more generally in the fields of electronics and vibration studies. During the period of the author's work at Southampton, the space-correlation equipment was completed and the author was able to assist in collaboration with Dr. R.E. Franklin and Mr. K.R. McLachlan in the measurements. The work is separately reported in Refs. 17, 18 and 19.

All the measurements reported in this section were made in the immediate neighbourhood of a two inch diameter cold-air jet. Succeeding sub-sections describe the equipment used and the measurements made. It was on the suggestion of Dr. Franklin that an investigation should be carried out close to and parallel with the jet boundary. The results of these measurements and a correspondence between Dr. Franklin and the author tends to confirm that turbulence in the jet mixing region is, over small but significant distances at any rate convected with some mean velocity downstream with only small changes in the eddy structure of the turbulence. This point is elucidated in 9.6.

9.2 Experimental arrangements.

The main items of equipment used in the experiments were :-

a) the two inch diameter air jet on which the measurements were made.

b) the probe microphones.

c) the correlator.

9.2.1 The two inch diameter air jet (Fig. 16).

The air jet was provided by exhausting high pressure air stored in a converted Lancashire steam boiler. The boiler stored compressed air up to a maximum pressure of 150 p.s.i. The air was compressed by an electric motor-driven air compressor taking about 75 minutes to pump the boiler up to full pressure. Control of the jet pressure ratio and hence the jet exit velocity was provided by a hand control throttling valve. The valve was controlled to give a constant up-stream settling chamber pressure recorded by a mecury manometer.

To the end of the second chamber could be fitted a variety of convergent nozzles giving the required jet exit diameter. The diameter chosen for these experiments was two inches. This diameter was influenced by several considerations.

Firstly, for correlation pressure measurements it is fundamental that the pressure measuring device measures sensibly at a point in space and not over an area; to this end a pair of matched probe microphones were developed (Ref. 21). These microphones were effectively the standard Bruel and Kjaer condenser microphones, diaphragm diameter approximately 1 inch, terminated by a fine bore hypodermic tube. inside diameter D.03". The probe is matched to the microphone through a carefully adjusted cavity to give a frequency response which, whilst falling off with increased frequency at 6 db/octave, has no resonances or anti-resonances in the

frequency range of interest (about 40-6000c/s). The two probe microphones were matched over this frequency range so that nowhere did their responses differ by more than 0.5 db.

With the fine bore microphones and the expectation that strong space correlations would be present in the range of one jet diameter it was clear that it would be quite practical to go to a jet as small as one inch diameter. However, two objections were raised to this; firstly that with the smaller diameter the spectrum of the pressure fluctuations would move up the frequency scale and possibly beyond the limit of the known response of the microphone probes; secondly with the smaller jet greater care must be taken in positioning the microphones.

The other nozzles available at the time were a two inch diameter and a four inch diameter. The four inch diameter was from the positioning point of view the best choice but with the limited supply of air available and the jet velocities which were to be used, the much larger mass flow associated with the four inch jet would have made the gathering of sufficient information prohibitively slow. The best compromise therefore was the two inch jet.

Fig. 17 shows a photograph of the jet with the microphones set in position. The moveable microphone is mounted on a screw threaded traversing gear and can traverse linearly past the fixed microphone.

9.2.2 The correlation computer.

The correlator was designed by Mr. K.R. Mclachlan of the Engineering Electronics Department of the University of Southampton as a general purpose

instrument covering the frequency range 0 - 10,000 c/s. It is fully described elsewhere (Ref. 19) and so only the salient features are described here.

A block diagram of the computer is shown in Fig. 18. The signals generated by the pressure fluctuations on the diaphragm are first passed through a cathode-follower mounted with the microphone; the cathode-follower matches the microphone to the long length of cable carrying the signal to the instrument room. The microphone frequency response falls away at 6db/octave hence the first components in the correlator are a pair of matched microphone amplifiers which can be selected to give a flat response curve or a response rising at 6db/octave to compensate for the probe response. A root mean square meter and fine control attenuators are built in at this stage in order to adjust the signal strength at the input to the correlator. The computer consists of a quarter-square multiplier incorporating a biased-diode function generator, followed by a pair of modified boot-strap integrators. An integrator circuit integrates the multiplier output over an interval of 10 seconds after which the integrator output is fed to an anlogue-to-digital converter and then to a digital register. This conversion process takes roughly two seconds and during the next eight seconds the integrator is error-corrected for drift by a servo-mechanism. At the end of a twenty second period from the start of the previous integration, the integrator again starts to integrate the multiplier output. Thus each integrator works on a cycle of twenty-second periods and the two are staggered so that the output of the multiplier is

continuously integrated and added in on the digital register which exhibits the 'count' on dekatron tubes. In this way an integration time of any multiple of ten seconds up to a hundred seconds and any multiple of a hundred seconds up to one thousand seconds is possible with very small errors.

9.3 Operating technique.

In these experiments three operators were required, one operating the control valve for the jet and moving the microphone, and two operating the computer and recording the results.

As regards the jet, the main difficulty was in controlling the pressure ratio and hence jet velocity; in fact it was not possible to control the upstream pressure to better than $\pm$ 0·1 p.s.i at a pressure differential of 9 p.s.i , this represents a velocity fluctuation of 5 f.p.s at about 890 ft/sec. This fluctuation was acceptable but at higher pressure ratios control fell away badly and some sort of servo-valve would be desirable.

The operation of the computer presented little difficulty once the instrument had warmed up and the servo mechanisms balanced. Three basic measurements were made at each microphone separation, each taking about twenty seconds. (This allows for a ten second integration time and time to record the integrated count and switch to the next measurement). These measurements were

1) the integration of the cross product $P_1 P_2$
2) " " " " (pressure)^2 on one microphone.
3) " " " " " the other microphone.

$\overline{P_1 P_2}$ is the correlation function which is normalised by $\sqrt{\overline{P_1^2}}\sqrt{\overline{P_2^2}}$ to give the correlation coefficient

$$R = \frac{\overline{P_1 P_2}}{\sqrt{\overline{P_1^2}}\sqrt{\overline{P_2^2}}}$$

The question of integration time was settled by computing R for several different integration times and it was established that in the present tests ten seconds was quite adequate; and so a ten seconds integration time was used for all subsequent experiments.

To achieve best accuracy with the computer care must be taken in setting the attenuators in order that the signal strength of each signal is about the same and gives a mid-scale deflection on the R.M.S. meter. The two signals were also monitored on a double-beam oscilloscope so that overloading or signal peculiarities could be quickly detected. It is also possible to display the correlation on the oscilloscope by having one signal on the x-plates and the other on the y-plates. This visual representation is very useful for quick surveys to establish the order of magnitude of correlation lengths in various directions.

9.4 Details of measurements and results.

In the complicated pressure field associated with the turbulent mixing of a free-jet, the number of correlation measurements one could take is almost without limit. To narrow the field somewhat the measurements were limited to the near "hydrodynamic" field; no measurements were taken in the far field where the fluctuations are acoustic. There is some conjecture as to the limit of the near field but it is considered that the region within three diameters is well within the limits of the near field.

A further restriction can be made by limiting the measurements to the first ten diameters downstream. This decision has proved to be sound in the light of Ribner's (Ref. 22) work on the distribution of sources along the jet. Ribner concludes that the main acoustic radiation emanates from a flat plateau of high intensity sources in the first few diameters and that beyond this position the intensity of noise source strength falls off as the seventh power of the distance from the jet-exit plane. Hence it would appear the region from zero to (at a maximum) ten diameters downstream is the region of most importance.

Having restricted the measurements to this region the question arose as to the traversing directions, or in effect, the choice of co-ordinate axes. Might there not be some planes on which the correlation would show symmetry? Possibly, such a traversing plane would be the conical surface with axis of symmetry coincident with the jet axis and with 'sides' parallel to the jet boundary. This was rejected since at the time the traversing gear was not obtainable; neither was there the time to enter on so ambititous a programme of measurement.

The traverses finally chosen were those parallel and perpendicular (outwards) to the jet boundary and also correlation over an area was measured; this area being in a typical plane where possible structure might be in a practical full scale case.

Fig. 19 shows the lateral correlation coefficient with reference to the fixed microphone 6.2 diameters downstream and 0.5 diameters from the jet boundary (the jet boundary was determined as the 1/10th velocity line

making the total spreading angle about 12°). Some scatter in the measurements is noticed for correlations below 0.2; this is probably explained by Fig. 21 where it is seen that the integrator 'count' (which is proportional to the mean square pressure fluctuation) falls off extremely rapidly over the first six inches outward from the jet. Under these conditions it was found difficult to adjust the signal strengths into the computer since at that time no fine attenuation adjustment had been fitted.

Fig. 20 shows longitudinal traverses parallel to the jet boundary at a position 5 diameters downstream and 0.5 diameters away from the jet boundary. These curves show two interesting features. Firstly there is apparently no change with jet velocity and secondly there is a marked difference between the longitudinal and lateral traverses. The independence with jet velocity will be returned to later whilst the difference between longitudinal and lateral traverses is further emphasised in Fig. 22.

In Fig. 22 space-correlation with respect to a point 5 diameters downstream and 0.5 diameters out from the jet boundary has been carried out over an area extending about 3 diameters upstream and 3 diameters vertically downwards. It is seen that if we consider a downward lateral traverse the correlation falls off slowly (as in the outward lateral traverse) compared with the longitudinal traverse.

9.5

9.5.1 Convected Turbulence

It was suggested by Dr. Franklin that a relationship might exist

between the auto-correlation coefficient and the space-correlation coefficient for traverses near and parallel to the jet boundary. This was based on the assumption that the microphones were sensing "hydrodynamic" incompressible pressure fluctuations associated with the turbulence washing past them and that it was this convection of an eddy containing a random wave-number structure that was causing the major fluctuation; the change in the eddy structure itself with time being relatively slow. The space and auto-correlations should then be equivalent on scaling with respect to the convected velocity; since, if the changes in the eddies are small, then a microphone at position B distance ξ downstream from A should correlate strongly with A if delayed in time by an amount $t = \frac{\xi}{u}$ which is just sufficient to allow the eddies at A to arrive at B substantially unchanged. u, the convection velocity was taken as half the local maximum jet velocity and this value used in all cases.

At the time when this was proposed, the auto-correlation unit was not yet available so that the auto-correlation curves were obtained by taking the Fourier transform of the normalised power spectra. The power sepctra were obtained using a Bruel and Kjaer third octave band analyser; the microphone signal being first fed to the correcting amplifier of the correlator and then to the spectrum analyser. The transformation was achieved by a straightforward numerical process and normalised to give the auto-correlation coefficient of unity for zero time delay. Fig. 23 shows a typical spectrum and its transformation to an auto-correlation coefficient.

It was decided to investigate this relationship at the four positions

shown in Fig. 24; 2 and 5 diameters downstream and 1 and 2 diameters out from the traverse line shown. Figs. 26 - 28, show the space and auto-correlation curves plotted together at positions 1, 2, 4; in each case the auto-correlation curves have been scaled to the space correlation curves using half the maximum local jet velocity as the convection velocity. It can be seen that for the inner positions, 1 and 2, the agreement is good but that for the outer position (4) this is not the case. It was concluded therefore that this relationship of convection would only hold nearer than about one diameter away from the jet boundary.

About this time, Dr. Franklin was conducting some full scale correlation measurements on a 21" diameter hot jet at Farnborough (R.A.E.) at the corresponding positions. Figs. 30 - 32 show the model and full scale measurements plotted together on a non-dimensional $\frac{r}{D}$ basis.

2.5.2

As a result of some correspondence between the author and Dr. Franklin, a simple theory based on the convection hypotheses was proposed which would explain some of the results noted above; namely - that the longitudinal correlation curves were independent of jet velocity and that the non-dimensional correlation curves (Figs. 30 - 32) should coincide in regions where convection was occuring. This work also yielded some interesting results on the effects of filtering and filter bandwidth.

Consider a frozen pattern of turbulence convected at a velocity U_c, with a wave-number spectrum $G(k)$, past a fixed point in space. The 'time' or frequency fluctuations seen at this fixed point will depend only on U_c

if $G(k)$ is fixed. A narrow band of wave number centred on K_o will produce a narrow band of frequency centred on ω_o where

$$\omega_o = U_c K_o \tag{9.1}$$

As U_c increases so does ω_o .

Now consider a non-dimensional wave-number spectrum $H(\eta)$ where

$$\eta = \frac{\omega D}{U_c} \tag{9.2}$$

This η may be considered as a non-dimensional wave number or frequency parameter. It is often referred to as the Strouhal number. It has been suggested by Lighthill (Ref. 24) that the Strouhal number is approximately constant for all jets and he uses this as part of the basis for his now famous similarity law for noise production from a jet. Thus the function $H(\eta)$ may be regarded as a universal function for all jets (see Fig. 29).

The auto-correlation coefficient is

$$R(\tau) = \frac{\int_0^\infty F(\omega) \cos \omega\tau \, d\omega}{\int_0^\infty F(\omega) \, d\omega} \tag{9.3}$$

From $F(\omega)$ the function $H(\eta)$ can be generated under the transformation $\omega = \frac{U_c \eta}{D}$ whence

$$R\left(\frac{U_c \tau}{D}\right) = \frac{\int_0^\infty H(\eta) \cos \frac{U_c}{D} \eta\tau \, d\eta}{\int_0^\infty H(\eta) \, d\eta} \tag{9.4}$$

Now under the hypothesis of convection $x = U_c \tau$ (9.4) becomes

$$R\left(\frac{x}{D}\right) = \frac{\int_0^\infty H(\eta) \cos \eta \frac{x}{D} \, d\eta}{\int_0^\infty H(\eta) \, d\eta} \tag{9.5}$$

This result, obtained by considering a rigid pattern of turbulence convected with velocity u_c confirms the observations noted in the previous section. $R(\frac{x}{D})$ is seen to be independent of η and hence independent of jet velocity (linearly related to u_c) and jet exit diameter D. These were noted in relation to Figs. 26 and 30.

9.5.3 Filtering

For structural response calculations it is necessary to know the correlation coefficient in narrow frequency bands. Filtering $F(\omega)$ in a frequency band $\omega_0 - \frac{\delta\omega}{2}$ to $\omega_0 + \frac{\delta\omega}{2}$ is equivalent to selecting $H(\eta)$ from $\eta_0 - \frac{\delta\eta}{2}$ to $\eta_0 + \frac{\delta\eta}{2}$ (9.5) becomes, assuming the bandwidth narrow so that $H(\eta)$ is flat over the range $2\delta\eta$ centred on η_0.

$$R_{\eta_0}\left(\frac{x}{D}\right) = \frac{\sin \frac{\delta\eta x}{2D}}{\delta\eta \frac{x}{2D}} \cos \eta_0 \frac{x}{D} \qquad (9.6)$$

$$R_{\omega_0}\left(\frac{x}{D}\right) = \frac{\sin \frac{\delta\omega}{2u_c} x}{\frac{\delta\omega}{2u_c} x} \cos \frac{\omega_0 x}{u_c} \qquad (9.7)$$

Thus $R_{\omega_0}\left(\frac{x}{D}\right)$ is independent of jet diameter but in contrast to the overall correlation it is dependent on the jet velocity since the distance to the first zero crossing x_1, is given by

$$\frac{\omega_0 x_1}{u_c} = \frac{\pi}{2}$$

$$x_1 = \frac{u_0 \pi}{2\omega_0} \qquad (9.8)$$

This result seems to contradict the observations of Callaghan, Howes

and Coles since in their measurements the filtered curves were independent of jet velocity (Fig. 8, Ref. 24) which is not in accordance with (9.8) above. From physical considerations one would expect the result (9.8) above since filtering with increasing jet speed means selection of progressively larger wave numbers to keep the frequency the same; this means progressively larger eddies and hence larger correlation scale, i.e. the distance to first zero crossing increasing with speed as in (9.8).

Due to the fact that the turbulence in practice is never completely "frozen" equation (9.7) probably only applies over a distance of 2 or 3 correlation lengths. The effect of bandwidth is shown in (9.7) by the factor

$$\frac{\sin \frac{\delta\omega}{2u_c} x}{\frac{\delta\omega}{2u_c} x} \qquad (9.9)$$

Now the first negative peak occurs at

$$x = \frac{x_1}{2} = \frac{u_c \pi}{4\omega_0} \qquad (9.10)$$

and the factor (9.9) controls the maximum amplitude if the bandwidth is large. The factor (9.9) is sensibly unity for $\frac{\delta\omega}{2u_c} x \sim 0.1$ making with (9.10) $\frac{\delta\omega}{\omega} \sim \frac{0.8}{2\pi} \sim 25\%$. This would indicate that 1/3 octave band filters (bandwidth 23%) would give sufficiently accurate filtered space correlation results. This could easily be checked experimentally by comparing with a narrow bandwidth filter.

9.6 Conclusions

The following are considered to be the main results of the limited space correlation measurements described above :-

1) the limited near field space-correlation measurements tend to support the hypothesis of a 'frozen' pattern of convected turbulence. The pressures measured are considered to be "hydrodynamic" rather than acoustic since the pressure field is convected at speeds related to the jet efflux and much lower than the speed of sound. The pressures are those associated with a group of turbulent eddies being convected downstream with a velocity of one-half the local maximum jet velocity.

2) the simple theory in 9.5.2 based on a convection hypothesis indicates that the space-correlations plotted on a non-dimensional basis should be the same for model and full-scale jets; this is borne out for positions within about one jet diameter of the jet boundary.

3) the question of filtering in a convective field is raised although it is felt that the results in 9.5.3 are of a tentative nature requiring experimental evidence to verify them or otherwise.

The author's opinion on the basis of the above work is that the region of most interest in the jet pressure field is the near field and that a detailed study of pressure correlations in this region and hot-wire

correlations of the turbulent eddies themselves will yield basic information in the jet study. Certainly there is a need for space-time correlation as well as space-correlation to further examine the convection of the pressure field associated with the turbulence eddies.

Also for structural response calculations, information is required of filtered space-correlation measurements and much work is required here. A relation is required too between model and full-scale work. A limited number of full-scale measurements are reported in the following chapter although it was not possible, due to lack of time, to pursue the work further than measurements of overall space-correlations.

CHAPTER 10

Space-correlation in the near field of a full-scale hot jet.

10.1

Very little work appears to have been done on the measurement of space-correlations on a full-scale hot jet; the only report available to the author's knowledge is one by Callaghan, Howes and Coles (Ref. 24).

It was felt that the right thing to do at this stage was, if possible, to take a set of full scale measurements with a view to comparing them with similar model experiments and also to gain some idea of the type of pressure field to which a structure might be subjected.

It was fortunate that, at this time, Vickers-Armstrongs Aircraft Ltd., had available their noise test rig at Chilbolton, nr. Andover, Hants. It was agreed that a set of measurements should be made and Vickers accordingly put the rig at the disposal of Mr. K.R. McLachlan and the author who together conducted the experiments described below.

10.2 Experimental arrangements.

10.2.1 The noise rig.

The Chilbolton noise rig consisted of a Rolls Royce R.A. 24 turbo-jet engine (see Fig. 33). The jet was shielded on one side by the aircraft fuselage and the rig itself enclosed in a pen. The walls of the pen were of the order of 20-30 diameters distant from the points where the measurements were taken. The walls were treated with absorbent material in order to reduce reverberation within the pen. From the measurement point of view this was undesirable but was thought to be not too serious. A short

calculation indicates (see Appendix F) that the result of these constraints will give a value of the space-correlation coefficient slightly low but accurate to about 5% which was considered adequate under the circumstances.

The traversing equipment shown in Fig. 33 was constructed from scaffolding materials and the microphone taped in position. Since the jet was pointing slightly downwards, the traversing rig had to be tilted slightly. During the running it was found that the rig was sufficiently rigid. Radial chalk lines were drawn on the ground and between each measurement the traversing arm was rotated to its new position. In this way, with the microphones at a given separation distance, the radial arm was rotated through increments of $11\frac{1}{2}^{\circ}$, a measurement taken at each position.

The measuring equipment was contained in a hut along with the engine controls.

10.2.2 The measuring equipment.

The correlator itself (briefly described in the previous chapter) is a fairly bulky piece of equipment and it was not considered feasible to transport it to Chilbolton. Also at Chilbolton there was not a sufficiently well stablised power supply. It was therefore necessary to record the microphone signals. This was done on a twin channel tape-recorder which records simultaneously the signals from each microphone on magnetic tape. In this particular recorder the recording heads were mounted side by side and hence the two tracks were 'staggered' slightly; this means that the same tape recorder must be used on play-back of the signals since the 'head' spacing is most critical (this latter point could possibly be overcome when

a time-delay system is available so that one channel could be delayed in time relative to the other by an amount that could give a previously established correlation between the two tracks).

The microphones were a matched pair of Standard Telephone's Type 4021F. These are moving coil microphones which are not ideal for low frequency measurements[1]. However, a laboratory test was conducted with the pair using tones generated by a loudspeaker. The signals were displayed as a Lissajou's figure on an oscilloscope and with the microphones coincident an investigation over the frequency range 50 - 1,000 c/s was conducted. It was found that the microphones showed little phase shift below 1,500 c/s and on the basis of this test it was felt that this pair would be adequate for these full scale measurements where significant signals above 1,500 c/s would not be present.

The microphone diaphragm was considered sufficiently small compared with the jet diameter (21 inches) and with the major proportion of the pressure fluctuations below 500 c/s the directional characterisitcs of the microphone would not effect the results significantly.

The microphone signals were amplified through a pair of matched oscilloscope amplifiers which were tested for relative phase shift and found to be satisfactory over the frequency range of interest. The signals were monitered on the oscilloscope to check against overloading and signal peculiarities.

10.3 Operating technique.

The engine was adjusted to the required R.P.M. setting and stabilised.

The amplifier attenuators were set to give the required signal level on to the tape (about 1 volt R.M.S.). The run number and microphone position recorded on the tape and also logged; the signals were then recorded simultaneously on each channel for 60 seconds followed by a 25 second break in which the traversing rig was rotated to its new position. The next measurement was then taken in the same manner; the engine conditions remaining constant all the time. When an angular traverse had been completed the engine was shut down to idling conditions and the microphone separation distance changed, the traversing rig returned to its initial angular setting and a set of measurements taken at the new separation.

The recorded tape was analysed through the correlator using the same tape recorder. Tests on integration time showed that 10 seconds was quite sufficient.

10.4 Details of measurements and results.

10.4.1

The following table shows the positions at which measurements were made. In order not to overload the microphone the engine R.P.M. was set at 65% of the maximum R.P.M. for all the measurements; this corresponds to a jet exit velocity of 823 ft/sec. The 0° - 180° line lies parallel to the jet boundary which was taken as 7° to jet centreline.

Fixed Microphone Position	Angular Coverage	Microphone Separation (inches)
2 jet nozzle diameters downstream and 5 jet		4.0 11.0

nozzle diameters perpendicular to the jet boundary	$0°(11\frac{1}{4}°)-360°$	23.0 35.0 47.0 60.0
2 jet nozzle diameters downstream and 3 jet nozzle diameters perpendicular to the jet boundary	$0°(11\frac{1}{4}°)-360°$	4.75 16.75 29.0 41.0 53.0 59.75
2 jet nozzle diameters downstream and 1 jet nozzle diameter perpendicular to the jet boundary	$0°(11\frac{1}{4}°)-180°$	4.5 17.75 28.75 41.0 53.0 59.5

The plane in which these measurements were taken is a nearly horizontal one containing the jet centreline but tilted slightly downwards because of the engine mounting in the rig. A plan view of the configurations is shown in Fig. 34.

10.4.2 The results.

For each angular position a correlation curve is obtained. By cross-plotting from each angular position a contour-map can be drawn thus displaying all the information together. Figs. 35, 36 and 37 show the contours of overall space correlation coefficient plotted at the three reference positions.

10.5 Discussion of Results.

Due to the sparsity of experimental data, it is possible to compare these results with other experiments at one position only, that is -

2 diameters downstream, 1 diameter out from the jet boundary and parallel to the jet boundary. Fig. 38 shows a comparison from three separate experimental data. There is a considerable divergence of results on this evidence which is not easy to explain. It should be stated that the dimension - 1 diameter from the jet boundary - is rather a nominal one since the Franklin curve corresponds to position 1 (Fig. 24) which is closer than 1 diameter and the Callaghan, Howes, and Coles curve is with reference to a point 2.16 diameters downstream and "along the jet boundary" (taken as a 9.8° semi-angle to the jet axis). It may well be that the correlation curves are very sensitive to position in these very close regions. This seems to be the only difference in between the experiments.

The interpretation of the contour-maps is not easy; their most striking feature is the elongated shape which is indicative of a "sound" wave front. In the case of a periodic acoustic plane wave the constant correlation contours would be straight lines perpendicular to the wave direction; the space correlation would be zero at a quarter wavelength spacing; the succeeding $-1, 0, +1$ contours would be at quarter wavelength spacing. In the case of a spherical wave front the correlation contours would be curved, concave towards the source, to confrom with the curved wavefronts.

In the present case of jet noise high spatial correlation would not be expected because the noise can be regarded as emanating from a distributed set of random sources in the jet mixing region. However, it can be seen in Figs. 35-37 that lines of constant correlation are curved; the

curvature roughly corresponding to noise sources positioned in the jet mixing region. It will be noticed that the curvature decreases in moving from position A (Fig. 35) close to the jet to position B (Fig. 36) and then the outermost position C (Fig. 37).

The distance to zero correlation in the wave direction also has an interesting feature. These spatial correlations are wideband; the peak acoustic intensity is known to be in the region of $\frac{\omega D}{U_c} = 2$. The distance to zero crossing may be expected to be approximately one-quarter wavelength of this peak frequency; this gives $\frac{\lambda}{4} = \frac{\pi c D}{4 U_c}$ which for the value of C and U_c in the present tests gives $\frac{\lambda}{4} \doteq D$. An examination of Figs. 35-37 shows that indeed the zero correlation contour is in the region of 1 jet diameter spacing in the wave direction from the reference point. This lends further weight to the notion that these iso-correlation contours represent the acoustic noise radiated by the jet.

There remains much more information to be extracted from the recordings before the overall picture is obtained; such information as the contour-maps in filtered bands would be most useful from the structural point of view and a comparison of these measurements with model experiments in the same position might indicate scaling properties. The question as to how these contours change with jet speed is also interesting and again could be determined by model testing.

10.6 Conclusions.

No firm conclusions can be drawn from the amount of information so far extracted from the recordings. However, for structural calculations, the filtered contour-maps are essential. A comparison with model experiments with these measurements would be most valuable. It is possible that a much

wider relationship exists between model and full-scale correlation measurements than that found in the previous chapter.

The experimental difficulties of site-working and also the high cost weigh heavily against full-scale measurements. The main use of these experiments may well be establishing a model-full-scale relationship making further detailed full-scale work unnecessary or at any rate restricted to isolated checking of model work.

The lack of agreement at the one point considered (Fig. 38) needs looking into with a possible indicated that microphone positioning is critical at any rate when one is close to the jet. A point also to be considered here is the velocity of the jet since at high speeds the jet turbulent structure may not be stable. Indeed, Johannesen (Ref. 24) suggests that there are very low frequency large scale turbulent fluctuations of the jet structure of a period of about one-minute. This could be of great importance very close to the jet.

CHAPTER 11

The response of a rectangular panel to noise pressure loading.

11.1

One of the main purposes of space-correlation measurements is to help in the assessment of the stresses induced in a light structure submitted to intense noise pressure fluctuations. Powell (Ref. 16) has used the Lagrangian - normal mode approach and obtains expressions for panel response. This method, of course, involves the generalised force of the noise pressure field acting in each mode. Powell shows that this generalised force is dependent on the space-correlation of pressure at every point of the structure. The number of space-correlation measurements required in one particular case is, in theory, enormous and therefore some justifiable simplifying assumptions must be made regarding the correlation field.

It is proposed in the following section to discuss Powell's method and to outline the main difficulties of measurement involved and theoretical limitations. Section 11.3 suggests a simplification of the correlation fields and 11.4 gives a numerical calculation of the root mean square panel stress in the fundamental mode.

11.2 Panel response.

For the problems considered in Part I, the generalised force could be expressedeas a function of time but for problems of noise excitation this is not possible; it is only possible to obtain average properties of the panel motion or stresses and therefore one looks for the spectrum of the

generalised force instead of the force itself. Now Powell shows that the spectrum of the generalised force in the mode mn is

$$\ell_{mn}(F) = \omega(F) \iint_{S\,S'} c(F, \vec{r}_1 - \vec{r}_2)\, a_{mn}(\vec{r}_1)\, a_{mn}(\vec{r}_2)\, dS\, dS' \qquad (11.1)$$

where $c(F, \vec{r}_1 - \vec{r}_2)$ is the space-correlation between the pressures on the panel at $\vec{r}_1$ and $\vec{r}_2$. $\omega(F)$ is the power spectral density of the pressure on the panel; an assumption is made here that $\omega(F)$ does not change over the panel. The double integration is over the panel area S . Powell terms the double integral the mode acceptance of the panel.

Liepmann (Ref. 26) shows that for a single degree of freedom system excited by a "noise" force it is possible to relate the input and output spectra by

$$g(F) = \frac{\ell(F)}{|Z(F)|^2} \qquad (11.2)$$

where $g(F)$ is the power spectral density of the output (displacement, stress, etc.) and $Z(F)$ is the impedance of the system containing the damping term and the mass-spring forces. Equation (11.2) is valid only for linear systems and this places a further restriction on the method. For a system with many degrees of freedom (11.2) can be generalised to

$$g_{mn}(F) = \frac{\ell_{mn}(F)}{|Z_{mn}(F)|^2} \qquad (11.3)$$

Now the mean square response in the mn^{th} mode is given by :-

$$\overline{a_{mn}^2} = \int_0^\infty g_{mn}(F)\, dF \qquad (11.4)$$

Hence Powell obtains (through equations 11.1, 3, 4)

$$\overline{a_{mn}^2} = \int_0^\infty \frac{\omega(F)\, A_{mn}(F)}{|Z_{mn}(F)|^2}\, dF \qquad (11.5)$$

It should be noted that equation (11.3) depends upon the fact that the mn equations obtained by the Lagrange method are independent and uncoupled. It was seen in Chapter 6 that there is a possibility of a damping coupling between modes. The extent of this coupling is unknown at present; Powell discusses this in a later paper (Ref. 27) and there is certainly need to investigate this point.

It is instructive to look at each of the terms under the integral sign in equation (11.5).

a) $\omega(F)$. $\omega(F)$ is the power spectral density of the pressure field at the plate surface. Two difficulties are presented by this quantity; firstly the accepted practice in acoustic measurements is an accuracy in pressure level of about ± one decibel. This represents a possible pressure error of ± 11% and accepting this the final answer cannot have a better accuracy. Secondly, and probably more serious, is the pressure doubling effect at a reflecting surface. It was seen in Chapter 3 that the pressure is increased by something approaching 6db at a semi-rigid surface (it is not 6db due to the finite impedance of the surface itself). Thus the free field pressure measurements should be factored by something like 6db (or nearly 100% increase) but the uncertainty

here produces a further source of error.

b) $|Z_{mn}(F)|^2$. For the purpose of discussion consider a flat panel length L, Breadth d, vibrating in simusoidal modes. The mechanical impedance of such a panel is shown by Timoshenko (Ref. 28) and reproduced in Appendix G.

$$|Z_{mn}(F)|^2 = S_{mn}^2 \left[\left(1 - \frac{F^2}{F_{mn}^2}\right)^2 + \delta^2 \frac{F^2}{F_{mn}^2} \right] \qquad (11.6)$$

where S_{mn} is the generalised stiffness, F_{mn} is the mode resonant frequency and δ is the damping ratio

$$\delta = \frac{b}{b_{crit}}$$

where b is the coefficient of the velocity term in the equation of motion and

$b_{crit} = \sqrt{M_{mn} S_{mn}}$, the critical damping.

The difficult term in equation (11.6) is the damping ratio δ. In the case of acoustic loading the damping is due to two effects, structural and acoustic; much work remains to be done on evaluating these terms since at resonance the amplitude is critically dependent on them. It is considered that the results of Chapter 6 throw some light on the acoustic damping and these will be used for a numerical calculation.

Another difficulty associated with $|Z_{mn}(F)|^2$ and also

$A_{mn}(F)$ is the mode shape; sinusoidal modes only are considered in this work, that is free rotation at the plate boundaries; one could equally well consider cosine modes with no rotation at the plate boundaries. However, in practice the boundaries will have some intermediate condition which will mean complicated mode shapes which are probably difficult to determine.

c) $A_{mn}(F)$, the modal acceptance. The modal acceptance contains the space-correlation coefficient in narrow frequency bands and a double integration of this over the panel. This in principle means a numerical integration of the pressure-correlations with reference to a lattice of points on the panel; such a process would mean a large number of experiments but if the correlation lengths are small and very appreciably over the panel then this would have to be done. A simplifying assumption is made in the following section which is that the space-correlation at one point on the panel can be referred to all other points, that is the field is homogeneous over the small region occupied by the panel. The author considers this justifiable on the basis of correlation measurements so far made and it enables a semi-analytic function for $A_{mn}(F)$ to be derived.

11.3 The modal acceptance in a homogeneous correlation field.

For $A_{mn}(F)$ one requires experimental data of filtered space correlation curves. Experiments to date indicate that a very fair approximation to

these curves is given by

$$R(x_1 - x_2) = \exp\left[-\frac{\pi b}{L}|x_2 - x_1|\right] \cos\frac{a\pi}{L}|x_2 - x_1| \qquad (11.7)$$

where L is a typical dimension (e.g. panel dimension or jet diameter).

is seen to depend on the two parameters a,, b; a can be regarded as fixing the distance to first zero crossing of R and b the "decay" of R with separation $|x_2 - x_1|$. It is considered that these two characteristics are the most important from the loading view point. a and b of course will depend on the filter frequency; a probably much more strongly than b. It is assumed that experimental evidence at one point on the panel will be sufficient for all points, that is, the field is homogeneous over the area occupied by the panel. Assuming (11.7), the integration in (11.1) can be carried through for a chosen mode shape; for sinusoidal modes in the $x\{\text{n modes}/\text{length } L\}$ and $y\{\text{m modes}/\text{breadth } d\}$ directions, and taking the correlation to be unity in the y direction one obtains

$$\rho_{mn}(f) = \omega(f) \int_0^d\int_0^d\int_0^L\int_0^L \exp\left[-\frac{b\pi}{L}|x_2 - x_1|\right] \cos\frac{a\pi}{L}(x_2 - x_1) \sin\frac{n\pi x_1}{L} \sin\frac{m\pi y_1}{d} \times \sin\frac{n\pi x_2}{L} \sin\frac{m\pi y_2}{d}\, dx_1\, dx_2\, dy_1\, dy_2 \qquad (11.8)$$

which on integration gives, with $\alpha = \frac{a}{n}$, $\beta = \frac{b}{n}$

$$\rho_{mn}(f) = \frac{4L^2d^2}{\pi^4 m^2 n^2}\omega(f)\left[\frac{b\pi\,(1+\alpha^2+\beta^2)}{(\{1+\alpha\}^2+\beta^2)(\{1-\alpha\}^2+\beta^2)} + \frac{2}{(\{1+\alpha\}^2+\beta^2)^2(\{1-\alpha\}^2+\beta^2)}\left\{\left[(\alpha^2-1-\beta^2)-4\alpha^2\beta^2\right]\left[1-e^{-b\pi}\cos(a-n)\pi\right]\right.\right. \qquad (11.9)$$
$$\left.\left. - (\alpha^2-1-\beta^2)\,4\alpha\beta\, e^{-b\pi}\sin(a-n)\pi\right\}\right] \quad (m \text{ odd})$$
$$= 0 \quad (m \text{ even})$$

This expression is plotted in Fig. 39 for $b = 0.6a$ this gives a first

negative overshoot of D.111.

The above expression (11.9) is well suited to digital computation as is the integral (11.5) giving the mean square response. If the acoustic damping digital programme of Chapter 6 is used then the whole problem can be computed automatically; the power spectral density $\omega(F)$ and a and b (found by experiment) are inserted along with the initial data. It was not possible in the time available to develope such a programme but a rough calculation based on the method is presented in the following section.

11.4 Approximate numerical calculation of the response in the fundamental mode of a panel

Consider a panel length l ; breadth d , thickness h , simply supported so that it vibrates in sinusoidal modes. The panel is situated in a "noise" pressure field with power spectral density $\omega(F)$ and modal acceptance $\rho_{mn}(F)$ given by (11.9). Then the mean square response in the fundamental mode (1.1) is

$$\overline{a_{11}^2} = \int_0^\infty \frac{\omega(F)\, A_{11}(F)\, dF}{S_{11}^2 \left[\left(1 - \frac{F^2}{F_{11}^2}\right)^2 + \delta^2 \frac{F^2}{F_{11}^2} \right]} \qquad (11.10)$$

Now if the damping ratio is small the main contribution to this integral will come from the neighbourhood $F = F_{11}$ thus the effects of $\omega(F)$ and $A_{11}(F)$ outside this region will make little difference unless they have very sharp peaks; Fig. 39 shows that this is not the case for $A(F)$; $\omega(F)$ may be more peaky but if the peak is well removed from $F = F_{11}$ it will make

only a small contribution to the integral. With this assumption $\omega(F) A_{11}(F)$ can be taken outside the integral sign. The solution of the definite integral remaining is given by Hardy (Ref. 29) giving

$$\int_0^\infty \frac{d\eta}{\eta^4 + (\delta^2 - 2)\eta^2 + 1} = \frac{\pi}{2\delta}, \quad \eta = \frac{F}{F_{11}} \tag{11.11}$$

and (11.10) becomes

$$\overline{a_{11}^2} = \frac{\omega(F_{11})\, A_{11}(F_{11})}{S_{11}^2} \cdot \frac{F_{11}\pi}{2\delta} \tag{11.12}$$

and the maximum panel stress at the centre of the panel in the outermost fibres (Ref. 28 and Appendix G) is

$$\overline{\sigma_{max}^2} = \left[\frac{Eh}{2(1-\nu^2)}\right]^2 \left[\frac{\pi^2}{L^2} + \frac{\nu\pi^2}{d^2}\right]^2 \overline{a_{11}^2} \qquad L \leq d$$

$$= \left[\frac{Eh}{2(1-\nu^2)}\right]^2 \left[\frac{\pi^2}{d^2} + \frac{\nu\pi^2}{L^2}\right] \overline{a_{11}^2} \qquad L \geq d \tag{11.13}$$

This is a generalisation of the work by Miles (Ref. 30) to a panel rather than a one-degree of freedom system.

Consider a typical practical example of an aluminium alloy panel situated parallel to the boundary of the jet, about 2 diameters downstream, panel dimensions L = 12", d = 6", h = 0.048", giving a resonant frequency (see Appendix G)

$$f_{11} = \frac{\pi}{2}\sqrt{\frac{Eh^2}{12\rho(1-\nu^2)}} \left[\frac{m^2}{d^2} + \frac{n^2}{L^2}\right] = 144 \text{ c/s}$$

From Fig. 11, Ref. 24 the distance to first zero crossing of the filtered space-correlation is estimated to be 0.65 nozzle diameters or about 14" at this frequency. From equation (11.7) the distance to first zero crossing is given by

$$\frac{a\pi x_0}{L} = \frac{\pi}{2}$$

$$\therefore \quad a = 0.43$$

and for the fundamental mode $n=1$, $\alpha = 0.43$

From Fig. 39 this gives for $A_{11}(F_{11})$

$$A_{11} = 648 \text{ in}^4$$

As regards $\omega(F_{11})$ the mean square level in the $\frac{1}{3}$ octave band centred on 160 c/s is required; a typical value close to the jet might be 140 db (allowing 6 db for pressure doubling). The filter bandwidth is allowed for by substracting 15.6 db = $10\log_{10}$(bandwidth) in the 160 c/s band giving a power spectral density level of 124.4 db/c/s (re 0.0002 dyne/cm^2), this corresponds to a pressure of about 0.7 lb ft^{-2}. The power spectral density is

$$23.7 \times 10^{-6} \text{ lb}^2 \text{ in}^{-4} \text{ sec}$$

The acoustic damping is obtained from Fig. 14; at this frequency

$$kL \equiv ka = 0.905$$

$$\frac{d}{L} \equiv \frac{b}{a} = 0.5$$

giving

$$\frac{b}{\rho c A} = 0.0125 \quad , \quad b = 1.33 \times 10^{-3} \text{ lb sec in}^{-1}$$

Now

$$S_{11} = 215 \text{ lb in}^{-1}$$

$$M_{11} = 0.101 \text{ lb}$$

$$b_{crit} = 0.238 \text{ lb sec in}^{-1}$$

the damping ratio $\delta = 0.0062$

Putting these values in equation (11.12)

$$\sqrt{\overline{a_{11}^2}} = 0.23 \text{in}$$

This is the root mean square amplitude in the fundamental mode ignoring structural damping. It has been calculated on a linear theory which, strictly, only applied for amplitudes smaller than the skin thickness (in this case 0.048") thus this is really a problem in non-linear vibrations hence the desirability of investigating non-linear plate vibration.

One can compute the mean stress level from equation (11.13).

$$\sqrt{\overline{\sigma_{max}^2}} = 9600 \text{ lb in}^{-2}$$

This is the maximum stress in the fundamental mode. A stress of this value would, on the experimental evidence of Hess, Fralich and Hubbard (Ref. 31) produce a fatigue failure in about 5 minutes. In this calculation the whole jet spectrum has not been used and only the fundamental mode has been calculated; thus the above value is optimistic and the failure time would probably be much less than this.

Whilst the above calculation is not claimed to be accurate, it has been useful to get the order of magnitude of the components contributing to the panel vibration.

CHAPTER 12

Conclusions to Part II.

Measurements have been described of the space-correlation of the pressure field close to the boundaries of subsonic air jets, both cold small scale model jets and hot fuel scale jets. The following conclusions are drawn :-

1) The spatial correlation of the pressure field in a direction parallel to the jet boundary is shown to be consistent with the hypothesis that the pressure field close to the jet boundary (roughly within one jet diameter) is a convected field; the convection velocity being approximately one half of the local maximum velocity in the jet. (Fig. 27)

2) Measurements of the broadband pressure spatial correlation shows that the correlation coefficients for model and full scale jets plot close to a common curve (Fig. 31) if the separation distance is normalised with respect to the jet diameter. A convection velocity hypotheses is used to show that this should be the case if the local non-dimensional power spectral density of the pressure field is dependent only on the Strouhal number $\frac{\omega D}{u}$. Measurements on a 2 inches diameter jet and a 21 inches diameter hot jet are consistent with this supposition. (Fig. 29)

3) The simple convection model also shows that the broadband correlation function is independent of jet speed, for a local universal Strouhal number spectrum, and the measurements again support the model. (Fig. 20)

4) The convection model also predicts the form of the filtered

space correlation function and suggests that the distance to the first zero crossing should be $x_1 = \frac{u_c \pi}{\omega}$. Information of the filtered space correlation function is particularly useful in the calculation of structural response to these pressure fields.

5) The work on the full scale hot jet (Chapter 10) on space correlation in the pressure field at points moving away from the jet shows a space correlation field having the characteristics of an acoustic pressure field. The correlation contours (Figs. 35 - 37) are shown to have the characteristics of an acoustic field and have a curvature consistent with sound sources located in the jet.

A simplified calculation has been carried out of the response in the fundamental mode of vibration of a flat rectangular panel. The calculation illustrates some of the difficulties in the way of accurate estimation of panel stresses under random noise loading. In particular the calculations show -

a) the need for space correlation data of the pressure field.

b) the need for data on modal damping - in the present calculation no account was taken of structural damping (the acoustic damping calculated in Chapter 6 was used).

c) the need to use non-linear vibration theory in intense noise fields.

Future work.

The measurements reported here are among the first of this type of a

systematic nature and have given knowledge which perhaps only scratches the surface of the problems. Much more work could profitably be done in the pressure field close to the jet.

The pressure field close to the jet is of particular interest for two important reasons -

a) it is the region in the immediate neighbourhood of the noise generating sources; a more detailed understanding of the noise generation mechanism is required and investigations of the near pressure field should aid this understanding.

b) the most severe structural vibration problems occur when structure is in the intense near field region.

Future work on measurement of the space-time correlation function in the near field would be valuable. This work would further elucidate the validity of the convection hypothesis discussed in Chapter 9. Measurements of the filtered space correlation function are also required for the structural response calculations.

Acknowledgements.

The author is grateful to Professor E.J. Richards for his encouragement and suggestions during the course of the work. To Dr. R.E. Franklin and later Dr. B.L. Clarkson go many thanks for their very helpful supervision. The author is also indebted to Messrs. K.R. McLachlan, D.J. Mead and P.R. Miller for many invaluable discussions. The help received from Dr. G.N. Lance and members of the staff of the Department of Computation at the University of Southampton is also gratefully acknowledged. The financial support for the project came from Vickers Armstrongs (Supermarine) Ltd. to whom the author extends his thanks.

The author is indebted to his wife, Jill, and Mrs. P. Rowlands for typewriting the work.

TABLE 1

n	$\lvert a_n \rvert / P_o$ (in. x 10^{-3})	n^o
0	5.0	172°27'
1	0.3	166°8'
2	1.4	352°44'
3	1.8	362°5'
4	2.4	164°59'
5	2.0	221°5'
6	2.5	231°20'
7	2.5	75°12'
8	4.0	104°13'
9	9.0	140°58'
10	26.0	193°10'
11	1.92	27°48'
12	1.38	105°40'
13	0.99	126°19'
14	0.69	185°
15	0.66	73°19'
16	0.51	152°21'
17	0.35	246°40'
18	0.18	348°42'
19	0.08	86°14'

The Response in the First 20 modes to a plane wave of Amplitude P_o p.s.i frequency 577 c/s. - no axial modes.

TABLE 2

The Response of a Stiffened Cylinder to an Oblique Sound Wave

Modal Amplitudes

Angle of Incidence $\theta = 15^{\circ}$, $F = 240$ c/s

$$10^3 \frac{\bar{C}_{mn}}{P_o} \quad Lb^{-1} in^3$$

n \ m	1	2	3	4	5	6	7	8	9	10
1	0.122	0.576	0.318	0.351	0.404	0.752	1.33	5.64	-	-
2	0.022	0.214	2.53	0.526	0.475	0.587	0.964	7.16	-	-
3	0.041	0.111	0.479	0.573	0.317	0.309	1.11	4.72	-	-
4	0.019	0.053	0.227	0.153	0.048	0.355	0.390	1.13	-	-
5	0.004	0.003	0.004	0.052	0.073	0.067	0.091	0.234	-	-
6	0.001	0.003	0.004	0.005	0.006	0.007	0.009	0.029	-	-
7	0.000	0.000	0.000	0.000	0.000	0.000	0.000	0.003	-	-
8	-	-	-	-	-	-	-	-	-	-
9	-	-	-	-	-	-	-	-	-	-
10	-	-	-	-	-	-	-	-	-	-

TABLE 2 contd.

$\theta = 30°$ F = 240 c/s

n \ m	1	2	3	4	5	6	7	8	9	10
1	0.059	0.284	0.163	0.194	0.252	0.599	2.311	2.32	-	-
2	0.034	0.339	4.09	0.878	0.843	1.19	3.48	2.97	-	-
3	0.156	0.427	1.88	2.31	1.35	1.49	9.36	5.6	-	-
4	0.165	0.447	1.95	1.35	0.453	3.81	7.64	4.24	-	-
5	0.066	0.059	0.079	0.975	1.46	1.56	4.01	1.67	-	-
6	0.053	0.097	0.134	0.177	0.248	0.358	0.825	0.432	-	-
7	0.004	0.009	0.015	0.023	0.031	0.046	0.129	0.081	-	-
8	0.000	0.001	0.002	0.002	0.003	0.005	0.018	0.012	-	-
9	0.000	0.000	0.000	0.000	0.000	0.000	0.002	0.002	-	-
10	0.000	0.000	0.000	0.000	0.000	0.000	0.000	0.000	-	-

TABLE 2 contd.

$\theta = 45^{\circ}$ F = 240 c/s

n \ m	1	2	3	4	5	6	7	8	9	10
1	0.039	0.196	0.118	0.157	0.270	6.27	0.435	0.257	-	-
2	0.011	0.116	1.55	0.396	0.560	9.15	0.639	0.666	-	-
3	0.091	0.255	1.19	1.65	1.29	13.9	1.49	0.230	-	-
4	0.167	0.461	2.12	1.63	0.717	57.0	1.95	0.725	-	-
5	0.108	0.098	0.139	1.92	3.81	40.3	1.98	0.567	-	-
6	0.136	0.255	0.371	0.554	1.06	15.5	0.696	0.242	-	-
7	0.017	0.038	0.067	0.112	0.210	3.15	0.171	0.071	-	-
8	0.003	0.007	0.011	0.018	0.035	0.591	0.036	0.016	-	-
9	-	-	-	-	-	-	-	-	-	-
10	-	-	-	-	-	-	-	-	-	-

TABLE 2 contd.

$\theta = 60°$ F = 240 c/s

n \ m	1	2	3	4	5	6	7	8	9	10
1	0.328	1.79	1.40	5.45	1.07	1.00	0.642	0.506	-	-
2	0.106	1.21	20.7	15.5	4.35	1.64	1.07	1.66	-	-
3	0.593	1.88	11.8	50.8	8.72	2.56	3.50	2.20	-	-
4	1.35	4.13	24.4	54.9	4.73	8.15	1.90	0.621	-	-
5	1.21	1.20	2.18	06.1	52.9	7.69	3.61	1.66	-	-
6	2.09	4.32	8.10	35.4	13.5	4.72	2108	1.10	-	-
7	0.359	0.976	2.01	10.01	3.82	1.56	0.717	0.445	-	-
8	0.089	0.209	0.453	2.18	0.861	0.341	0.201	0.136	-	-
9	0.028	0.042	0.091	0.495	0.189	0.079	0.050	0.035	-	-
10	0.003	0.008	0.018	0.094	0.040	0.017	0.011	0.000	-	-

TABLE 2 contd.

$\theta = 75°$ F = 240 c/s

n \ m	1	2	3	4	5	6	7	8	9	10
1	1.11	21.7	2.56	0.962	0.541	0.543	0.489	0.564	-	-
2	0.393	15.6	38.4	2.59	1.07	0.634	0.437	0.545	-	-
3	2.18	24.5	22.9	9.36	2.55	1.33	2.35	1.85	-	-
4	4.40	47.8	42.5	9.18	1.30	4.31	1.65	0.448	-	-
5	4.23	14.7	3.87	13.7	7.59	2.67	1.37	0.803	-	-
6	8.77	63.2	17.3	6.91	4.03	2.43	1.34	0.814	-	-
7	1.84	15.8	5.35	2.48	1.47	0.910	0.593	0.412	-	-
8	0.552	4.57	1.46	0.656	0.403	0.275	0.199	0.150	-	-
9	0.129	1.07	0.348	0.161	0.104	0.075	0.058	0.045	-	-
10	0.029	0.244	0.081	0.038	0.025	0.019	0.015	0.012	-	-

NOTATION

Part I.

ρ air density

ω angular frequency

t time

d distance between plate and rigid backwall

S plate stiffness/unit area

m plate mass/unit area

T_T total kinetic energy

S_T total strain energy

w radial cylinder shell displacement

v circumferential cylinder shell displacement

u axial cylinder shell displacement

r, ϕ, z cylinder co-ordinates

p_0 incident pressure field

p_i internal pressure field

p_s scattered pressure field

n circumferential mode number

m axial mode number

c velocity of sound

Y_n, J_n Bessel functions

$k = \omega/c$

a = cylinder radius, panel length (Chapter 6)

b = panel breadth (Chapter 6)

a_{mn}, b_{mn}, c_{mn} generalised co-ordinates

$\epsilon_n = 1$	$n = 0$
$\epsilon_n = 2$	n 1
A_n, B_n etc.	coefficients
R_A	acoustic radiation damping
X_A	acoustic reactive impedance
h	shell thickness
β	$\frac{1}{12}(\frac{h}{a})^2$
$2L$	length of cylinder
θ	angle of plane wave axis to cylinder axis
a_{mn}	generalised co-ordinate
X_M	mechanical impedance
$A, B, C \ldots Q$	see Appendix A.
$A_L, A_F, \ldots A_F^{(n)}$	see Appendix A.
Φ_{mn}	generalised force
ϵ	phase difference between plane waves
$\alpha_n, \beta_n, \theta_n$	see equation 5.14
C_1, γ_n	see equation 5.15

PART II

f	frequency c/s $= \frac{\omega}{2\pi}$
R	correlation function
λ	wavelength
k	wave number
U_c	convection velocity
D	jet exit diameter
η	$\frac{\omega D}{U_c}$

L length of panel

d breadth of panel

h thickness of panel

REFERENCES

No.	Author(s)	Title, etc.
1.	J.H. Foxwell and R.E. Franklin	Acoustic effects in the vibration of structures. A.R.C. 19,495 L.A. 41 August 1957.
2.	Lord Rayleigh	Theory of Sound Vol. 1. Dover Pub. 1945 P. 403.
3.	M. Junger	Sound scattering by thin elastic shells. Journal of the Acoustical Society of America, Vol. 24, P. 367, 1952.
4.	P.R. Miller	Free Vibrations of a Stiffened Cylindrical Shell. A.R.C. 19,338. May, 1957.
5.	R.N. Arnold and G.B. Warburton	The Flexural Vibrations of Thin Cylinders. Proc. of Inst.Mach.Eng. (A) Vol.167, 1953.
6.	See end.	
7.	J.H. Foxwell and R.E. Franklin	The Vibration of a Thin-walled Stiffened Cylinder in an Acoustic Field. Aero. Quarterly, Vol.X, February, 1959.
8.	M. Junger	The Physical Interpretation of the Outgoing Wave. Journal of the Acoustical Society of America Vol. 25, P.40, 1953.
9.	F.M. Wiener	The Scattering of Sound by Cylinders and Spheres. Journal of the Acoustical Society of America Vol. 19, P.444, 1947.
10.	-	Mathematical Tables, Vol.VI, X, Bessel Functions. British Assn. for the Advancement of Science, Cambridge University Press, 1952.
11.	C.A. Coulson	Waves. University Mathematical Texts (Oliver and Boyd).
12.	H.B. Dwight	Tables of Integrals and Other Mathematical Data. (MacMillan Book Co.)

No.	Author(s)	Title, etc.
13.	N.W. McLachlan	Bessel Functions for Engineers. (Oxford University Press).
14.	Ming Chen Wang and G.E. Uhlenbeck	Noise and Stochastic Processes (Ed. N. WAX) Dover Pub. 1954.
15.	N. Weiner	Generalised Harmonic Analysis ACTA MATH. 55, 117 (1930)
16.	A. Powell	The Problem of Structural Failure Due to Jet Noise. A.R.C. 17,514. 1955.
17.	R.E. Franklin and J.H. Foxwell	Pressure Fluctuations near a cold, small-scale air jet (measurement of space correlations) A.R.C. 20,182. May, 1958. R & M 3162.
18.	R.E. Franklin and J.H. Foxwell	Correlation in the random pressure field close to a jet. A.R.C. 20,264. June, 1958. R & M 3161.
19.	K.R. McLachlan	Thesis - University of Southampton.
20.	K.R. McLachlan and J.H. Foxwell	Space correlation measurements near a jet engine (unpublished).
21.	See end.	
22.	H.S. Ribner	On the strength distribution of noise sources along a jet. U.T.I.A. REP. 51, April, 1958.
23.	M.J. Lighthill	On sound generated Aerodynamically. PROC. ROY. SOC. A,211, P.564. 1952.
24.	E.E. Callaghan, W.L. Howes and W.D. Coles	Near Noise Field of a Jet-Engine Exhaust. II - cross correlation of sound pressures. N.A.C.A. T.N. 3764.
25.	N.H. Johannesen	The mixing of free Axially symmetric jets of Mach Number 1.40. A.R.C. 18967. Jan. 1957.
26.	H.W. Liepmann	On the application of statistical concepts to the buffeting problem. Journal of Aero. Science. Dec.1952.

No.	Author(s)	Title, etc.
27.	A. Powell	On Structural Vibration excited by Random pressures, with reference to structural fatigue and boundary layer noise. Douglas Rep. No. S.M. 22795.
28.	S. Timoshenko	Engineering Vibrations. (Van Nostrand)
29.	G.H. Hardy	Pure Mathematics. Cambridge University Press - 1948.
30.	J.W. Miles	Structural fatigue under random loading. Journal of Aero. Science 1954.
31.	R.W. Hess, R.W. Fralich and H.H. Hubbard.	Studies of structural failure due to acoustic loading. N.A.C.A. T.N.4050. July, 1957.
32.	L. Cremer	See references in "Technical Aspects of Sound". Vol. 1. Ed. Richardson.
33.	P.G. Kafka	Private Communication.
6.	A.E.H. Love	The Mathematical Theory of Elasticity 4th edition. Cambridge University Press, 1952.
21.	R.A. Archbold and R.E. Franklin	The matching of a fine-bore probe into a condenser microphone.

APPENDIX A

Structural Energies.

1.1

In order to set up the Lagrange equations it is necessary to know the total kinetic and strain energies of the structure (including the skin, frames and stringers) when vibrating in the form

$$u = \sum\sum a_{mn} \cos n\phi \cos \frac{m\pi z}{L}$$

$$v = \sum\sum b_{mn} \sin n\phi \sin \frac{m\pi z}{L}$$

$$w = \sum\sum c_{mn} \cos n\phi \sin \frac{m\pi z}{L} \qquad (A.1)$$

where u, v, w are the axial, tangential and radial displacements and a_{mn}, b_{mn}, c_{mn} are periodic functions of time.

Miller (Ref. 4) has extended the theory of cylindrical shell vibrations (Ref. 5, 6) to include the effects of stiffening. The method consists of representing the principal direct strains and shear strain for an element of the structure in terms of u, v, w and their derivatives; the displacement of a general element is also found. It is then possible to find the stresses in the structure and hence the potential energy (strain energy) in terms of the generalised co-ordinates; the kinetic energy is easily found since the displacement (and therefore the velocity for simple Harmonic motion) is known for a general element. A full development on the above lines is given in Ref. 4 and it is proposed to quote only the final results for the strain and kinetic energies of the skin, frame and stringers. The following notation is used :-

E Young's modulus.

h Skin thickness.

a Cylinder radius.

ν Poisson's ratio.

λ $\frac{m\pi a}{L}$

β $\frac{1}{12}\left(\frac{h}{a}\right)^2$

$(q-1)$ Number of frames in Length L.

A_F Cross sectional area of frame.

$A_F^{(1)}$ First moment of area of frame about skin (note Z (Fig.1) is measured +ve outwards).

$A_F^{(2)}$ Second moment of area of frame about skin.

$A_F^{(3)}$ Third moment of area of frame about skin.

A_L Cross sectional area of stringer.

$A_L^{(1)}$ First moment of area of stringer about skin.

$A_L^{(2)}$ Second moment of area of stringer about skin.

$A_L^{(3)}$ Third moment of area of stringer about skin.

ρ_s Density of skin material.

ρ_f Density of frame material.

ρ_L Density of stringer material.

p Number of stringers.

The total strain energies and kinetic energies for a stiffened cylinder of length 2L with $(q-1)$ frames in length L and p stringers are given by

Total strain energy $S_T = S_s + S_f + S_L$

Total kinetic energy $T_T = T_s + T_F + T_L$

where S_s strain energy of skin for deflection (A.1) over length 2L.

$$S_S = \frac{Eh\pi}{2(1-\sigma^2)}\left(\frac{h}{a}\right)\Big[\bar{a}_{mn}^2\left\{\lambda^2+n^2\left(\frac{1-\sigma}{2}\right)\right\} - a_{mn}b_{mn}\lambda n(1+\sigma)$$
$$- a_{mn}c_{mn}2\sigma\lambda + b_{mn}^2\left\{n^2+\lambda^2\left(\frac{1-\sigma}{2}\right)\right\} + 2n b_{mn}c_{mn} + c_{mn}^2$$
$$+ \beta\left\{a_{mn}^2\left(\frac{1-\sigma}{2}\right)n^2 + \lambda a_{mn}c_{mn}\left(n^2(1-\sigma)-2\lambda^2\right) + b_{mn}^2\left(\frac{3(1-\sigma)}{2}\lambda^2\right)\right.$$
$$\left. + b_{mn}c_{mn}n\lambda^2(3-\sigma) + c_{mn}^2\left((\lambda^2+n^2)^2 - 2n^2+1\right)\right\}\Big] \qquad \text{(A.4)}$$

S_F = strain energy of 2(q-1) frames over length $\underline{2L}$.

$$= \frac{E\pi q r}{2a}\Big[b_{mn}^2 n^2\left\{A_F + \frac{A_F^{(1)}}{a}\right\} + 2n b_{mn}c_{mn}\left\{A_F + \frac{n^2 A_F^{(1)}}{a}\right\}$$
$$+ c_{mn}^2\left\{A_F - \frac{A_F^{(1)}}{a} + \frac{A_F^{(2)}}{a^2} - \cdots + 2n^2\left(\frac{A_F^{(1)}}{a} - \frac{A_F^{(2)}}{a^2} - \cdots\right)\right.$$
$$\left. + n^4\left(\frac{A_F^{(2)}}{a^2} - \frac{A_F^{(3)}}{a^3} - \cdots\right)\right\}\Big] \qquad \text{(A.5)}$$

S_L = strain energy of p longerons over length $\underline{2L}$

$$= \frac{ELp}{2a^2}\left[A_L\lambda^2 a_{mn}^2 - 2\frac{A_L^{(1)}}{a}\lambda^3 a_{mn}c_{mn} + \frac{A_L^{(2)}}{a^2}\lambda^4 c_{mn}^2\right] \qquad \text{(A.6)}$$

And for the kinetic energies.

T_S = kinetic energy of skin over length $\underline{2L}$

$$= \frac{\rho_2 a\pi h L}{2}\Big[\dot{a}_{mn}^2 + \dot{b}_{mn}^2 + \dot{c}_{mn}^2 +$$
$$\beta\left\{3\dot{b}_{mn}^2 + 4n\dot{b}_{mn}\dot{c}_{mn} + \dot{c}_{mn}^2(\lambda^2+n^2) - 2\lambda\dot{a}_{mn}\dot{c}_{mn}\right\}\Big] \qquad \text{(A.7)}$$

T_F = kinetic energy of 2(q-1) frames over length $\underline{2L}$

$$= \frac{\rho_F a\pi}{2}\Big[\left(\frac{qr}{2}-1\right)\left\{\dot{a}_{mn}^2\left(A_F + \frac{A_F^{(1)}}{a}\right) - \dot{a}_{mn}\dot{c}_{mn}2\lambda\left(\frac{A_F^{(1)}}{a} + \frac{A_F^{(2)}}{a^2}\right)\right.$$
$$\left. + \dot{c}_{mn}^2\lambda^2\left(\frac{A_F^{(1)}}{a} + \frac{A_F^{(2)}}{a^2}\right)\right\}$$
$$+ \frac{qr}{2}\left\{\dot{b}_{mn}^2\left(A_F + 3\frac{A_F^{(1)}}{a} + \frac{3A_F^{(2)}}{a^2} + \frac{A_F^{(3)}}{a^3}\right) + \dot{c}_{mn}^2\left(n^2\left(\frac{A_F^{(2)}}{a^2} + \frac{A_F^{(3)}}{a^3}\right) + \right.\right.$$
$$\left.\left. + A_F + \frac{A_F^{(1)}}{a}\right) + 2n\dot{b}_{mn}\dot{c}_{mn}\left(\frac{A_F^{(1)}}{a} + \frac{2A_F^{(2)}}{a^2} + \frac{A_F^{(3)}}{a^3}\right)\right\}\Big] \qquad \text{(A.8)}$$

T_L = kinetic energy of p longerons over length $\underline{2L}$

$$= \frac{\rho_L L}{2}\frac{p}{2}\left[A_L \dot{a}_{mn}^2 + \dot{b}_{mn}^2\left(A_L + 2\frac{A_L^{(1)}}{a} + \frac{A_L^{(2)}}{a^2}\right)\right.$$
$$+ \dot{C}_{mn}^2\left(\frac{A_L^{(2)}}{a^2}(\lambda^2+n^2) + A_L\right) - \dot{a}_{mn}\dot{C}_{mn}\,2\frac{A_L^{(1)}}{a}\lambda$$
$$\left. + \dot{b}_{mn}\dot{C}_{mn}\,2n\left(\frac{A_L^{(1)}}{a} + \frac{A_L^{(2)}}{a^2}\right)\right] \qquad (A.9)$$

1.2

The above expressions are not valid when

$$m = 0, q, 2q, \qquad (A.10)$$

and $n = 0, \frac{p}{2}$,

This is not a serious limitation in the light of the calculations presented in Chapter 4 where it will be seen that it is the lower modal configurations which appear to be important in practice. The (0,0) mode was not investigated in these calculations but slight modifications of the Pegasus programme would enable this to be done.

The reader is referred to Miller (Ref. 4) for an appraisal of the method he uses when stiffening is taken into account. One of the more important conclusions is in fact that the above expressions are only valid when the stiffener spacing is small compared with the mode spacing and this again restricts the problem to the lower order modes.

1.3

The derivatives of the strain and kinetic (with respect to the generalised co-ordinates a_{mn} , b_{mn} , C_{mn} ,) energies are required in the Lagrange equations. Differentiating equations A.2 - 9 the following results are obtained :-

$$\frac{\partial S_T}{\partial a_{mn}} = A a_{mn} - B b_{mn} - C c_{mn} \tag{A.11}$$

where

$$A = \frac{E_L h \pi}{(1-\nu^2)}\left(\frac{h}{a}\right)\left[\lambda^2 + n^2\frac{(1-\nu)}{2} + \beta n^2\frac{(1-\nu)}{2}\right] + \frac{E_L}{2a^2} p\lambda^2 A_L \tag{A.12}$$

$$B = \frac{E_L h \pi}{(1-\nu^2)}\left(\frac{h}{a}\right)\lambda n\frac{(1+\nu)}{2} \tag{A.13}$$

$$C = \frac{E_L h \pi}{(1-\nu^2)}\left(\frac{h}{a}\right)\left[\nu\lambda - \frac{\beta\lambda}{2}\left\{n^2(1-\nu) - 2\lambda^2\right\}\right] - \frac{E_L}{2a^2} p\frac{A_L^{(1)}}{a}\lambda^3 \tag{A.14}$$

$$\frac{\partial S_T}{\partial b_{mn}} = D b_{mn} - B a_{mn} + E c_{mn} \tag{A.15}$$

where

$$D = \frac{E_L h \pi}{(1-\nu^2)}\left(\frac{h}{a}\right)\left[n^2 + \lambda^2\frac{(1-\nu)}{2} + \beta\left\{\frac{3(1-\nu)}{2}\lambda^2\right\}\right] + \frac{E\pi q r}{2a}\left\{2n^2\left(A_F + \frac{A_F^{(1)}}{a}\right)\right\} \tag{A.16}$$

$$E = \frac{E_L h \pi}{(1-\nu^2)}\left(\frac{h}{a}\right)\left[n + \beta n\lambda^2\frac{(3-\nu)}{2}\right] + \frac{E\pi q r}{a}\left[n\left(A_F + n^2\frac{A_F^{(1)}}{a}\right)\right] \tag{A.17}$$

$$\frac{\partial S_T}{\partial c_{mn}} = F c_{mn} + E b_{mn} - G a_{mn} \tag{A.18}$$

where

$$F = \frac{E_L h \pi}{(1-\nu^2)}\left(\frac{h}{a}\right)\left[1 + \beta\left\{(\lambda^2+n^2)^2 - 2n^2 + 1\right\}\right] + \frac{E_L}{2a^2} p\lambda^4 \frac{A_L^{(2)}}{a^2}$$
$$+ \frac{E\pi q r}{2a}\left[2\left(A_F - \frac{A_F^{(1)}}{a} + \frac{A_F^{(2)}}{a^2}\right) + 2n^2\left(\frac{A_F^{(1)}}{a} - \frac{A_F^{(2)}}{a^2}\right) + n^4\left(\frac{A_F^{(2)}}{a^2} - \frac{A_F^{(3)}}{a^3}\right)\right] \tag{A.19}$$

$$G = \frac{E_L h \pi}{(1-\nu^2)}\left(\frac{h}{a}\right)\left[\nu\lambda - \frac{\beta\lambda}{2}\left\{n^2(1-\nu) - 2\lambda^2\right\}\right] - \frac{E_L \rho}{2a^2}\frac{A_L^{(1)}}{a}\lambda^3 \tag{A.20}$$

$$\frac{\partial T_T}{\partial \dot{a}_{mn}} = H \dot{a}_{mn} - J \dot{c}_{mn} \tag{A.21}$$

where

$$H = \rho_s a h \pi h + \rho_f a\pi\left(\frac{q}{2} - 1\right)\left(A_F + \frac{A_F^{(1)}}{a}\right) + \rho_L \frac{1}{2} p A_L \tag{A.22}$$

$$J = \rho_s a h \pi L \beta \lambda + \rho_f a \pi \left(\frac{q}{2} - 1\right)\left(\frac{A_f^{(1)}}{a} + \frac{A_f^{(2)}}{a^2}\right) + \rho_L \frac{LP}{2} \frac{A_L^{(1)}}{a} \lambda \tag{A.23}$$

$$\frac{\partial T_I}{\partial \dot{b}_{mn}} = M \dot{b}_{mn} + N \dot{c}_{mn} \tag{A.24}$$

where

$$M = \rho_s a h \pi L \left[1 + 3\beta\right] + \rho_f \frac{a \pi q}{2} \left[A_f + 3\frac{A_f^{(1)}}{a} + 3\frac{A_f^{(2)}}{a^2} + \frac{A_f^{(3)}}{a^3}\right]$$

$$+ \rho_L \frac{LP}{2} \left[A_L + 2\frac{A_L^{(1)}}{a} + \frac{A_L^{(2)}}{a^2}\right] \tag{A.25}$$

$$N = \rho_s a \pi h L 2\beta n + \rho_f \frac{a \pi q}{2} n \left[\frac{A_f^{(1)}}{a} + \frac{A_f^{(2)}}{a^2} + \frac{A_f^{(3)}}{a^3}\right]$$

$$+ \rho_L \frac{LPn}{2} \left[\frac{A_L^{(1)}}{a} + \frac{A_L^{(2)}}{a^2}\right] \tag{A.26}$$

$$\frac{\partial T_I}{\partial \dot{c}_{mn}} = -J \dot{a}_{mn} + N \dot{b}_{mn} + Q \dot{c}_{mn} \tag{A.27}$$

where

$$Q = \rho_s a \pi h L \left[1 + \beta(\lambda^2 + n^2)\right] + \rho_f a \pi \left(\frac{q}{2} - 1\right) \lambda^2 \left(\frac{A_f^{(1)}}{a} + \frac{A_f^{(2)}}{a^2}\right) \tag{A.28}$$

$$+ \rho_f \frac{a \pi q}{2} \left[n^2 \left(\frac{A_f^{(2)}}{a^2} + \frac{A_f^{(3)}}{a^3}\right) + A_f + \frac{A_f^{(1)}}{a}\right]$$

$$+ \rho_L \frac{LP}{2} \left[\frac{A_L^{(2)}}{a^2} (\lambda^2 + n^2) + A_L\right]$$

APPENDIX B

Details of the calculation for the plane-wave excitation of the frame stiffened cylinder with no axial modes.

The cylinder constants were :-

radius	= a	=	60 ins.
thickness	= h	=	4.8×10^{-3} in
density	= ρ_s	=	0.117 lb/in^3
Young's Modulus	= E	=	10^7 Lb/in^2
Poisson's ratio	= ν	=	0.3

The frame section chosen was :-

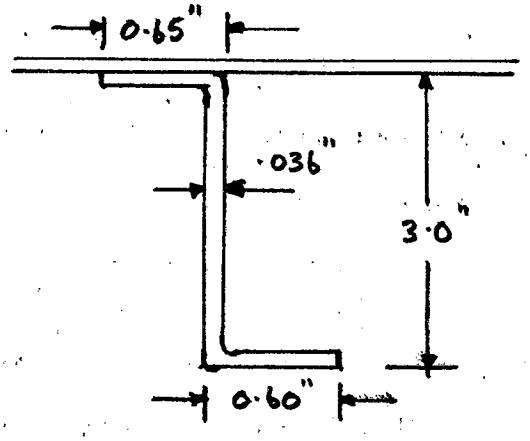

whence

Area of the frame = A_f = 0.153 in^2

Second moment about skin = I_f = 0.560 in^4

Distance of centre of frame from skin = 1.5 in.

The calculation was carried out for the mode n = 10.

Using the above values the constants in the expression for (eqn. (3.35)) are

$$A = 2.688 \times 10^{-3} \quad \frac{\text{lb sec}^2}{\text{in}^2}$$

$B = 5.393 \times 10^4$ lb/in^2

$C = 2.149 \times 10^5$ lb/in^2

$D = 3.170 \times 10^6$ lb/in^2

Other constants used were -

speed of sound $= a = 1120$ ft/sec.

density of air $= \rho = 2.38 \times 10^{-3}$ slugs/ft^3

The functions J_n and Y_n were obtained from Ref. 10 and J_n', Y_n' computed from recurrence relationships.

$$J_n' = \tfrac{1}{2}\left[J_{n-1} - J_{n+1}\right]$$

$$Y_n' = \tfrac{1}{2}\left[Y_{n-1} - Y_{n+1}\right]$$

APPENDIX C

'Pegasus' programme for the response of a stiffened cylinder to an oblique plane sound wave.

1.

The numerical evaluation of $\bar{C}_{mn}$ (4.29) involves a wide range of numerical values which makes the scaling of numbers (necessary for normal fixed point working on 'Pegasus') impractical; also since the sub-routine for the Bessel function evaluation works in floating point arithmetic the whole programme for finding $\bar{C}_{mn}$ has been written in floating point form. This unfortunately makes the computation rather slow.

The main programme computes X_M and separate sub-routines compute P_n, X_n, and Q_{mn}. This allows for incident fields other than the oblique plane wave considered in this work.

2. Operation of the programme

(1) The main programme requires a data tape; this is assembled from data obtained from the DATA CALC. programme.

(2) DATA CALC. Programme :- The 'data calc' programme is fed into the machine with the floating point library containing the sub-routines 101, 610, 11. The initial data has then to be fed in; this data tape is punched in the following way :-

T	0.0	
C	101	
0.2	500	
1	142	
0+	0 72	
0.0+	0 60	
80	- 000	Note: 80 signifies the address where the first piece of data is stored and 27 denotes the number of the data.
27		

			Units
J	0.0		
.0	$E/1-\nu^2$	E = Young's Modulus = Poisson's ratio	(Lb/ft^2)
.1	L	cylinder length = 2L	(ft)
.2	π		-
.3	h	shell thickness	(ft)
.4	a	cylinder radius	(ft)
.5	E		(Lb/ft^2)
.6	+ 2.0		
.7	q	q + 1 = number of frames in length L	
.0	ν		-
.1	P	number of longerons	
.2	$A_L^{(1)}$	1st moment of area of longeron about skin (positive outwards)	(ft^3)
.3	q		
.4	A_F	area of frame	(ft^2)
.5	$A_F^{(1)}/a$	$A_F^{(1)}$ = 1st moment of area of frame about skin (positive outwards)	(ft^2)
.6	$\frac{A_F^{(2)}}{a^2}$	$A_F^{(2)}$ = 2nd moment of area of frame about skin (positive outwards)	(ft^2)
.7	$\frac{A_L^{(2)}}{a^2}$	$A_L^{(2)}$ = 2nd moment of area of longeron etc.	(ft^2)

			Units.
.0	$\frac{A_P(3)}{a^3}$	$A_P(3)$ = 3rd moment, etc.	(ft^2)
.1	ρ	density of material	
.2	q/2 - 1		
.3	P/2		
.4	q/2		
.5	+ 12.0		
.6	A_L		(ft^2)
.7	+ 1.0		
.0	$A_L^{(1)}/a$		(ft^2)
.1	+ 3.0		
.2	+ 2.0		
E	+ 2.0		

Z

This data tape is then fed through the tape recorder.

E 2.0, inhibit optional stop, START and RUN will then do the calculation resulting in the processed data being punched out. This data is used to form a data tape for the main programme which is made up as follows :-

(3) M.P. data tape -The data tape for the main programme is written :-

T	0.0
C	101
0.2	5 00
1	1 42
0+	0 72
0.0+	0 60
128	- 000
42	
J	0.0

This is followed by the 24 numbers obtained from the DATA CALC. programme. Then the following is punched :-

.0	f	frequency	c/s
.1	2π		
.2	c	speed of sound (1120)	ft/sec.
.3	π		
.4	L	Half length of cylinder	ft.
.5	+ 0.0025		
.6	a^2	a = radius of cylinder	ft.
.7	$+ 2/\pi$	+ 0.63661977	
.0	$2\omega L\rho$	ρ = density of air	$\frac{\text{slugs}}{\text{ft. sec.}^2}$
		$\omega = 2\pi F$	
.1	a		ft.
.2	$\cos\theta$		
.3	$\sin\theta$		
.4	$-2\pi a P_o\sqrt{2}$		Lb/ft.
15	π/L		1/ft.
.6	$\sqrt{1-\cos Y}$	$= 2 L k \cos$	
.7	$\frac{\sin Y}{1-\cos Y}$		
.0	+ 180		
.1	+ 90		
E	1.5		

This data tape is fed in after the main programme tape and floating point library tape. Operation of the start key will run the programme.

The print will be :-

n = 1

m	R_A	X_A	ϵ_{mn}	C mn
1				
2				

When the cut off point is reached*, i.e. $km^2 < 0$, the programme prints 0 > KMA ADN, and m is returned to unity; n advanced by one, then :-

n = 2

m	R_A	X_A	ϵ_{mn}	C mn
0				
1				
2				

n is advanced by unity each time.

To investigate a particular m and n, say m_1, n_1, the following short data tape is used :-

T	1.5
n_1	1.40
m_1	2.40
2.1	1 10
2.3	2 10
1 +	0 72
0.0	0 60
E	1.5

Then run, - unless the programme is stopped, n will be advanced on each cycle of the range of m.

* If this does not occur for m = 10 then m is returned to m = 1.

APPENDIX D

Pegasus programme for computing radiation damping from a rectangular panel (Chapter 6)

1.

The analysis of the panel radiation problem in Chapter 6 required the evaluation of an integral of the type (eqn. 6.10) :-

$$I = \int_0^1 \int_0^1 G(ka, m, n, \alpha, \beta, u, v)\, du\, dv \qquad D.1$$

A Pegasus programme has been developed to evaluate this integral over the frequency range (ka) for mode combinations m, n and panel aspect ratio β. The programme is in fixed point working and will work to any required degree of accuracy by altering element size $\Delta u \Delta v$.

Briefly the programme works by dividing the 'square' uv into N^2 elements, evaluating G (D.1) at each co-ordinate (taken as the mid-point of each element) and summing the results. I is thus obtained by multiplying the sum by the area of the element $\Delta u \Delta v$ where

$$\Delta u = \Delta v = N^{-1}$$

2. Flow diagram.

The flow diagram for evaluating I is :-

Set N, m, n, β and $\Delta = 1/N$

Set ka

Set u = $\Delta/2$ and counter Nu

Set v = $\Delta/2$ and counter Nv

Evaluate G using sine, cos, $\int$, S/Rs

Add to sum [illegible] Nu

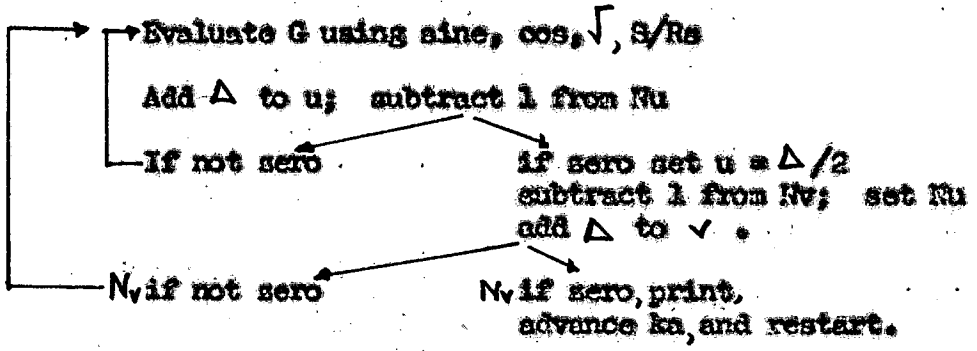

3. Operation of the Programme

The main programme and the fixed point library sub-routines are fed into the machine. The following data tape is then fed through the tape reader :-

	N	
m = m_1	n = n	B = B_1 (< 1) I = I (< 1)
	ϕ	
	- ϕ	
T 3.0		
+ 1/N	Note:- N is the number of sub-divisions	
+1/2N	of the integration	
+ N		
+ N		
+ m1	modes m = $m_1 \geq 1$, n = $n_1 \geq 1$	
+ n1		
+ B1	$B_1 = \beta = b/a$ b the short side. For	
+ I1	$\frac{k_1 a_1}{20}$ b = a put B_1 = + 0.99999.	
T 11.4		
+ P	the programme will evaluate $\frac{R_A}{\rho c A}$ at the points	
J 2.0	$k_1 a_1$, 2 $k_1 a_1$, - - - (P+1) $k_1 a$	

4. Accuracy

The function under the integral sign in equation 6.10 contains the oscillatory terms of the form

$\sin ka v \quad (ka = 2\pi\alpha)$

$\sin m\pi u$ etc.

In the method of computation, the function is evaluated over a lattice of elements thus it is assumed that the gradient of the function is slowly varying over the area of an element. Thus for higher ka, m, n the lattice becomes finer and finer with corresponding increase in computation time. This accuracy should be examined by doing the same computation with a different number of sub-divisions N. The value of N chosen in the computation presented in Fig. 14 is 10 this should be sufficiently accurate for $m, n \leq 2$, $ka < 5$; the accuracy falling away for larger ka.

APPENDIX B

The transformation of the quadruple integral (6.9)

The quadruple integral (6.9) can be converted to a double integral in the following way

Put $\frac{a}{\lambda} = \alpha$, $\frac{b}{a} = \beta$ then from (6.9)

$$\frac{R A_{mn}}{\rho c A} = \frac{\alpha\beta}{4} \int_0^{1}\int_0^{1}\int_0^{1}\int_0^{1} F(\eta-\eta', \xi-\xi') \left[\cos n\pi(\eta-\eta') - \cos n\pi(\eta+\eta')\right] \times \left[\cos m\pi(\xi-\xi') - \cos m\pi(\xi+\xi')\right] d\eta\, d\eta'\, d\xi\, d\xi'$$

$$F(\eta-\eta', \xi-\xi') = \frac{\sin 2\pi\alpha \sqrt{(\eta-\eta')^2 + \beta^2(\xi-\xi')^2}}{\sqrt{(\eta-\eta')^2 + \beta^2(\xi-\xi')^2}} \qquad \text{(E.1)}$$

Change the variables to

$$u = \eta + \eta'$$
$$v = \eta - \eta'$$

The Jacobian

$$J = \left| \frac{\partial(\eta, \eta')}{\partial(u, v)} \right| = -\frac{1}{2}.$$

This maps the interior of the square in the $\eta\eta'$ plane into the interior of the diamond in the u - v plane formed by the lines $v=-u$, $v=-u+2$, $v=u$, $v=u-2$. This is obtained by considering the limits of integration. Looking now at the $\eta\eta'$ integration in (E.1) the inner integral is

$$I_1 = \iint F(v, \xi-\xi') \left[\cos n\pi v - \cos n\pi u\right] |J|\, du\, dv \qquad \text{(E.2)}$$

The u integration may now be done keeping v fixed; the limits are

$u = v$ to $2-v$ $\quad v>0$

$u = -v$ to $2+v$ $\quad v<0$

Integrating w.r.t u and noting that $F(-v) = F(v)$

$$I_2 = \int_0^{1} F(v, \xi-\xi') \left[2(1-v)\cos n\pi v + \frac{2}{n\pi}\sin n\pi v\right] dv \qquad \text{(E.3)}$$

In a precisely similar manner the $(\xi-\xi')$ integral can be reduced, giving the final form

$$\frac{R_{Amn}}{\rho c A} = \frac{\alpha\beta}{4}\int_0^1\int_0^1 F(u,v)\left[2(1-u)\cos m\pi u + \frac{2}{m\pi}\sin m\pi u\right]\times \left[2(1-v)\cos n\pi v + \frac{2}{n\pi}\sin n\pi v\right] du\,dv \qquad (E.4)$$

APPENDIX F.

Space-correlation in a reverberant noise field.

Consider the noise pressure at points P_1, P_2 distant $\vec{r}_1, \vec{r}_2$ from the source which is situated in a reverberant field. The pressures at P_1 and P_2 will consist of direct p_1, p_2 pressures and "reflected" pressures π_1, π_2. The space-correlation coefficient between the points P_1, P_2, will be

$$R(\vec{r}_1 - \vec{r}_2) = \frac{\overline{(p_1+\pi_1)(p_2+\pi_2)}}{\sqrt{\overline{(p_1+\pi_1)^2}}\sqrt{\overline{(p_2+\pi_2)^2}}} \qquad \text{(F.1)}$$

where $\overline{\ }$ indicates a time average. Now since this is a noise source π_1 and π_2 will be the result of random reflections from the walls of the enclosure and if one is a long way from the wall it can be said that :-

a) π_1 and π_2 will be uncorrelated i.e. $\overline{\pi_1\pi_2} = 0$

b) π_1, π_2 and p_1 will be uncorrelated i.e. $\overline{\pi_1 p_1} = 0 = \overline{\pi_2 p_1}$

c) π_1, π_2 and p_2 will be uncorrelated i.e. $\overline{\pi_1 p_2} = 0 = \overline{\pi_2 p_2}$

hence F.1 becomes

$$R(\vec{r}_1 - \vec{r}_2) = \frac{\overline{p_1 p_2}}{\sqrt{\overline{(p_1+\pi_1)^2}}\sqrt{\overline{(p_2+\pi_2)^2}}} \qquad \text{(F.2)}$$

as against the true free field value

$$R(\vec{r}_1 - \vec{r}_2) = \frac{\overline{p_1 p_2}}{\sqrt{\overline{p_1^2}}\sqrt{\overline{p_2^2}}} \qquad \text{(F.3)}$$

Close to the source and a long way from the walls of the enclosure the pressure will be predominated by the direct component p. If $\pi = \frac{p}{4}$ then the error in R would be about 6% too low. In the Chilbolton full-scale

tests it is considered that the reflected pressure would not approach this value of ½ and that the inaccuracy of R due to the reverberation is at worst 5% and probably much better since the "hydrodynamic" preasures in the near field are much greater than the "acoustic" reflections. The same applies to the near field model measurements.

APPENDIX G

The stresses in a vibrating rectangular plate.

Timoshenko (Ref. 28) derives expressions for the modal displacements and stresses in a rectangular simply supported (round the edges) plate.

The plate displacement is specified by

$$W = \sum_m \sum_n \phi_{mn} \sin \frac{n\pi x}{a} \sin \frac{m\pi y}{b} \qquad (G.1)$$

Expressions are derived for the strains in an element distance z from the mid plane of the plate, total thickness h. From these, the direct and shear stresses follow :-

$$\sigma_x = \frac{-Ez}{(1-\nu^2)} \left[\frac{\partial^2 W}{\partial x^2} + \nu \frac{\partial^2 W}{\partial y^2} \right]$$

$$\sigma_y = \frac{-Ez}{(1-\nu^2)} \left[\frac{\partial^2 W}{\partial y^2} + \nu \frac{\partial^2 W}{\partial x^2} \right] \qquad (G.2)$$

$$\tau = \frac{-Ez}{(1-\nu^2)} \frac{\partial^2 W}{\partial x \partial y}$$

Using G.2, the strain energy of the plate may be found; the kinetic energy follows from

$$K.E = \frac{\rho h}{2} \iint \dot{w}^2 \, dx \, dy \qquad (G.3)$$

and the Lagrange equations then give

$$M_{mn} \ddot{\phi}_{mn} + \beta_{mn} \dot{\phi}_{mn} + S_{mn} \phi_{mn} = Q_{mn}(t) \qquad (G.4)$$

where β_{mn} is the damping term and

$$M_{mn} = \frac{\rho hab}{4} \quad = \text{the generalised mass.}$$

$$S_{mn} = \frac{\pi^4 ab E h^3}{48(1-\nu^2)}\left[\frac{m^2}{a^2}+\frac{n^2}{b^2}\right]^2$$ = the generalised stiffness.

From G.4 the mechanical impedance is

$$|Z(\omega)|^2 = S_{mn}^2\left[\left(1-\frac{\omega^2}{\omega_{mn}^2}\right)^2 + \delta_{mn}^2\left(\frac{\omega}{\omega_{mn}}\right)^2\right]$$

where

$$\delta_{mn} = \left[\frac{\beta}{\beta_{crit}}\right]_{mn}, \quad \beta_{crit} = \sqrt{M_{mn} S_{mn}}, \quad \omega_{mn} = \sqrt{\frac{S_{mn}}{M_{mn}}}$$

From G.1 and G.2 the mean square stress can be related to the mean square displacement in any mode, viz.

$$\overline{\sigma_x^2}_{mn} = \left[\frac{Ez}{(1-\nu^2)}\right]^2 \overline{\phi^2}_{mn}\left[\frac{m^2\pi^2}{a^2}+\nu\frac{n^2\pi^2}{b^2}\right]^2 \qquad (G.5)$$

which is a maximum at

$$z = \frac{h}{2}$$

This theory assumes that the displacement w is small compared with the plate thickness; in the case of thin panels under intense acoustic loading, this will not be the case, hence the need for non-linear terms to be included.

FIGURES.

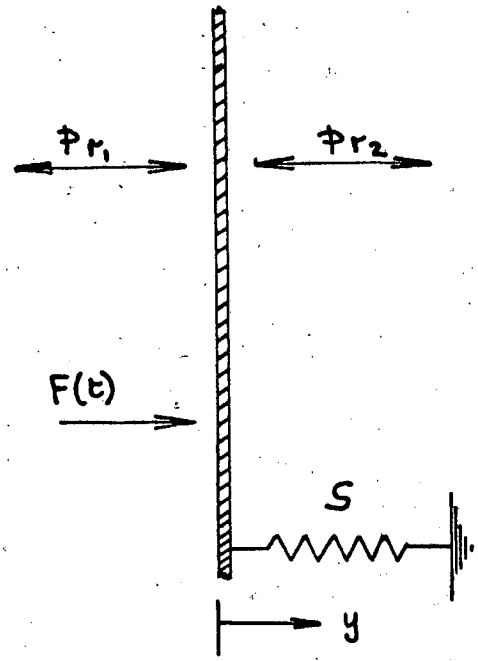

FIG.1

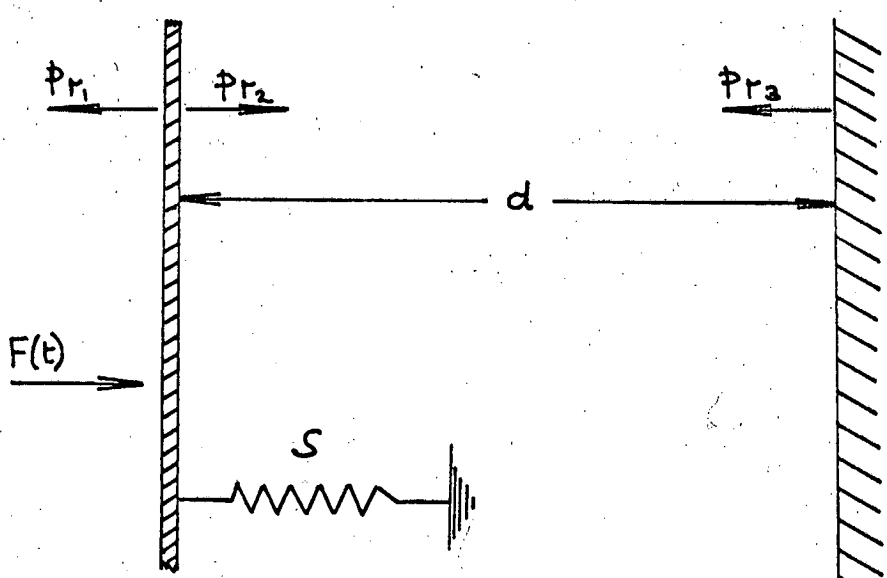

FIG.3

FIG.2

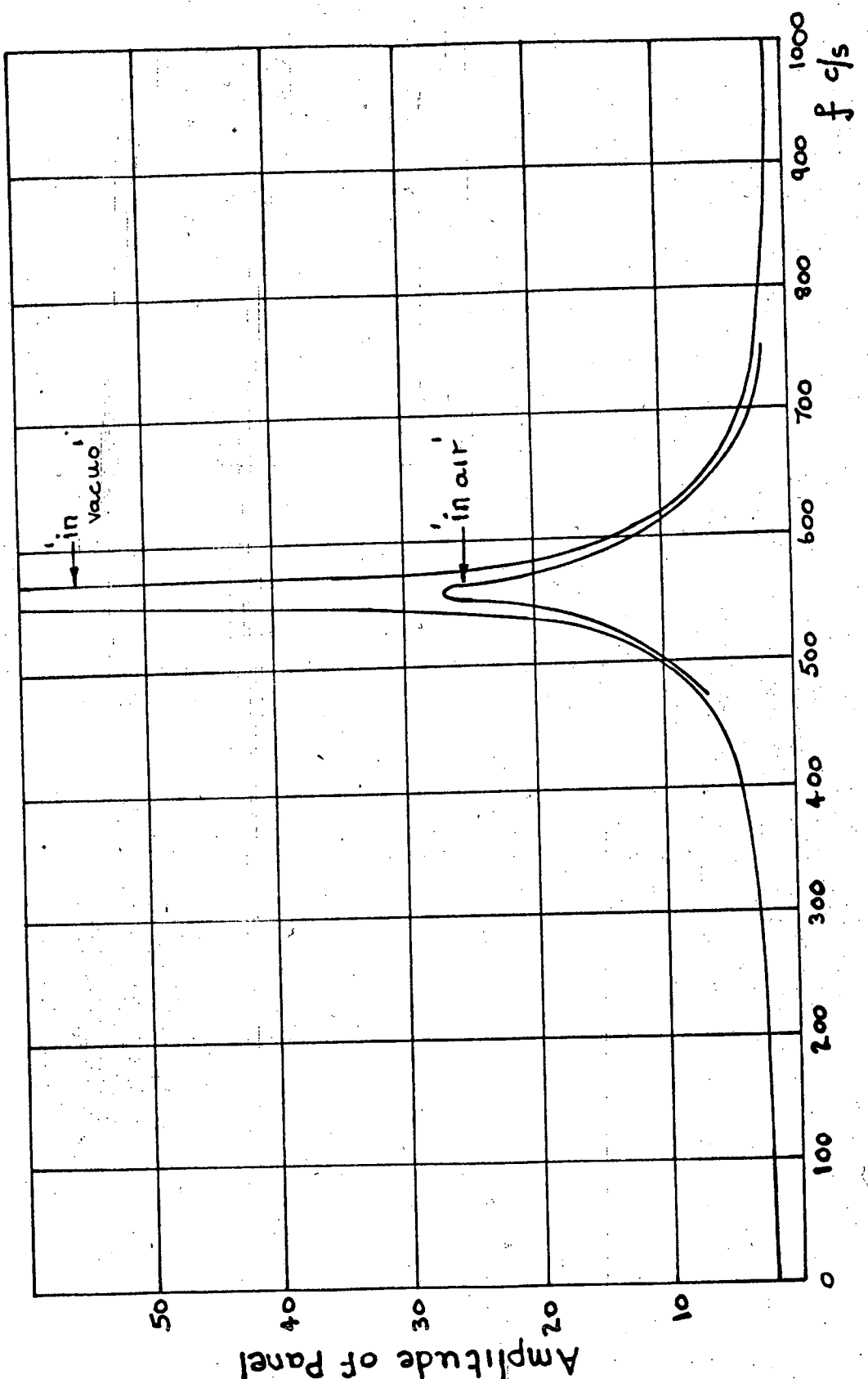

Panel response [resonance 560 c/s]

FIG.4

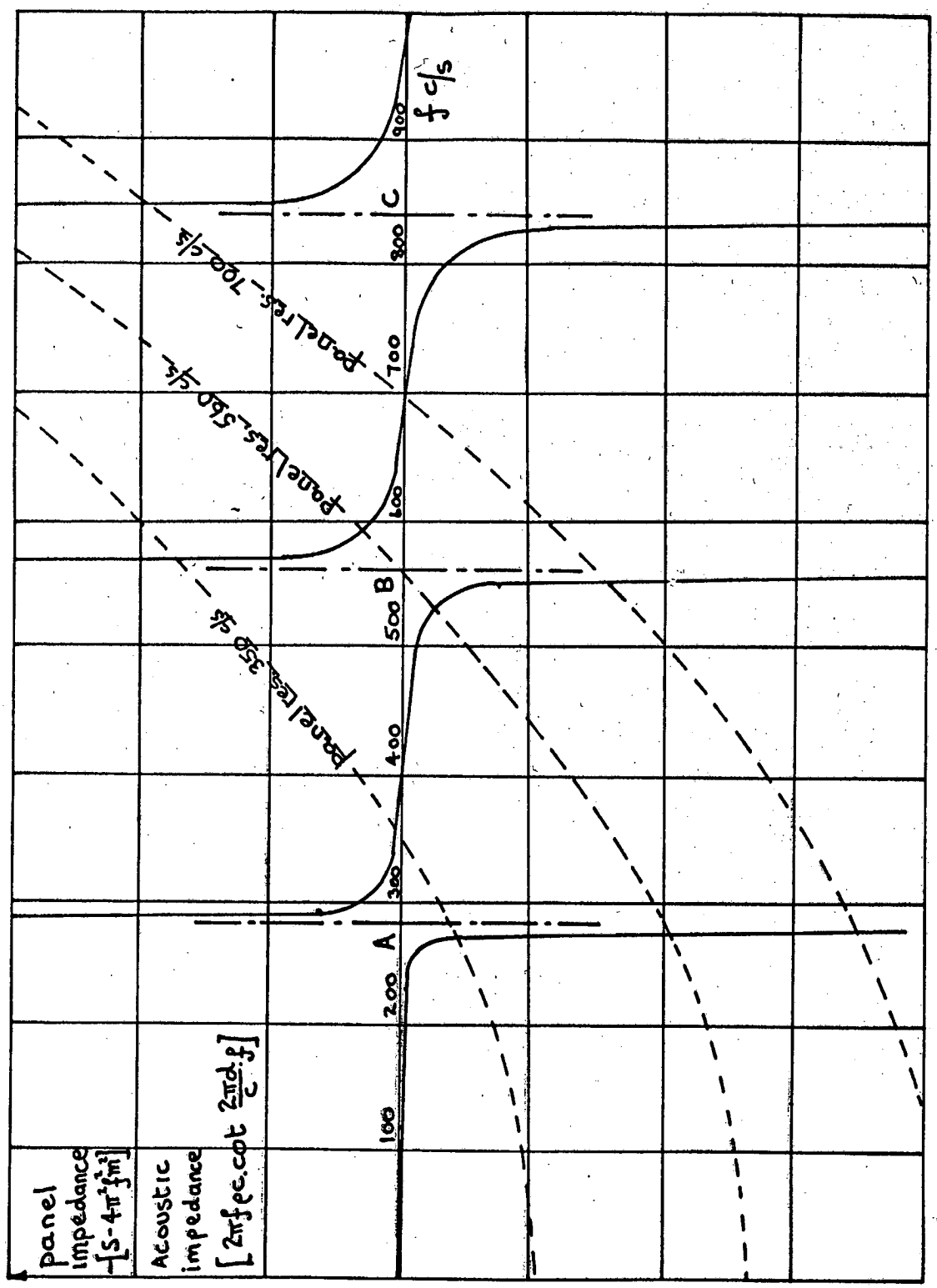

Mechanical and acoustic impedances of panel and cavity.

[intersections of these curves denote resonances.]

FIG.5

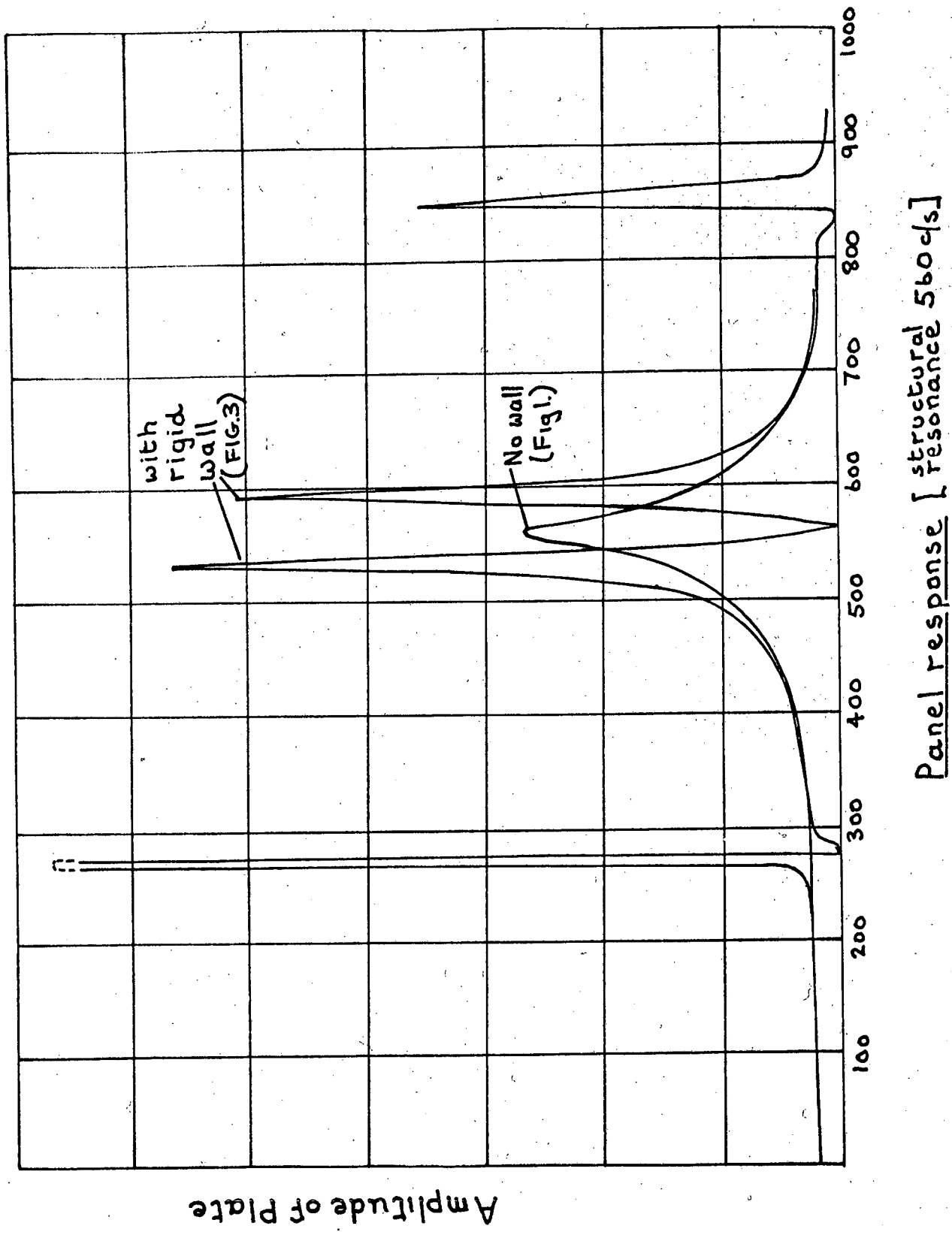
Amplitude of plate
100
200
300
400
500
600
700
800
900
1000
Panel response [structural resonance 560 c/s]
with rigid wall (FIG.3)
No wall (Fig.1.)

FIG.6

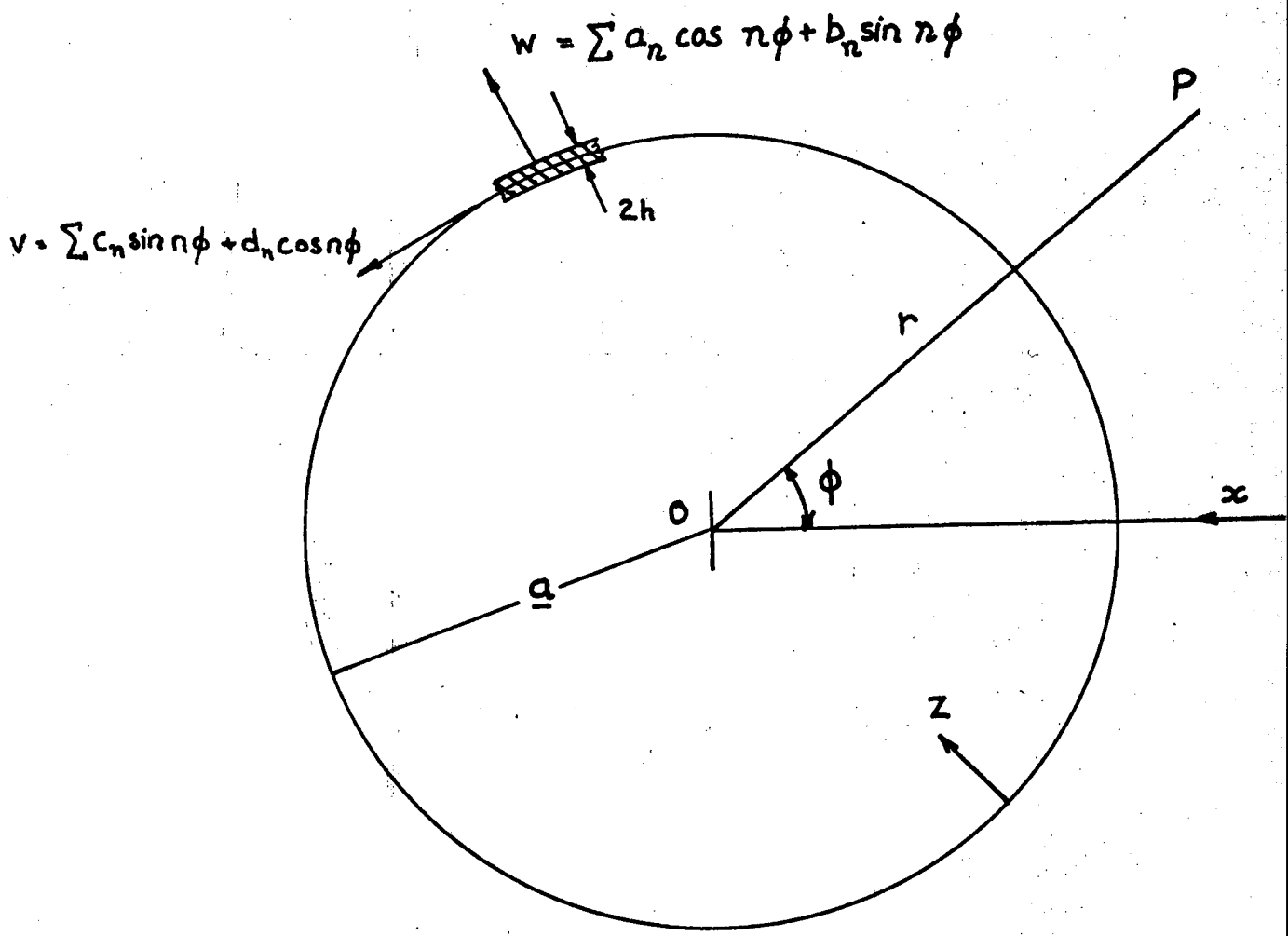

Coordinate System.

FIG.7

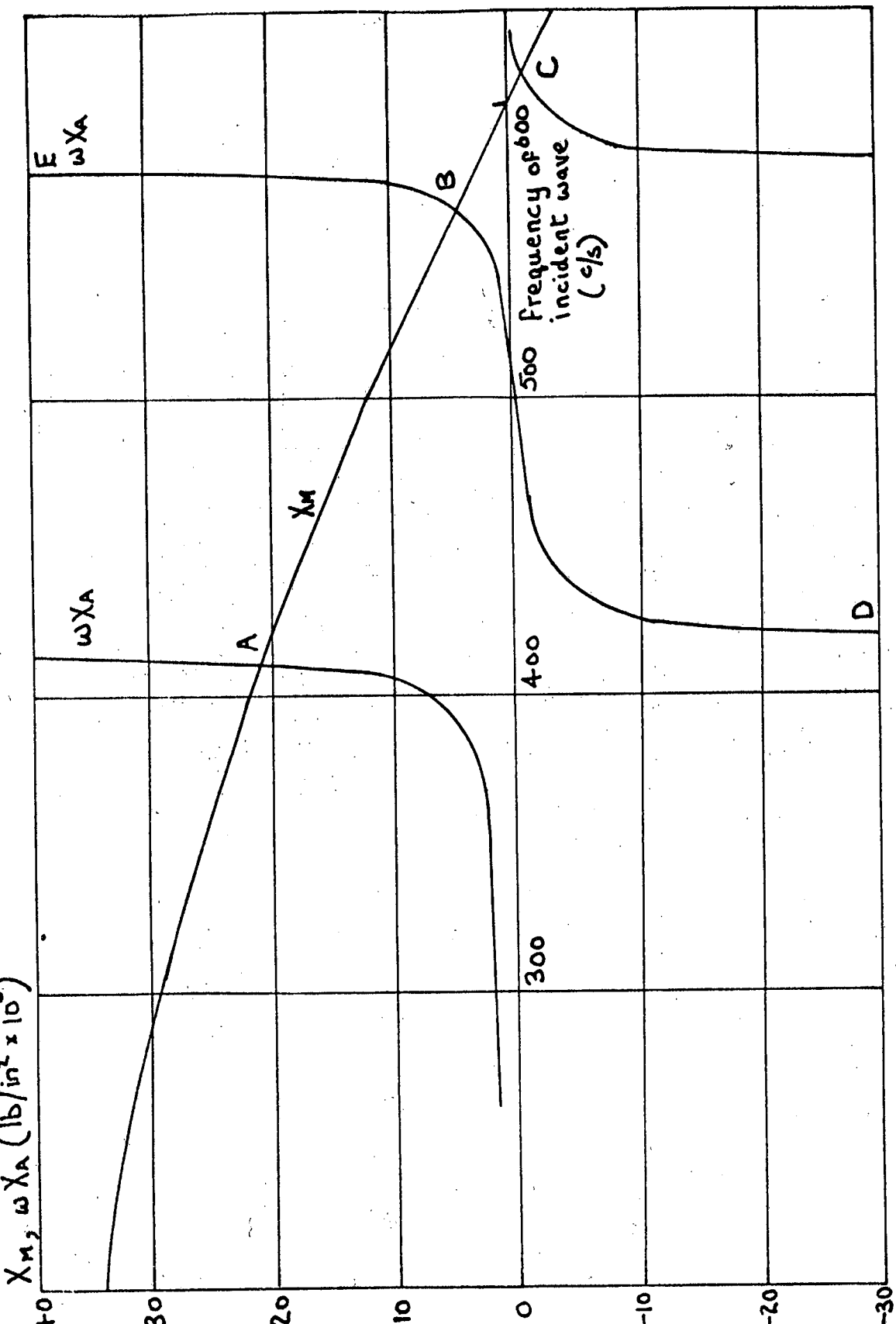

Cylinder impedances for mode n = 10

FIG. 8

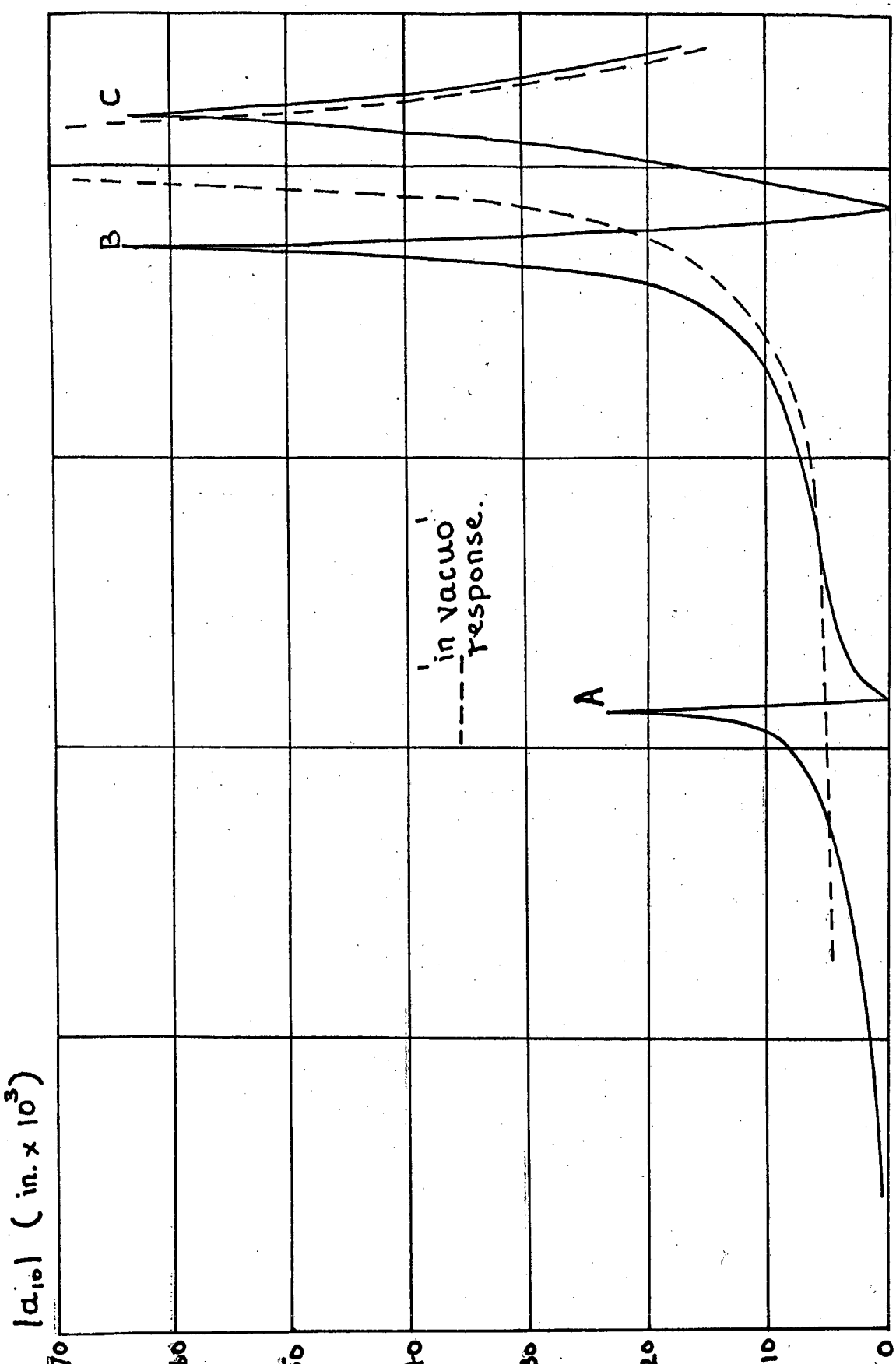

Response of cylinder in mode n = 10 excited by a plane sound wave - amplitude 1 p.s.i.

FIG. 9.

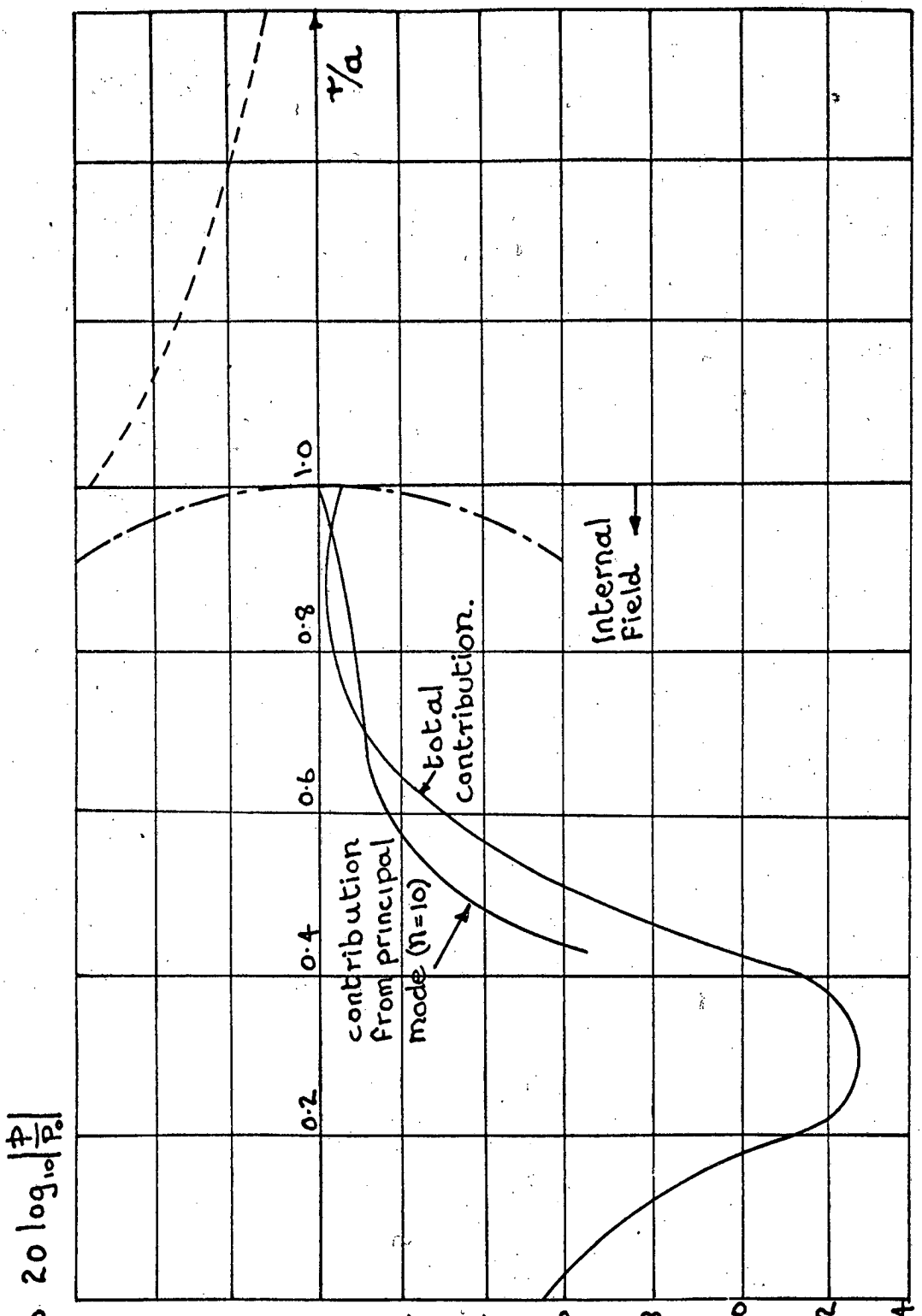

The sound field along $\phi = 0$ for an incident plane wave of amplitude P_0 and frequency 577 c/s.

FIG.10.

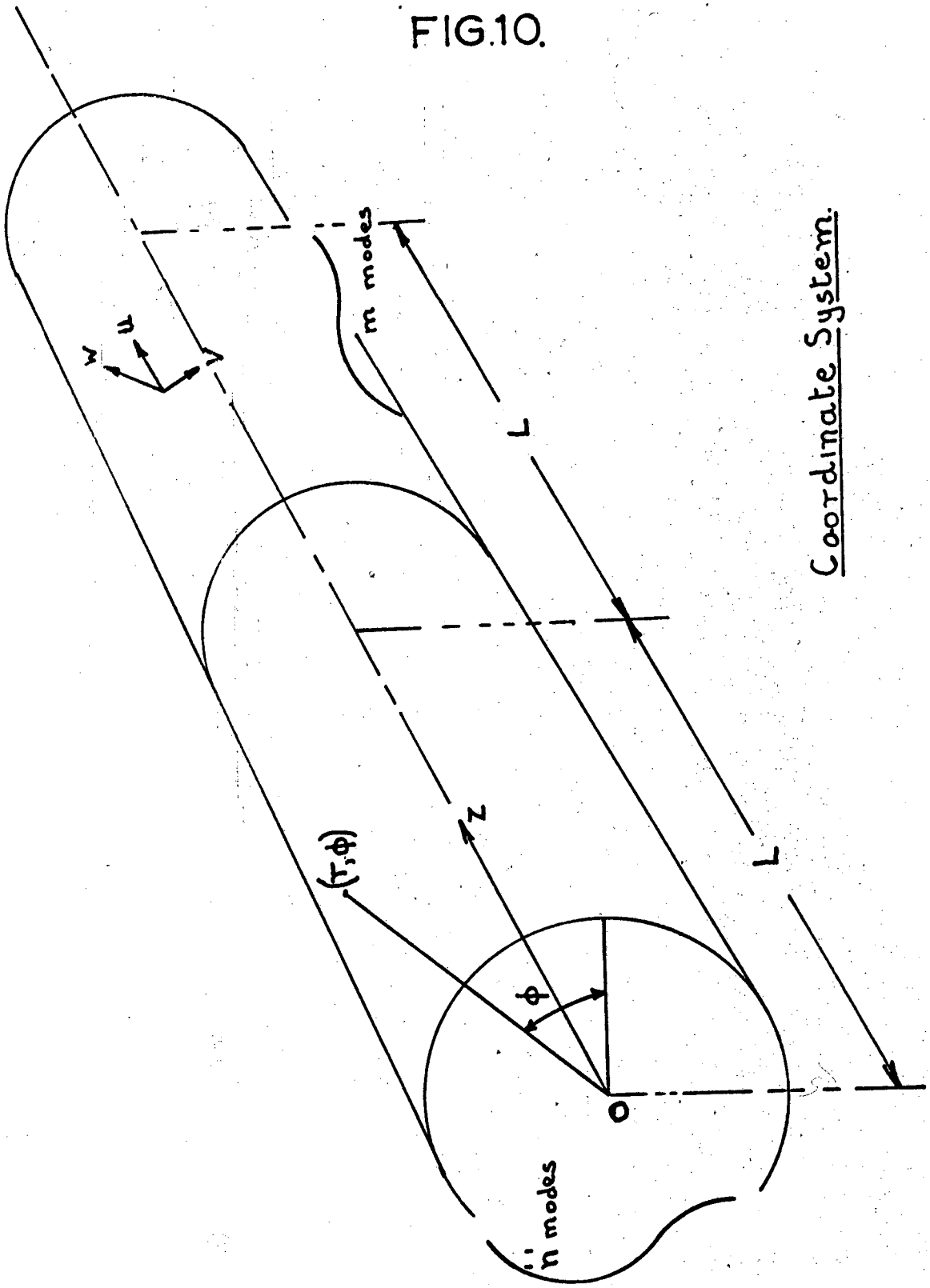

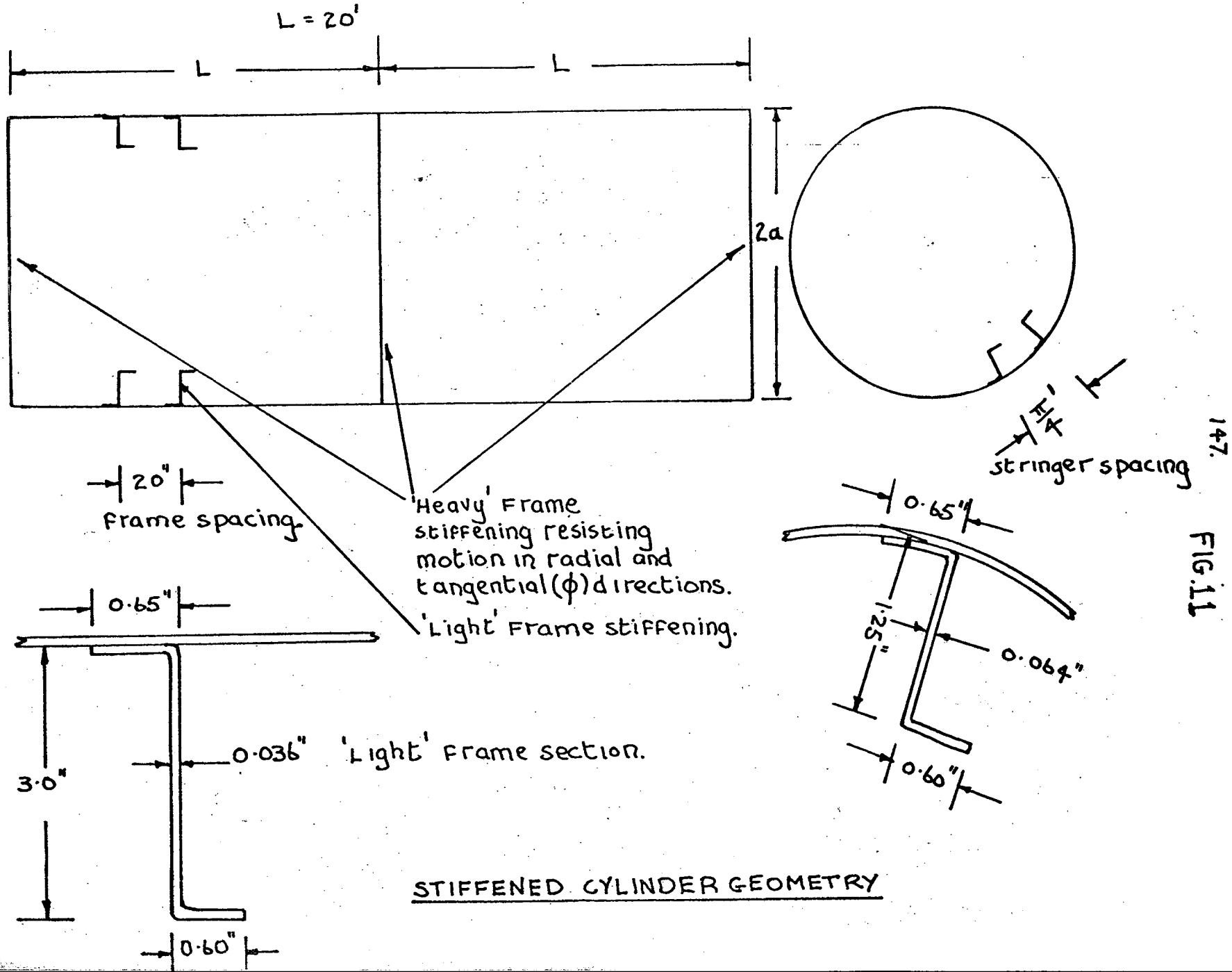

STIFFENED CYLINDER GEOMETRY

FIG. 11

FIG.12.

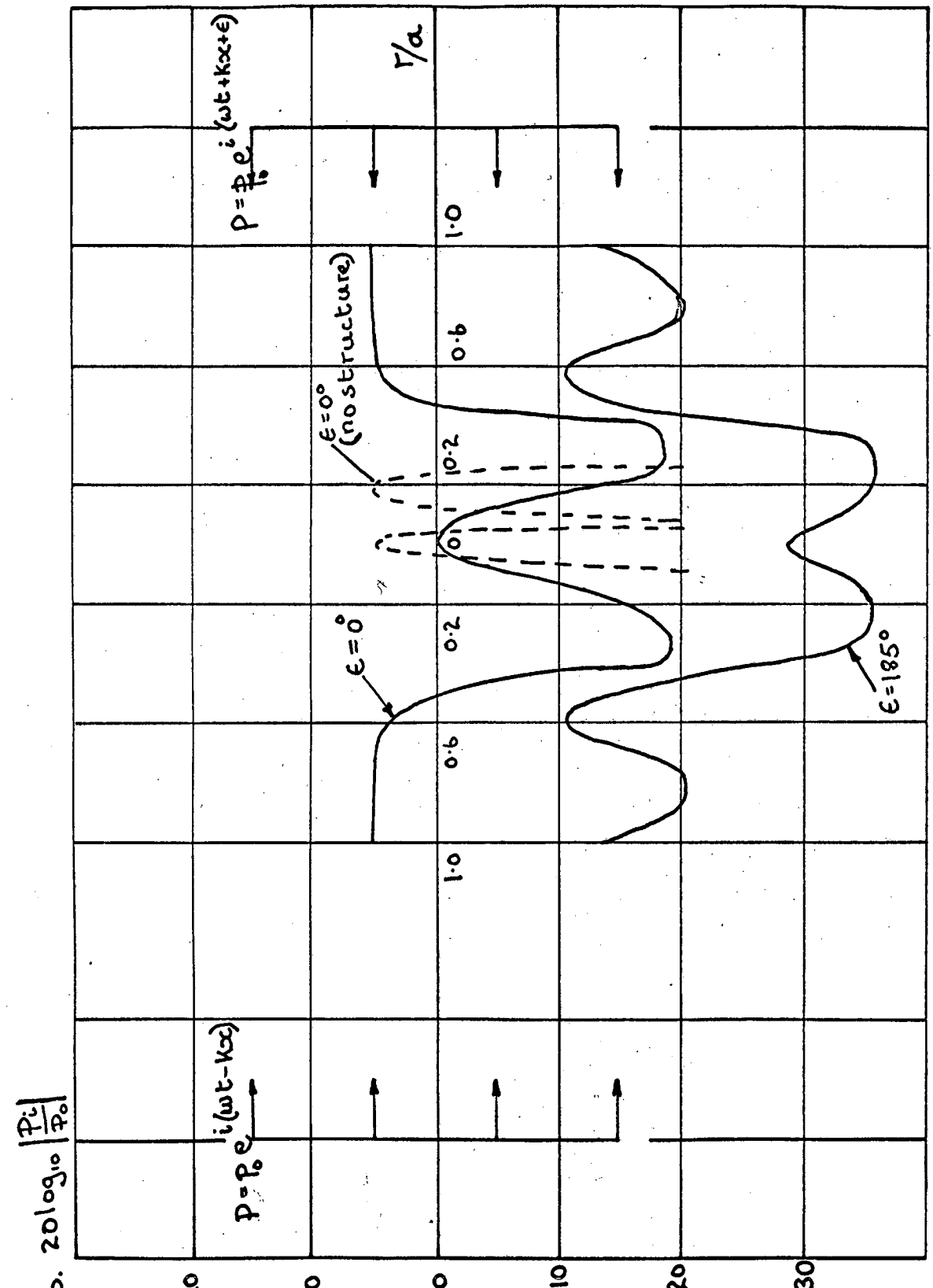

The effect of the phase angle between plane sound waves incident on opposite sides of a thin-walled cylinder

Frequency 577 c/s.

FIG.13.

Flexible panel in infinite rigid wall.

FIG.14.

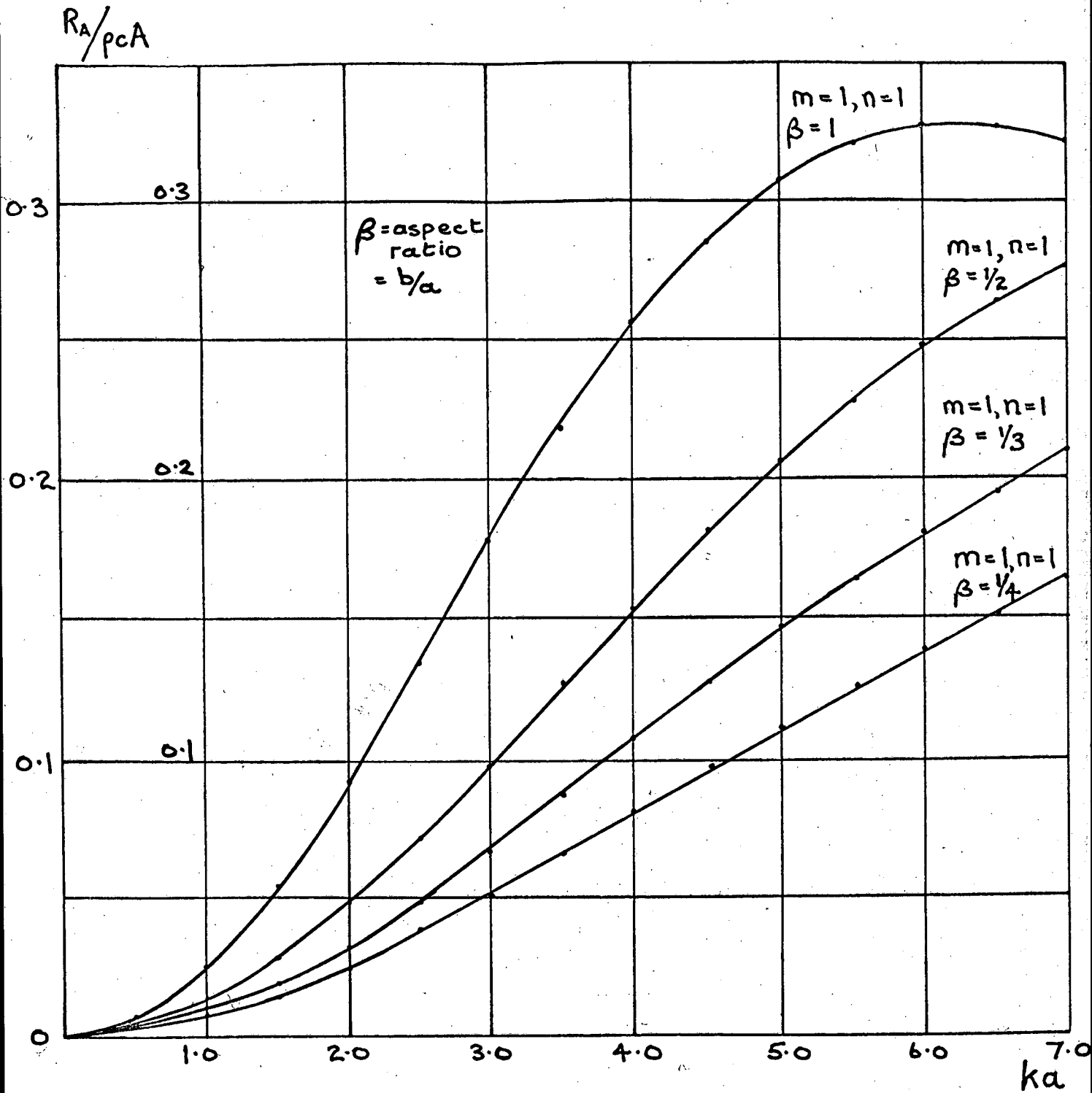

Acoustic damping in the fundamental mode of a panel set in an infinite rigid wall.

FIG.15.

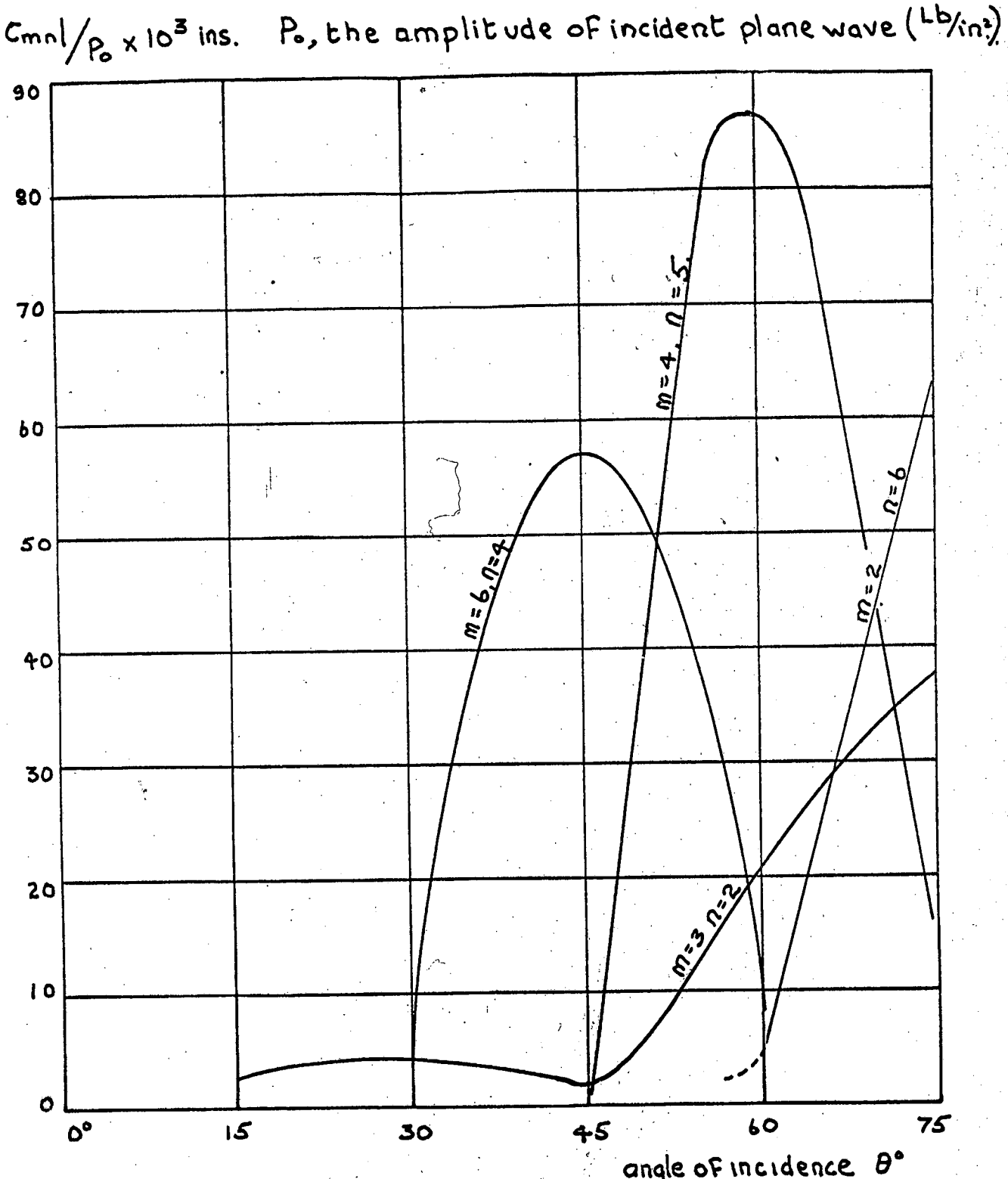

RESPONSE OF STIFFENED CYLINDER TO OBLIQUE PLANE SOUND WAVE. F = 240 c/s - SOME IMPORTANT MODES (SEE ALSO TABLE 2.).

FIG.16.

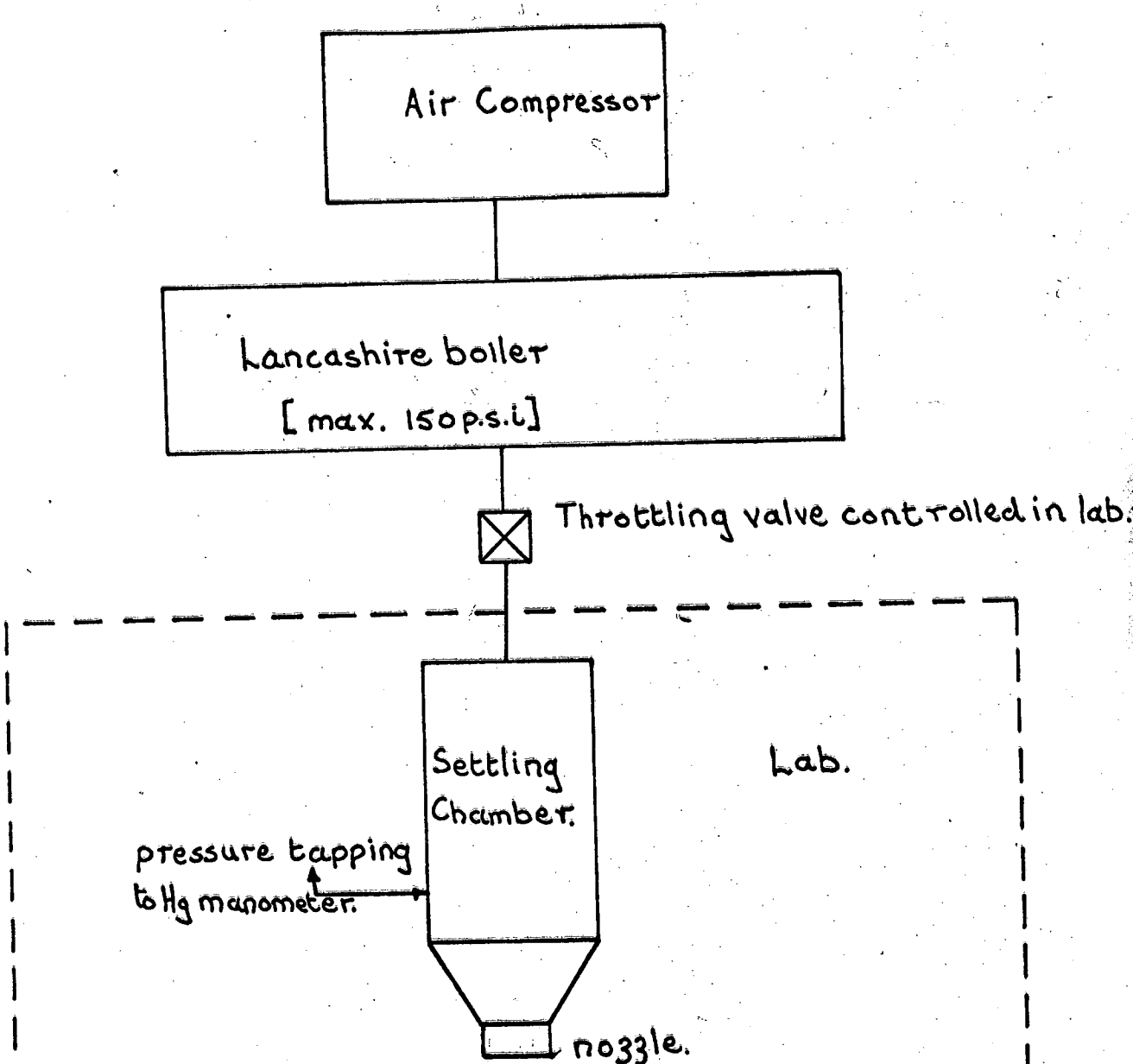

Sketch of air supply system.

FIG.17.

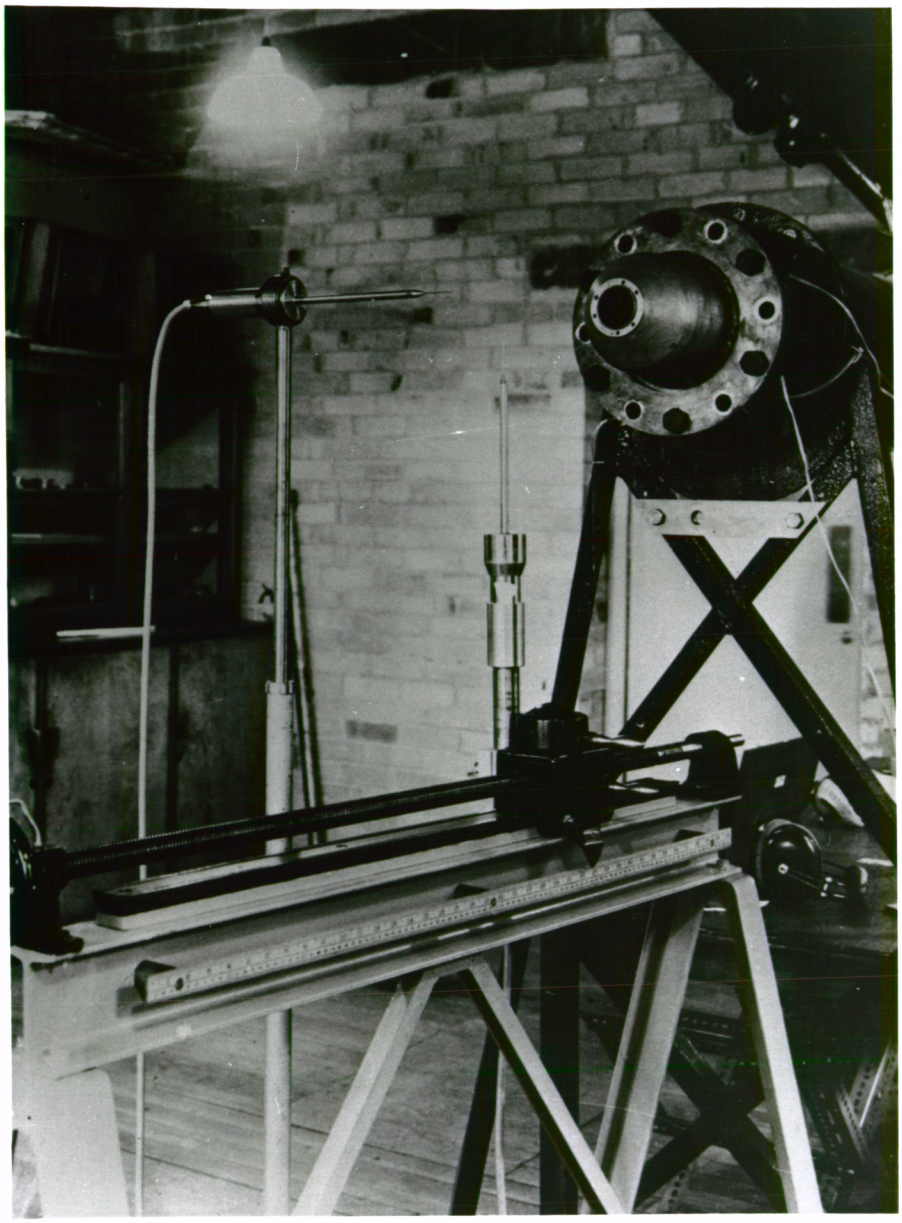

2" MODEL JET SHOWING PROBE MICROPHONES AND TRAVERSING RIG.

FIG.18.

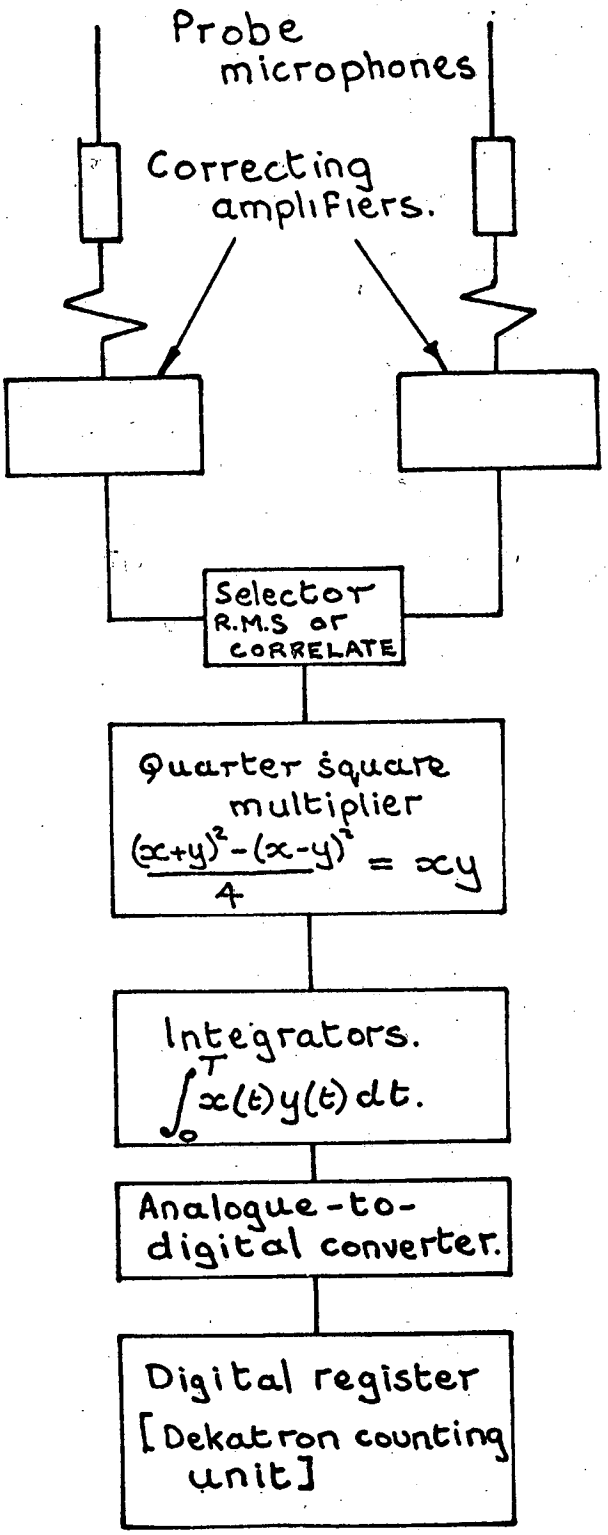

Block Diagram of Correlator

FIG.19.

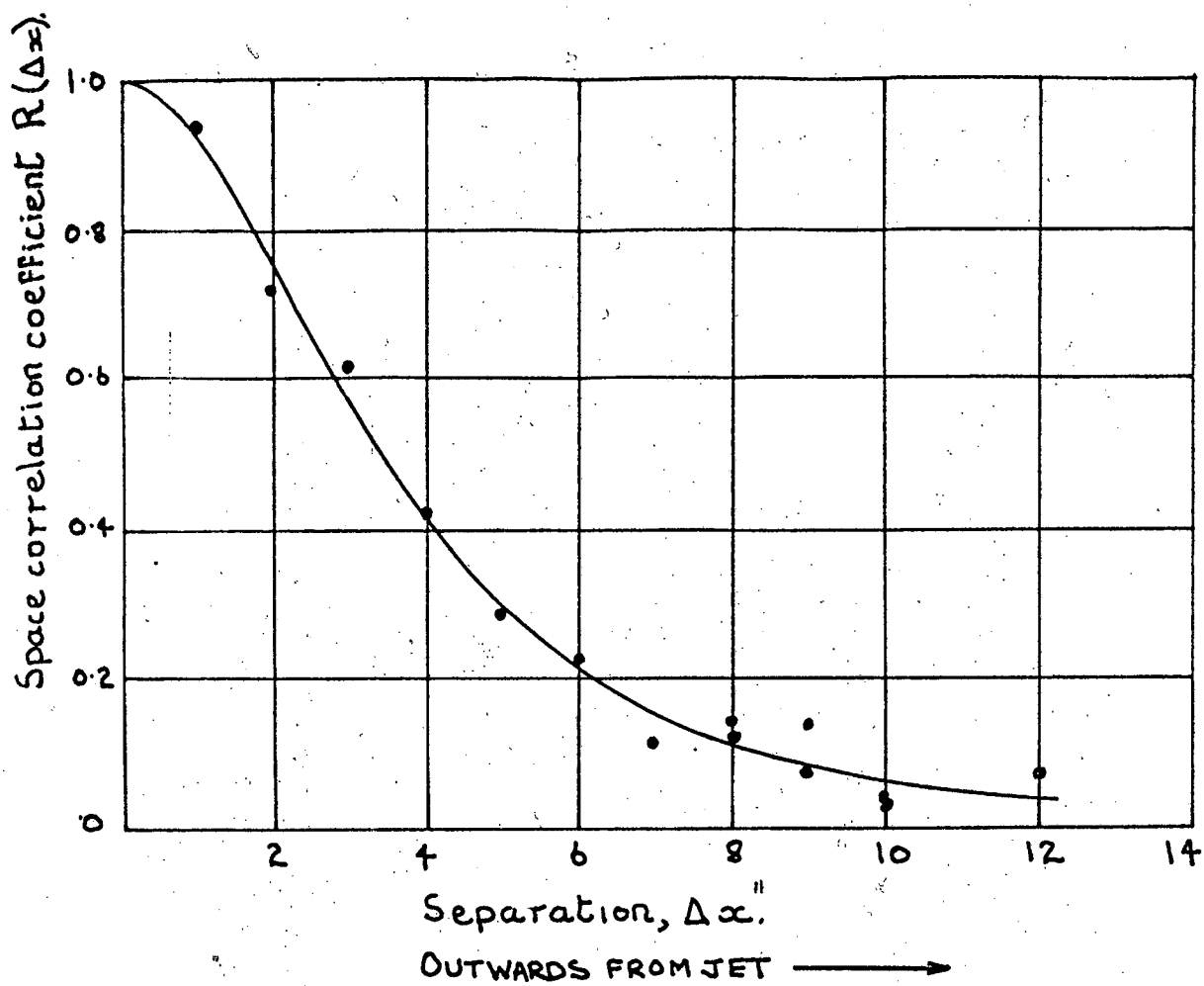

2" dia. cold jet, jet velocity 490 ft/sec, reference point 6·2 dias. downstream 0·5 dia. from jet boundary.

SPACE CORRELATION COEFFICIENT OF PRESSURES.

LATERAL TRAVERSE.

FIG.20

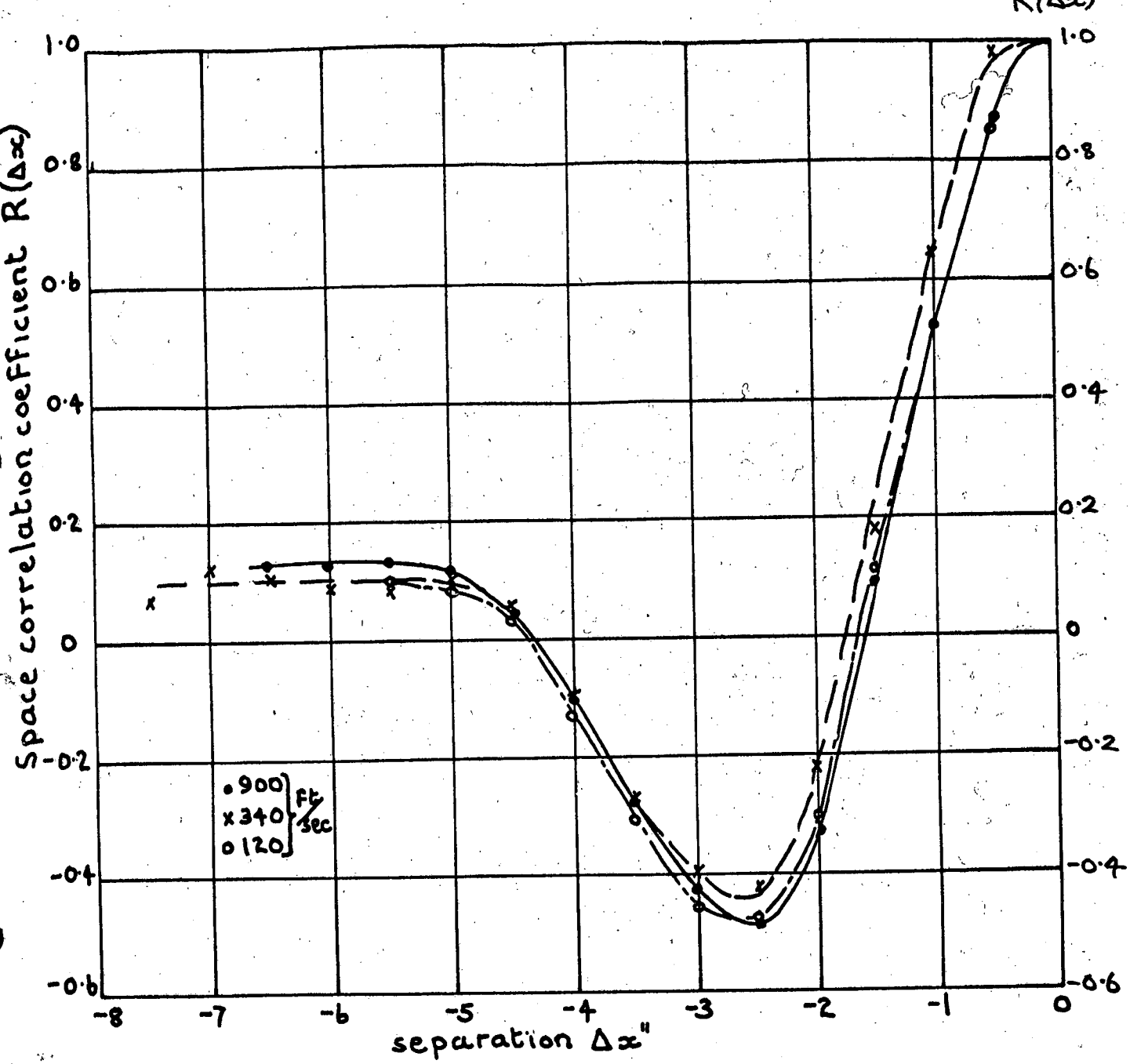

——— upstream.

reference microphone 5 dia. downstream, 0·5 dia. from jet boundary.

VARIATION OF LONGTITUDINAL SPACE-CORRELATION CURVES WITH JET VELOCITY.

FIG.21.

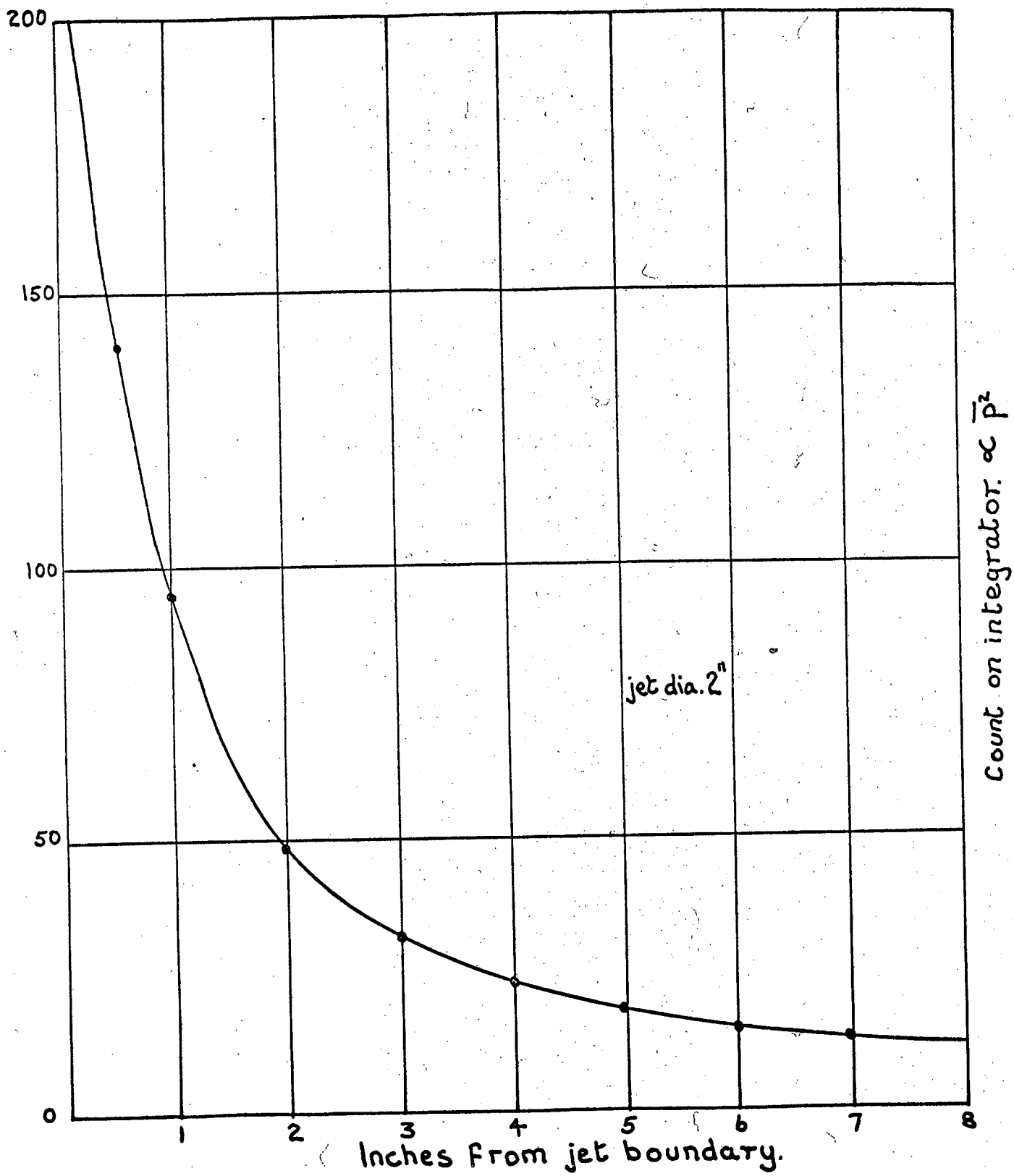

Variation in signal from traversing microphone during lateral traverse.

FIG.22.

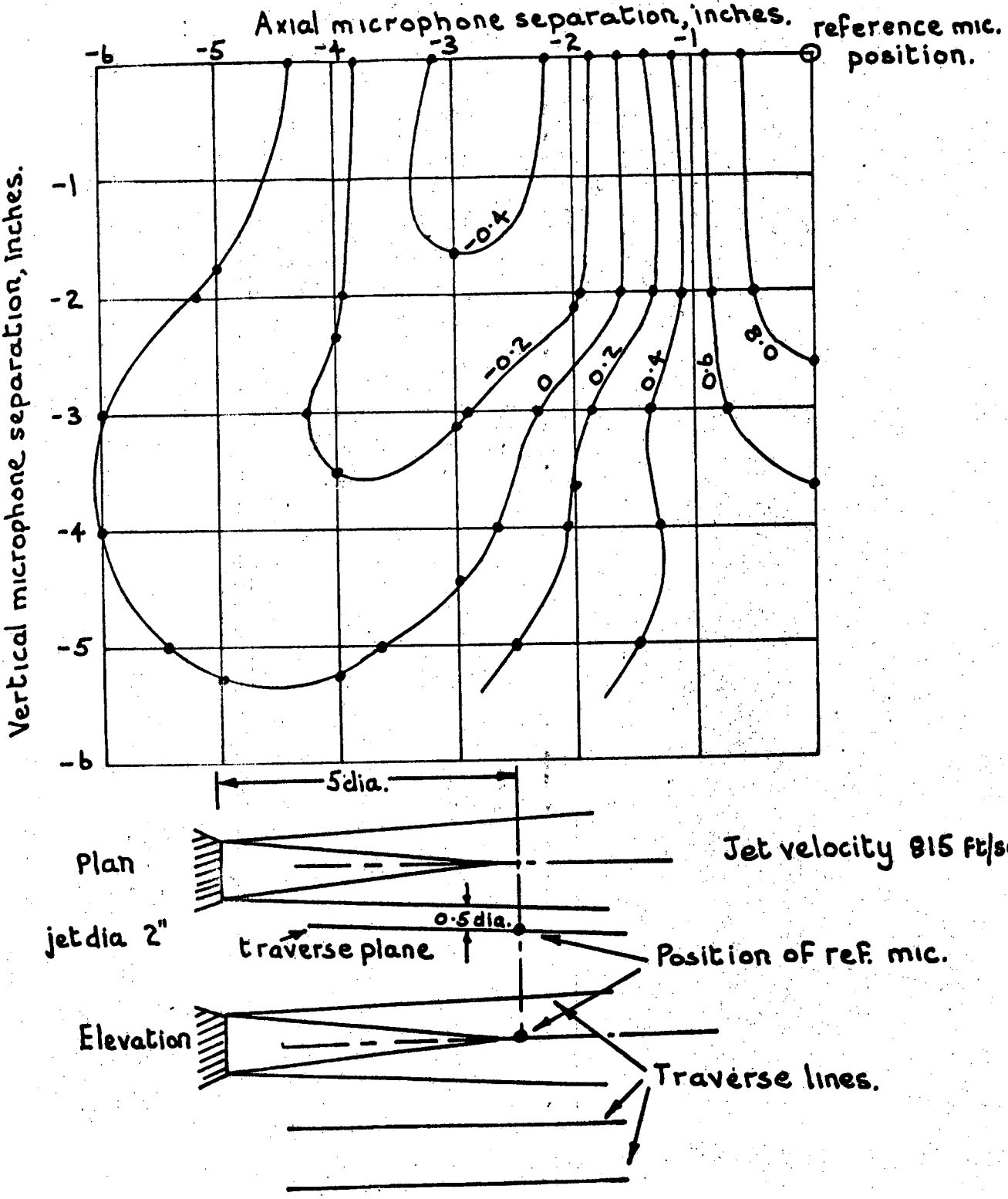

CONTOURS OF ISO-SPACE-CORRELATION COEFFICIENT

FIG.23

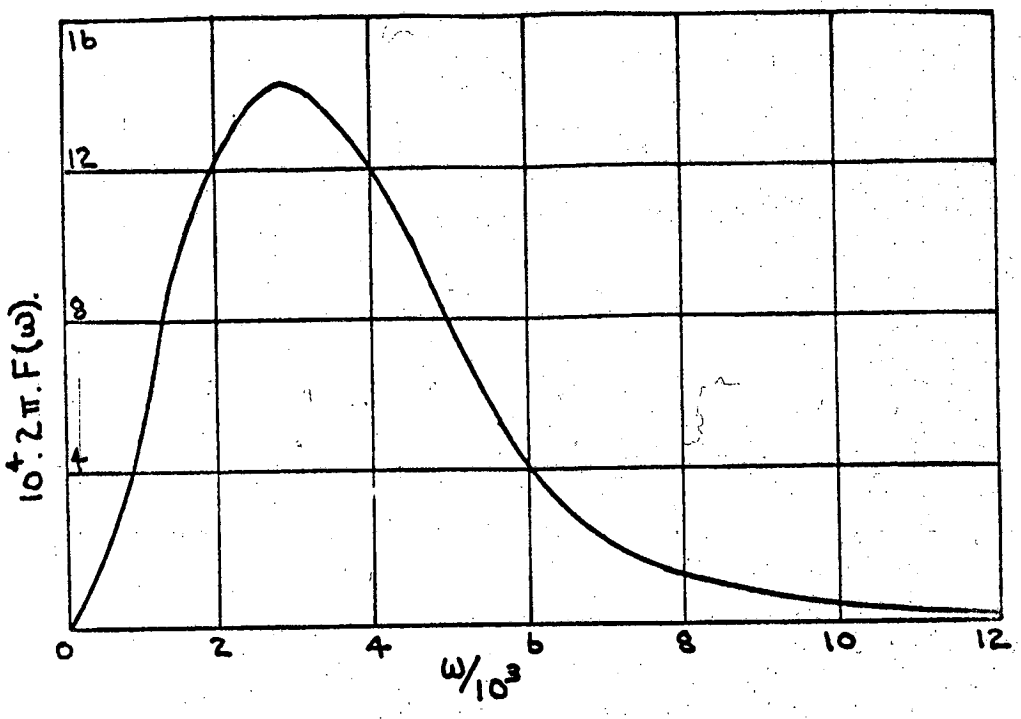

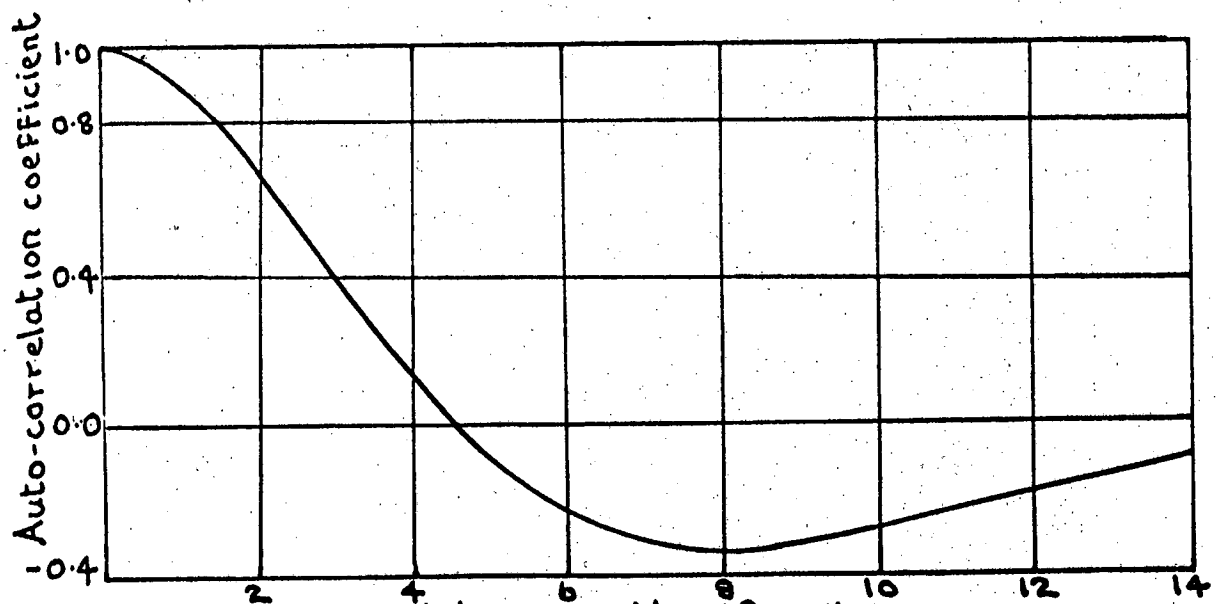

jet velocity 710 ft/sec, jet dia. 2"

NORMALISED POWER SPECTRAL DENSITY AND AUTO-CORRELATION COEFFICIENT.

FIG.24.

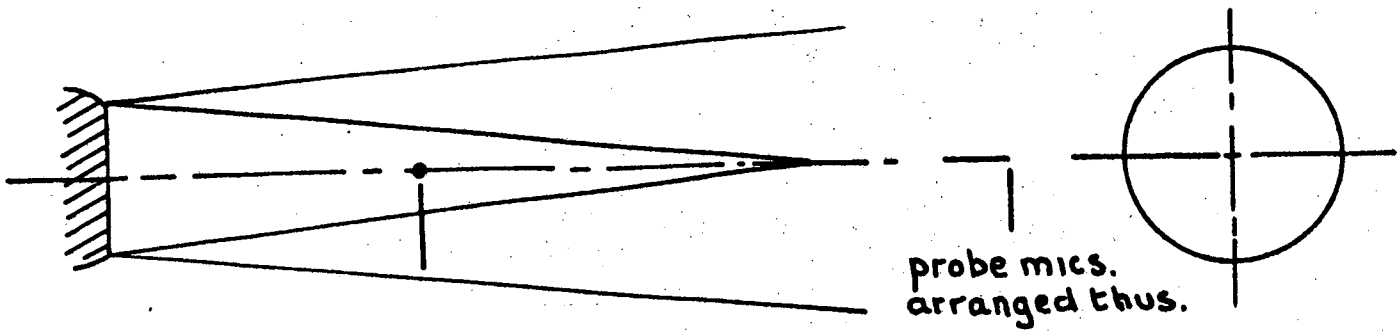

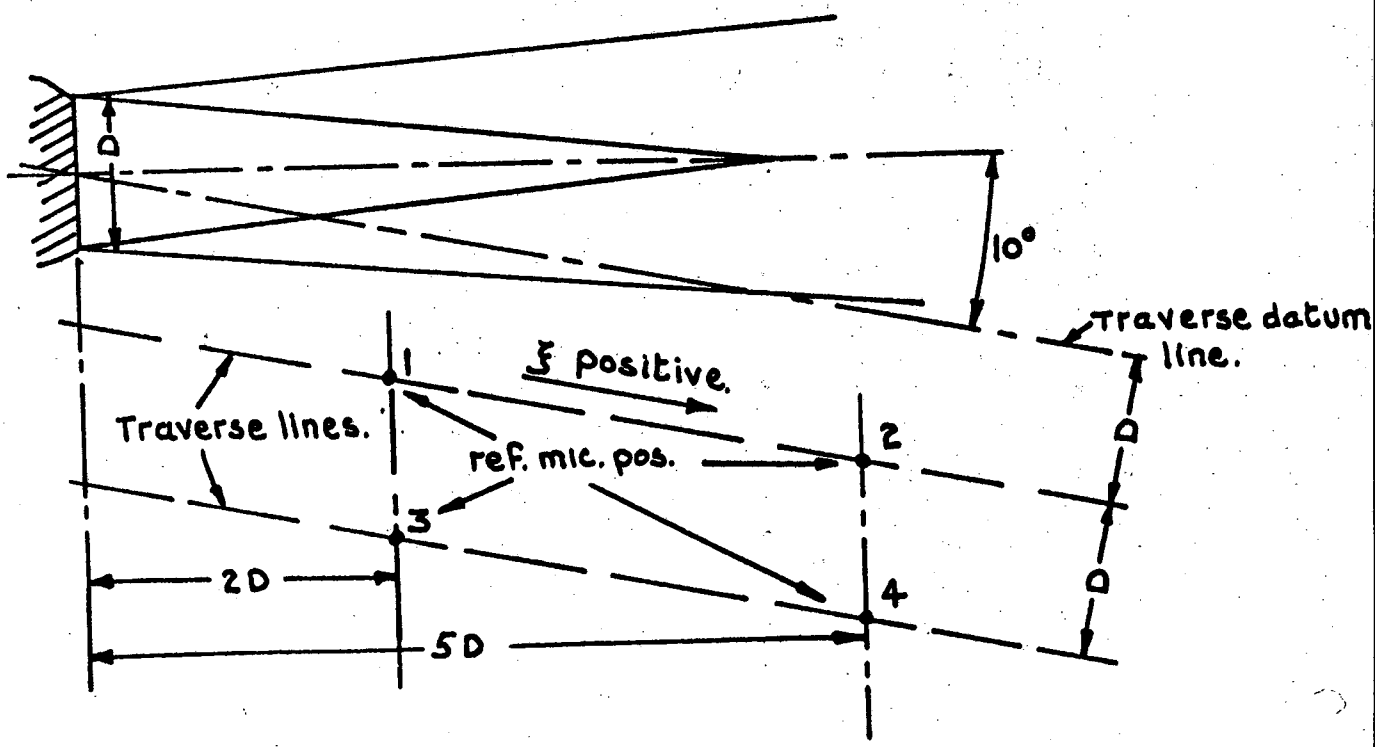

DIAGRAM SHOWING DETAILS OF MEASURING POSITIONS FOR INVESTIGATING CONVECTION OF PRESSURE FLUCTUATIONS.

FIG.25.

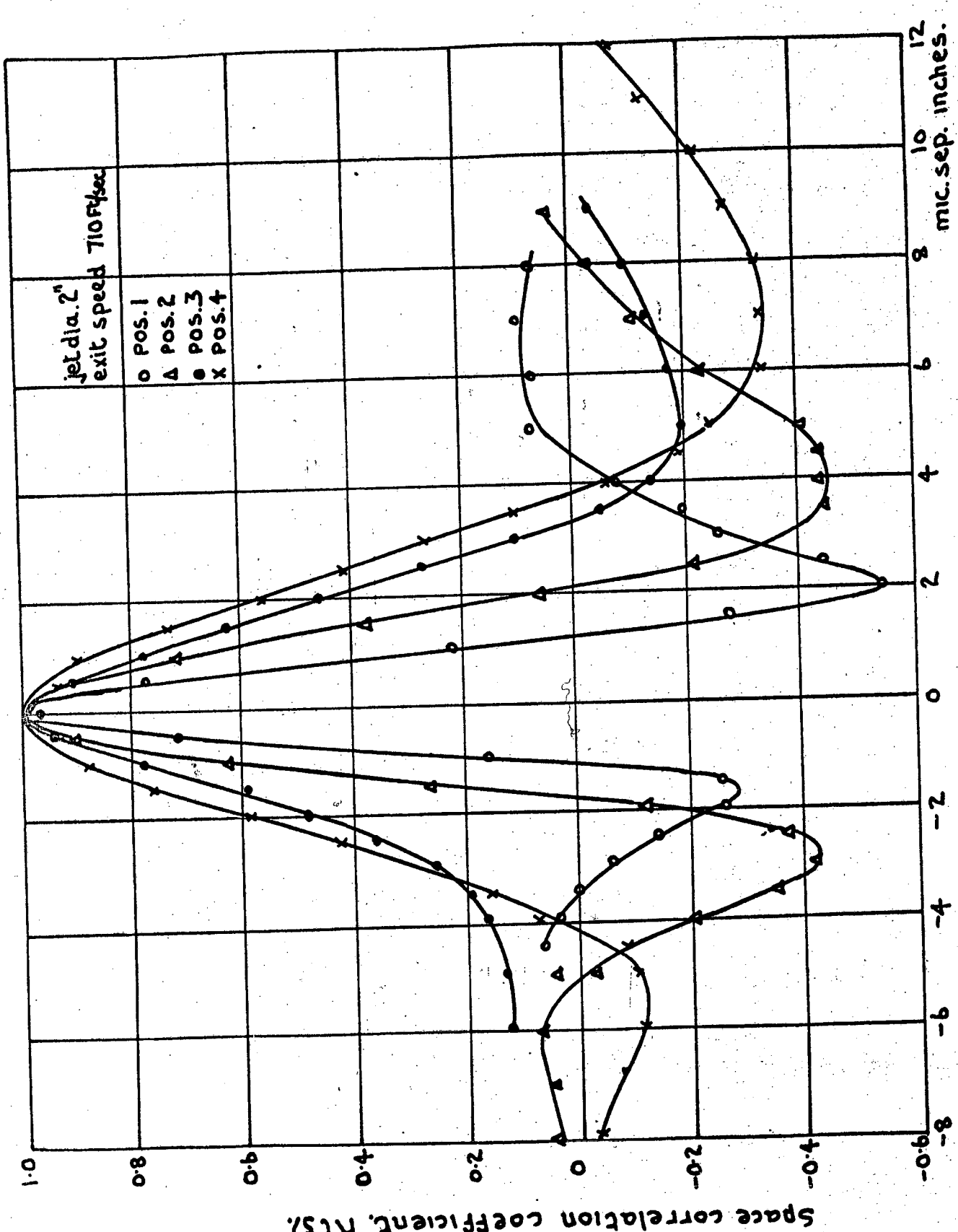

SPACE-CORRELATIONS CURVES FOR POSITION 1,2,3,4 (SEE FIG. 24)

FIG.26

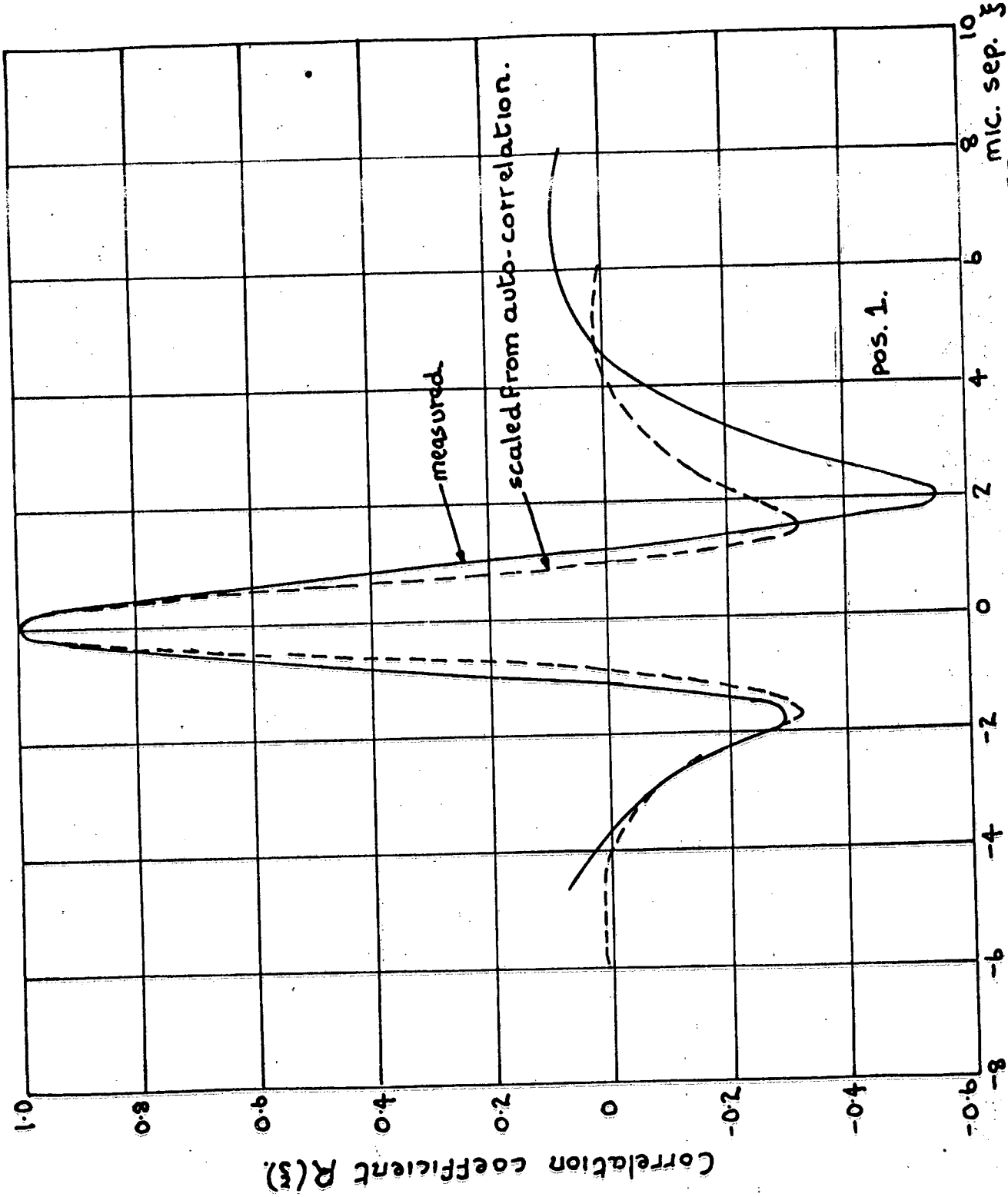

COMPARISON OF MEASURED SPACE-CORRELATION AND SCALED AUTO-CORRELATION - 2" DIA JET, VELOCITY 710 FT/SEC.

FIG. 27.

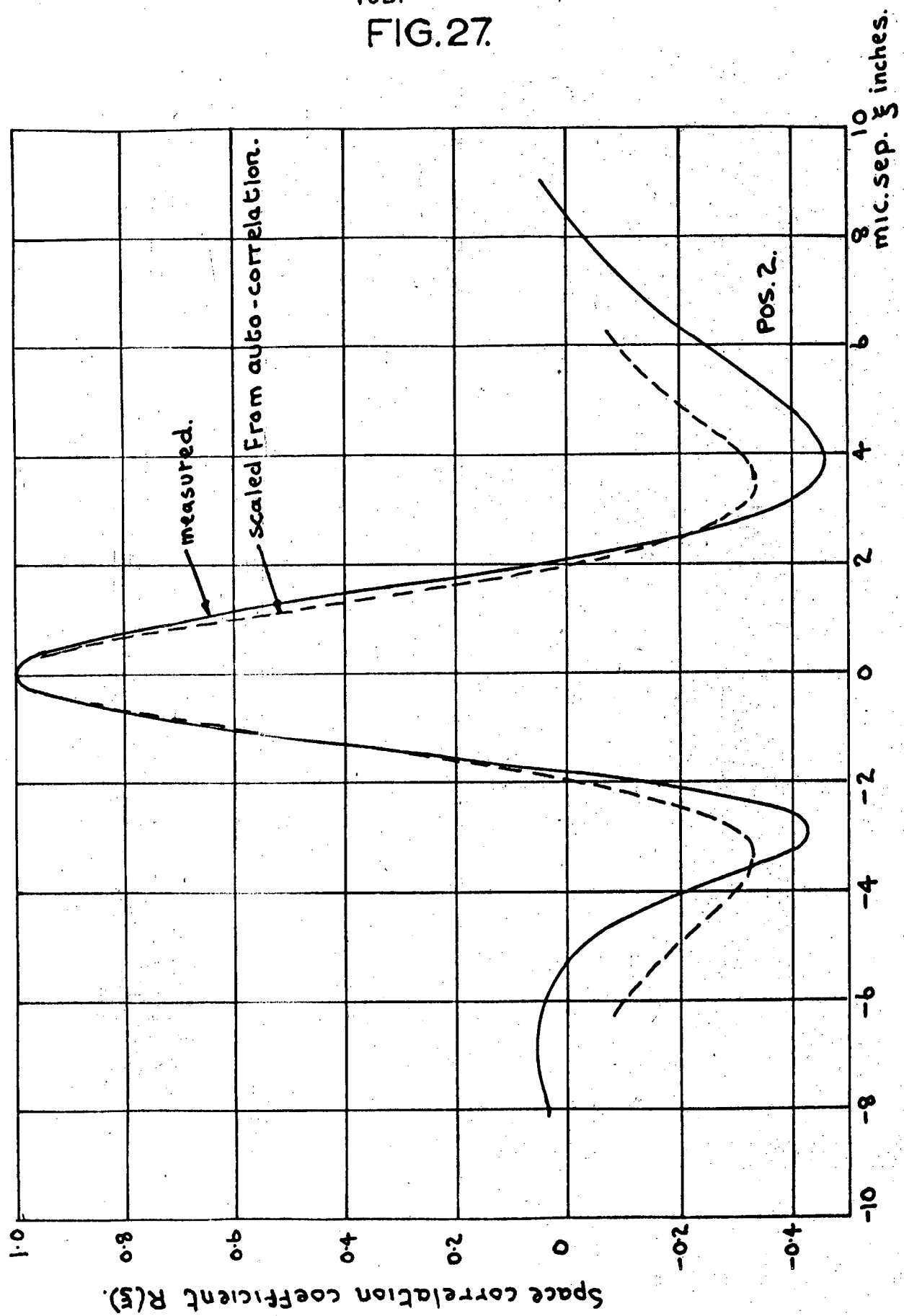

COMPARISON OF MEASURED SPACE-CORRELATION AND SCALED AUTO-CORRELATION. JET DIA. 2" VELOCITY 710 Ft/SEC.

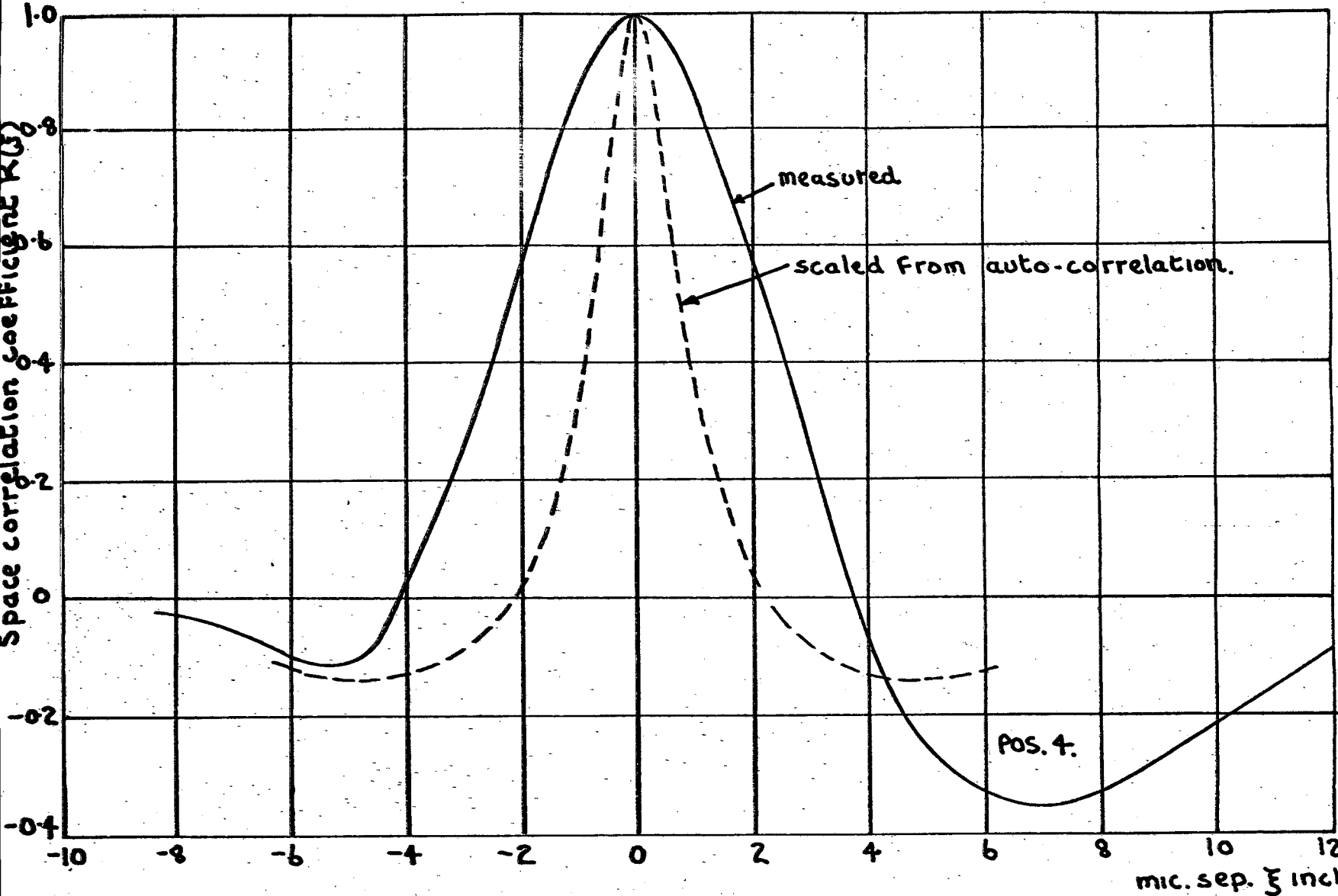

FIG. 28.

COMPARISON OF MEASURED SPACE CORRELATION AND SCALED AUTO-CORRELATION

2" DIA. JET, VELOCITY 710 FT/SEC.

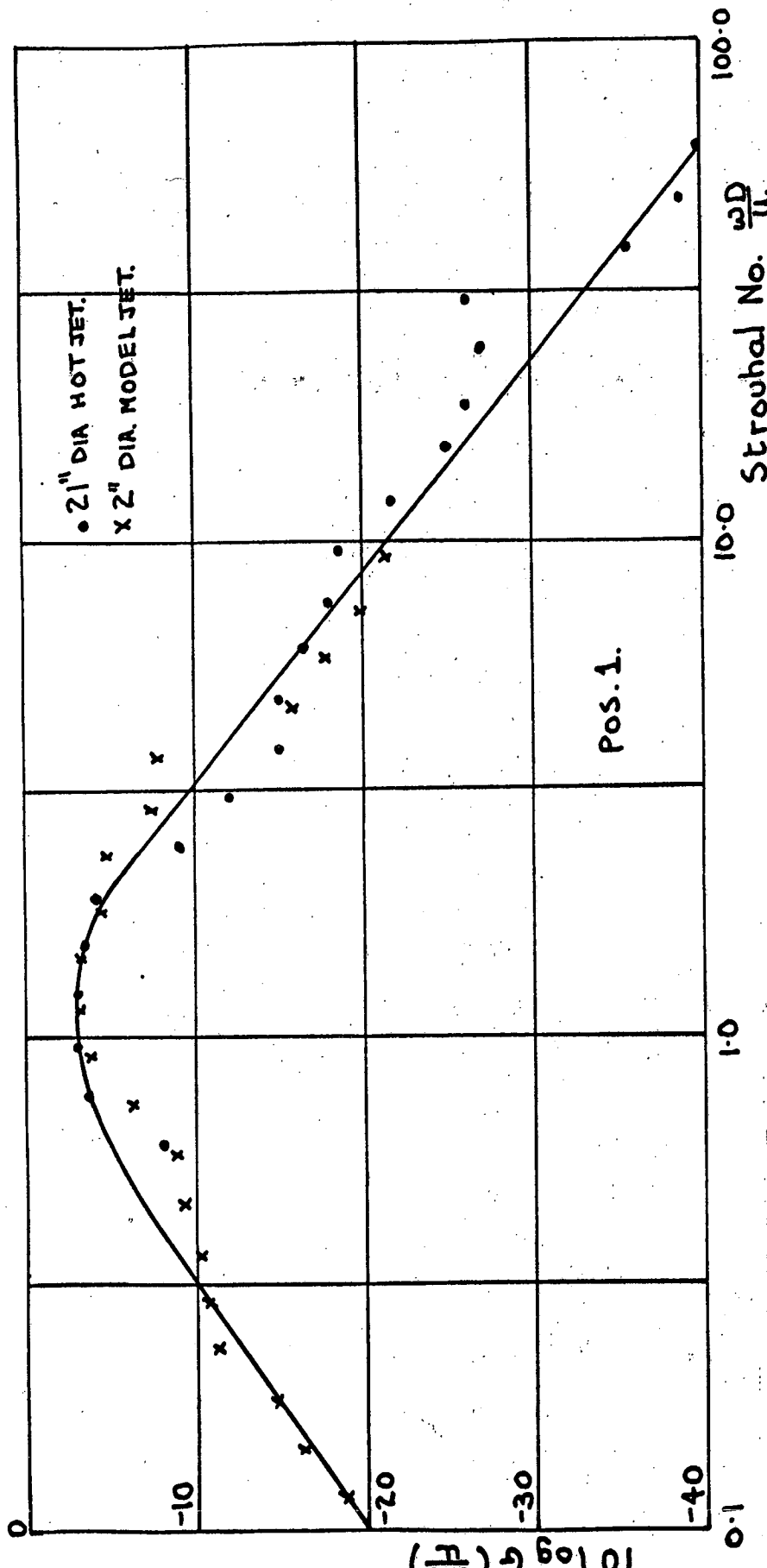

FIG. 29.

NON DIMENSIONAL POWER SPECTRUM - COMPARISON OF MODEL AND FULL SCALE RESULTS.

FIG.30.

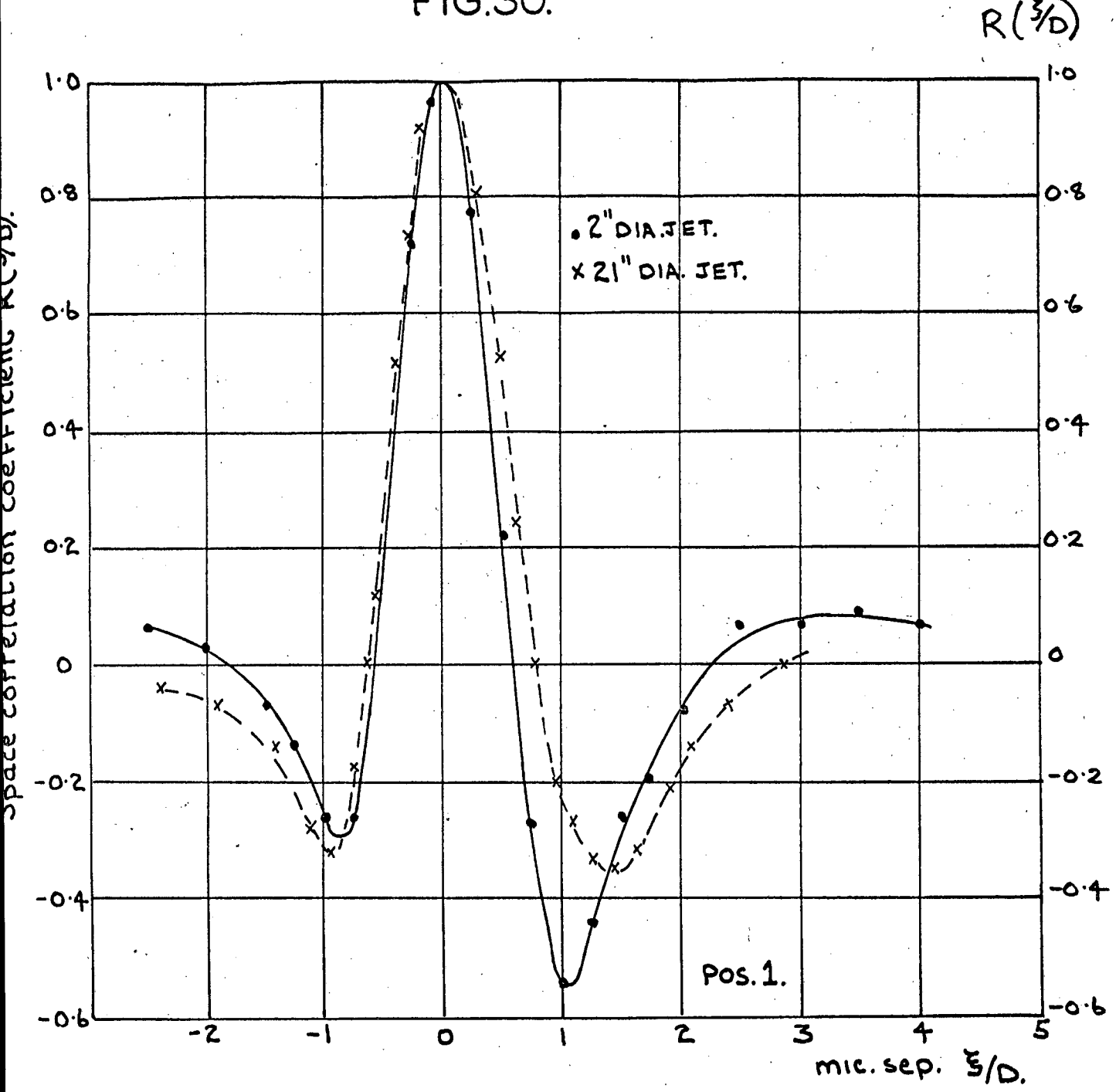

NON DIMENSIONAL SPACE-CORRELATIONS.
COMPARISON OF MODEL AND FULL SCALE RESULTS.

FIG. 31.

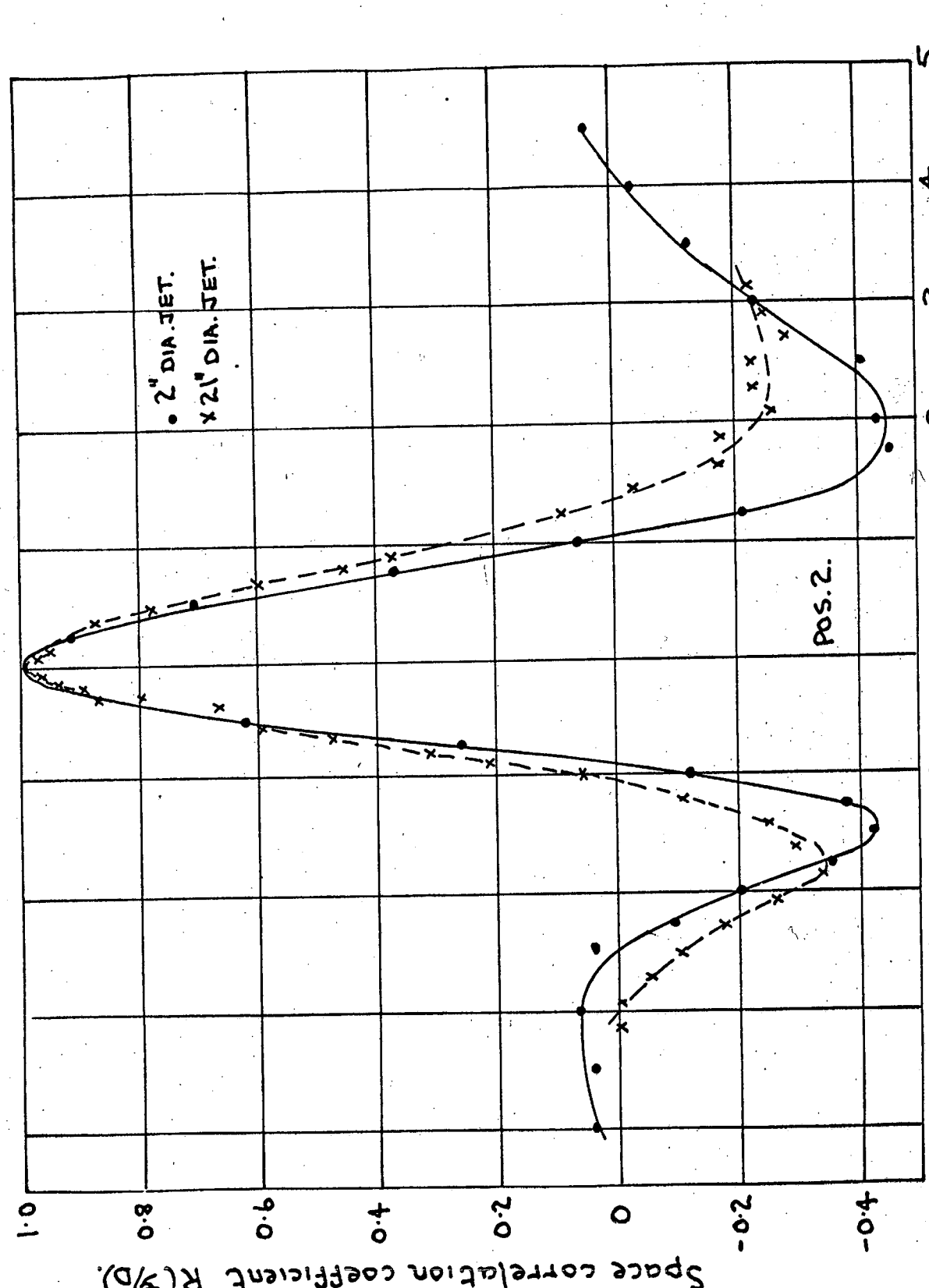

NON-DIMENSIONAL SPACE CORRELATIONS.

COMPARISON OF MODEL AND FULL-SCALE RESULTS.

FIG.32

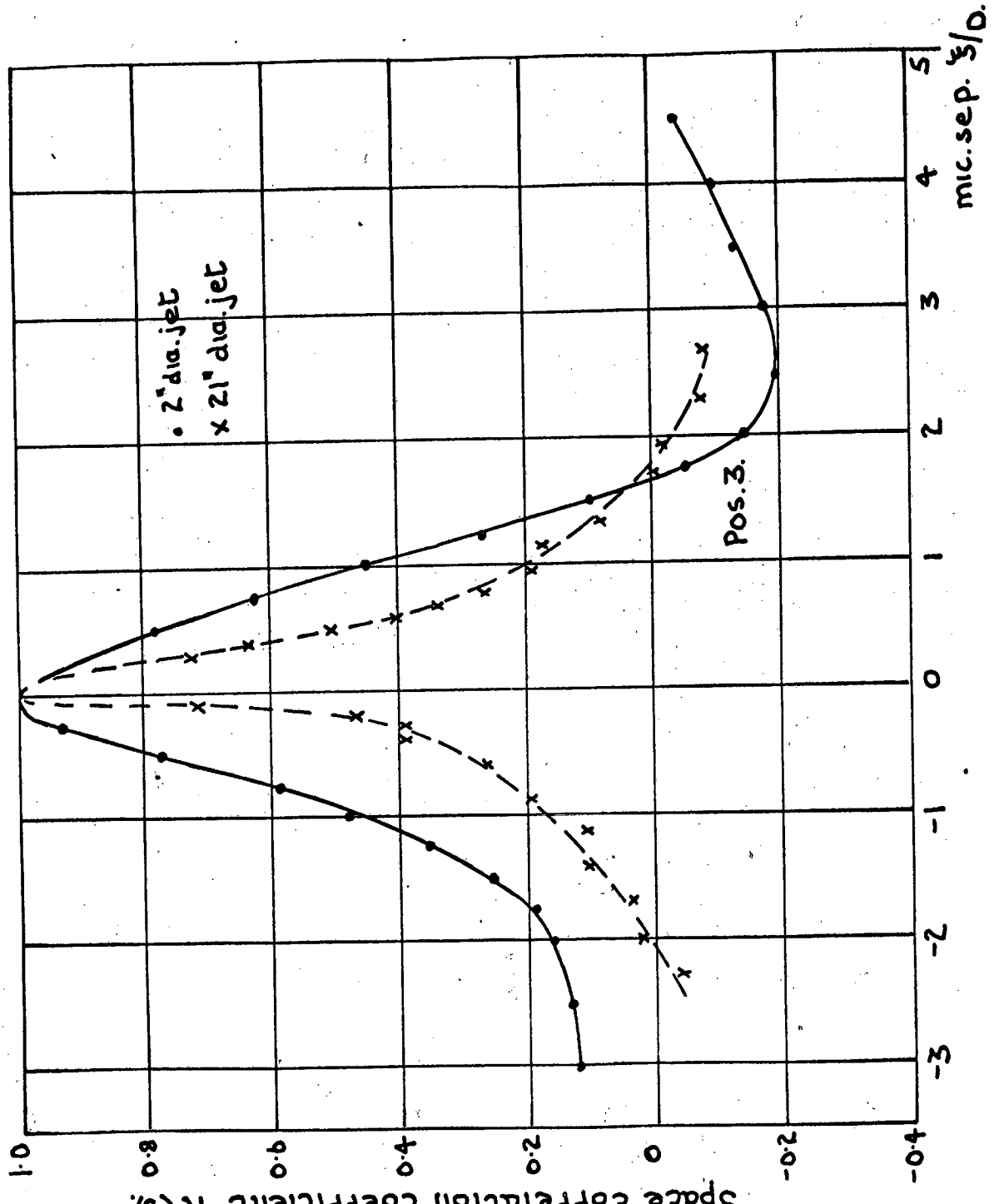

NON-DIMENSIONAL SPACE-CORRELATIONS.

COMPARISON OF MODEL AND FULL-SCALE

FIG. 33.

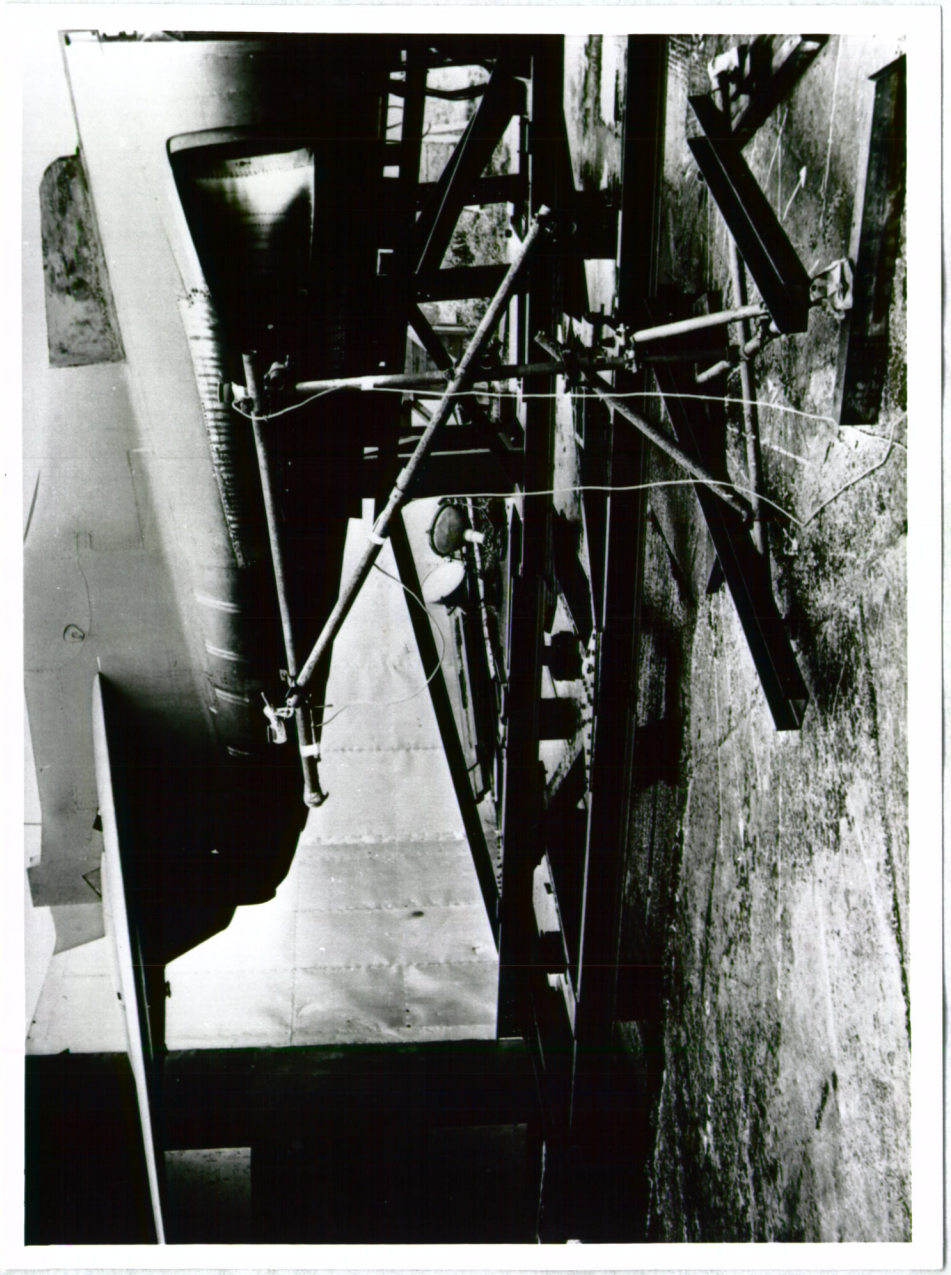

FULL SCALE JET RIG WITH MICROPHONES IN POSITION.

FIG.34.

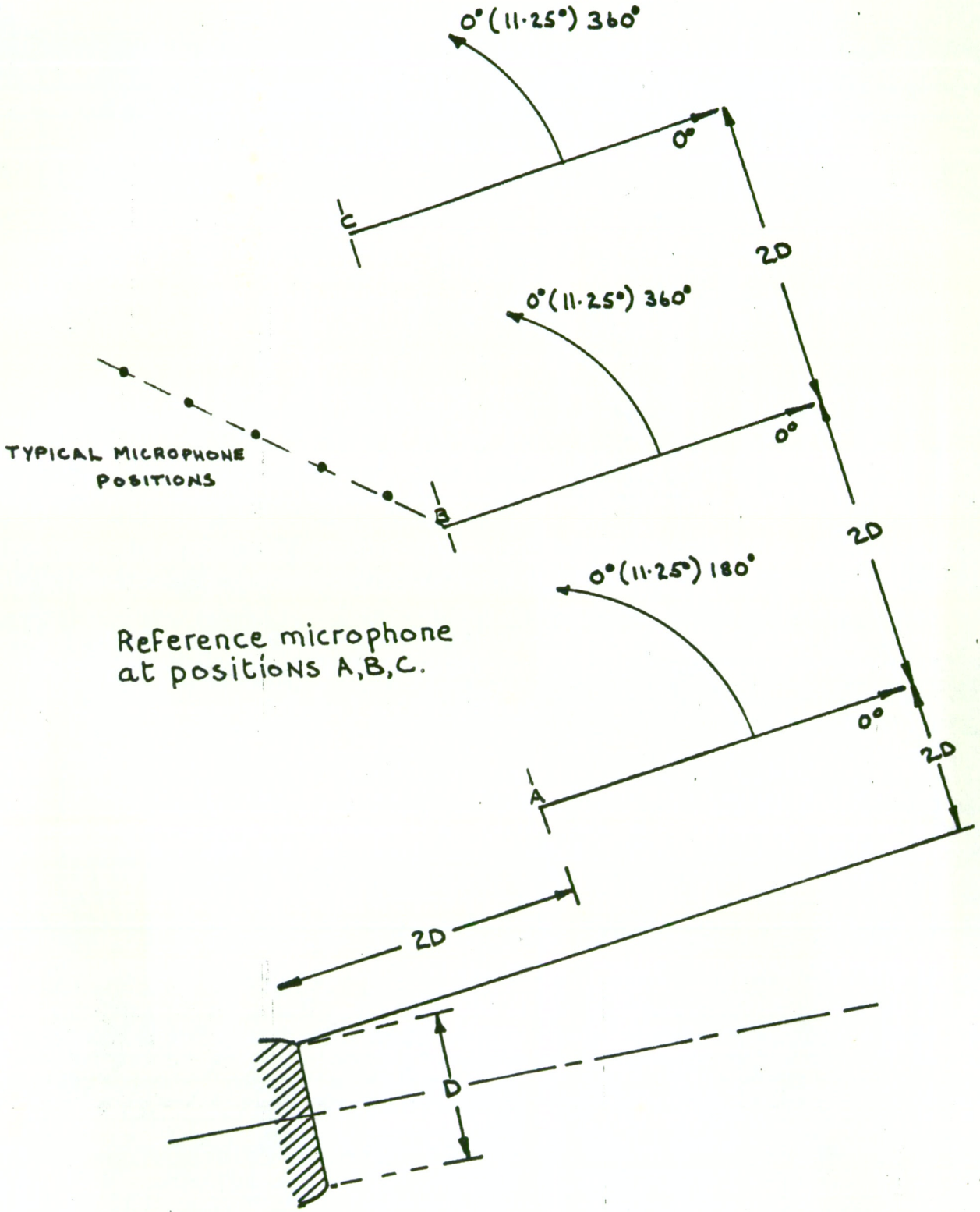

MEASURING POSITIONS FOR FULL SCALE. CHILBOLTON EXPERIMENTS.

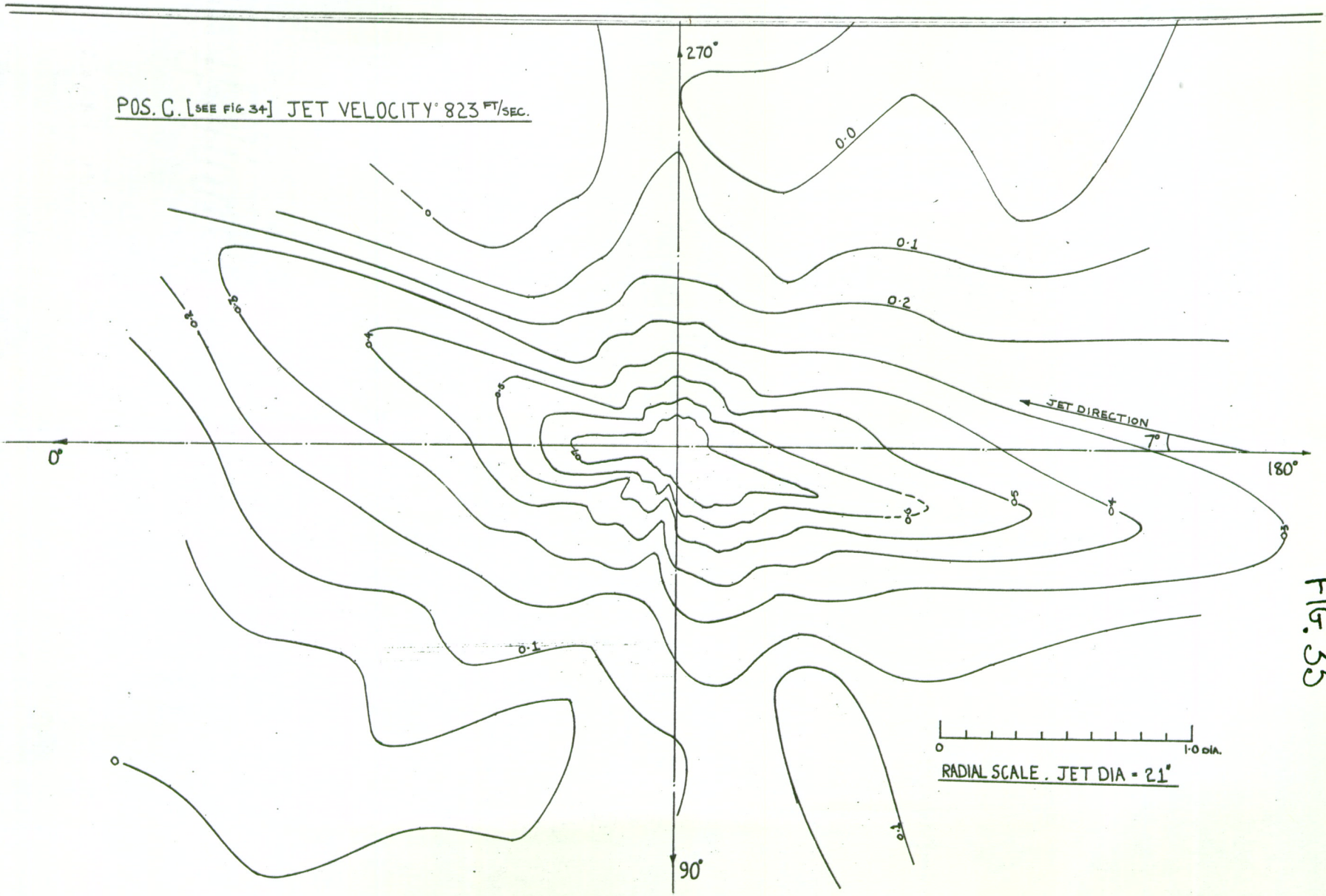
POS. C. [SEE FIG 34] JET VELOCITY 823 FT/SEC.
270°
0°
90°
180°
0·0
0·1
0·2
0·3
0·4
0·5
JET DIRECTION
7°
0
1·0 DIA.
RADIAL SCALE . JET DIA = 21"

FIG. 35

FIG. 36.

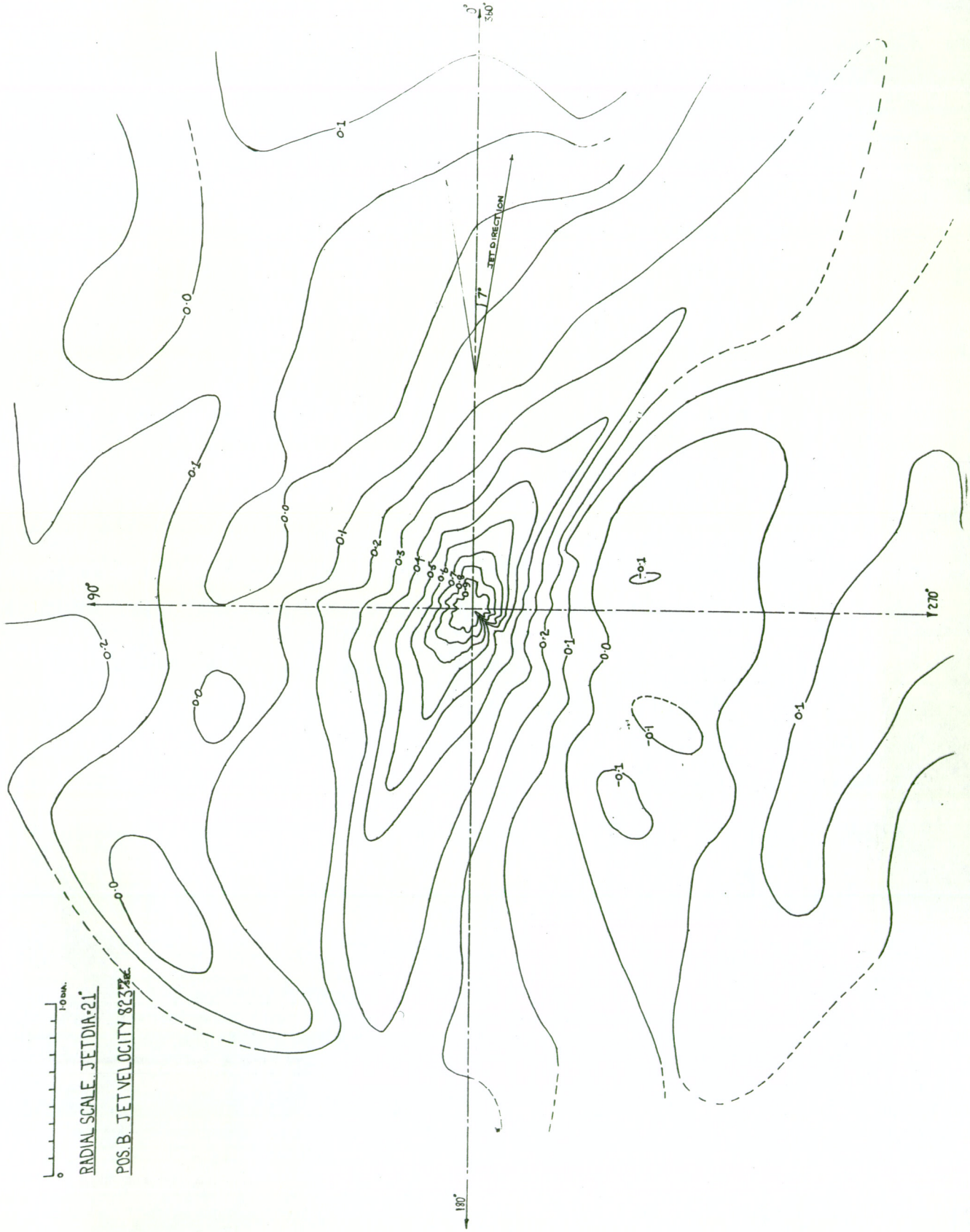
0°
360°
90°
180°
270°
JET DIRECTION
7°
0·0
0·1
0·2
0·3
0·4
0·5
0·6
0·7
0·8
0·9
-0·1
1·0 MM.
RADIAL SCALE. JETDIA=21'
POS. B. JET VELOCITY 823 ft/sec

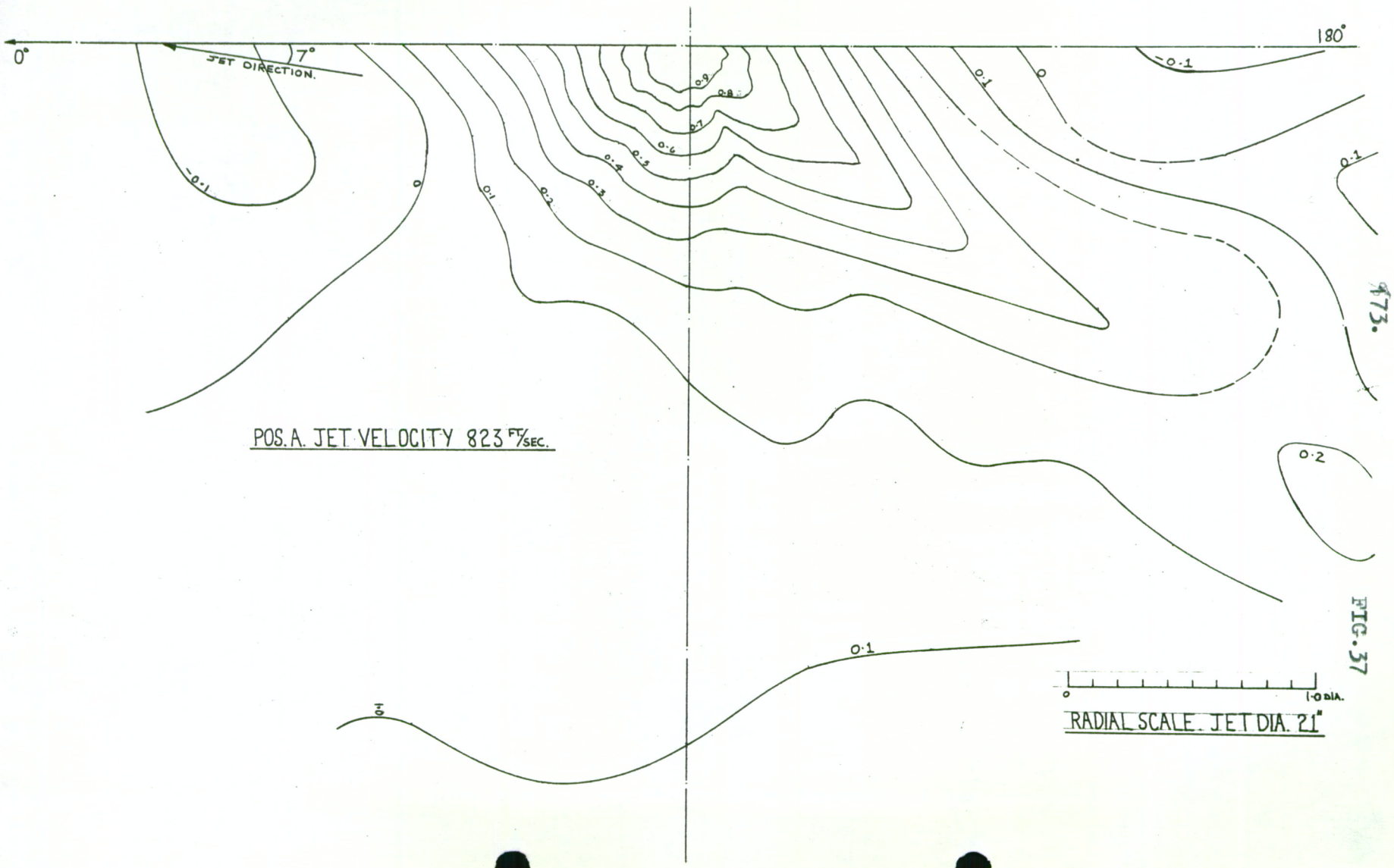
0°
180°
7°
JET DIRECTION.
-0·1
0
0·1
0·2
0·3
0·4
0·5
0·6
0·7
0·8
0·9
0·1
0
-0·1
0·1
0·2
0·1
0
1·0
POS. A. JET VELOCITY 823 FT/SEC.
0
1·0 DIA.
RADIAL SCALE. JET DIA. 2.1"

FIG. 37

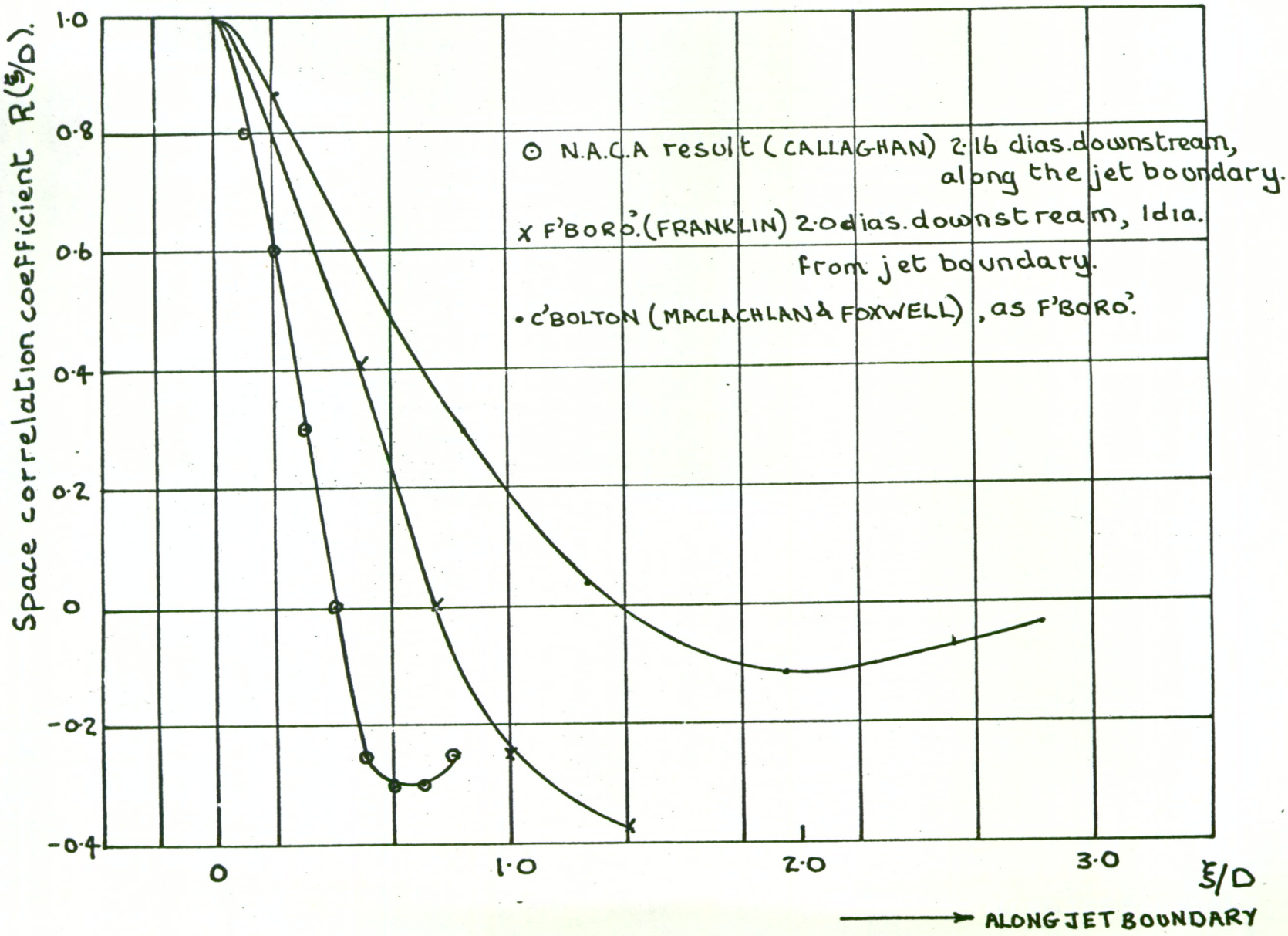

COMPARISON OF FULL-SCALE HOT JET SPACE CORRELATIONS.

FIG. 38.

FIG.39.

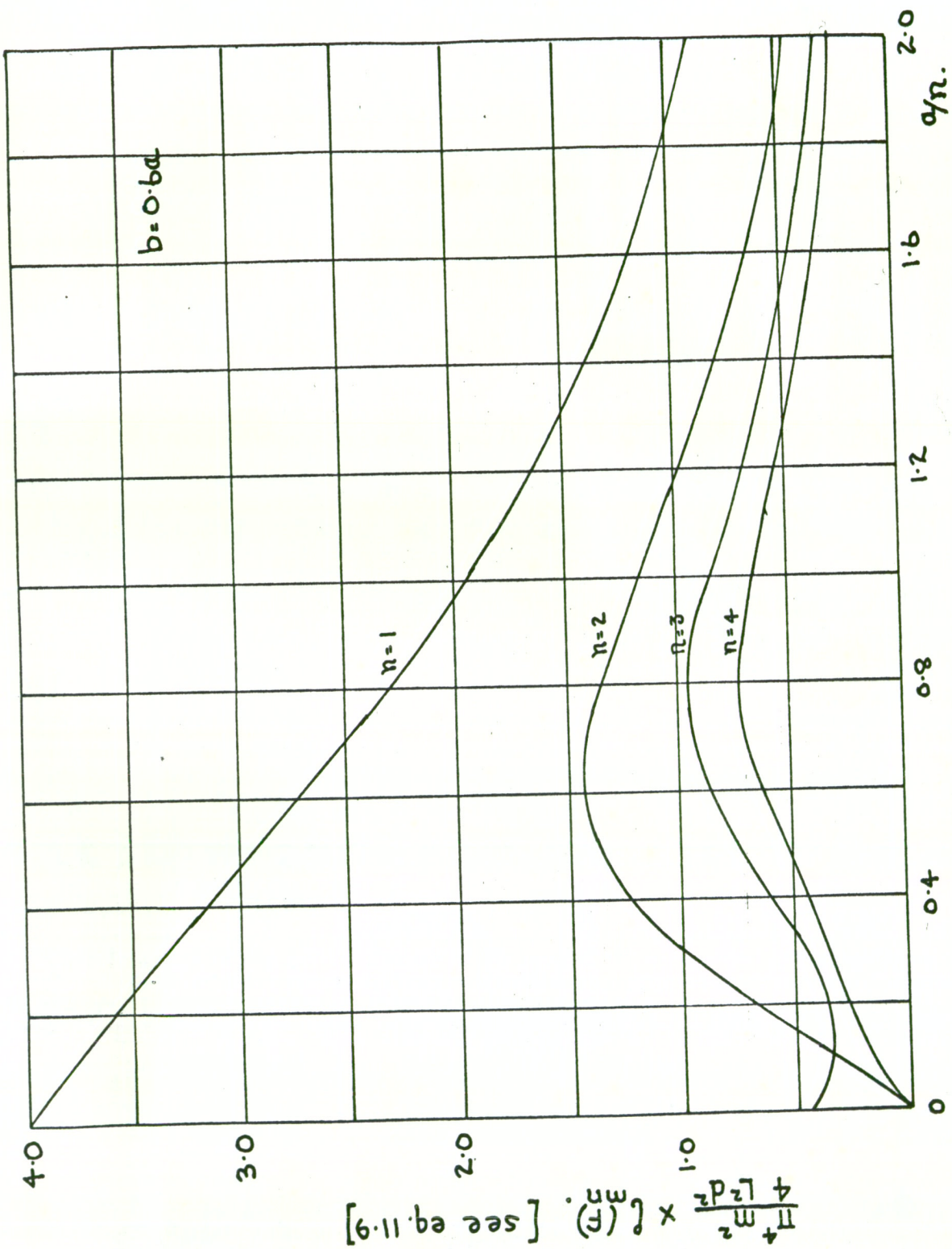

MODAL ACCEPTANCE FOR PRESSURE CORRELATION FIELD OF THE TYPE $\exp[-b\pi/L\,|x_2-x_1|\cos a\pi/L\,(x_2-x_1)]$.